Politecnico di Milano
Department of AEROSPACE SCIENCE AND TECHNOLOGY
Doctoral Programme In 2015

GENERALIZED AEROSERVOELASTIC STABILITY ANALYSIS OF ROTORCRAFT

Doctoral Dissertation of:
Aykut Tamer

Supervisor:
Prof. Pierangelo Masarati

Tutor:
Prof. Carlo L. Bottasso

The Chair of the Doctoral Program:
Prof. Luigi Vigevano

2012 – 27th cycle

Abstract

ROTORCRAFT aeroservoelasticity is inherently multidisciplinary, including aerodynamics of streamlined bodies, dynamics of flexible structures and flight control systems. The related engineering branches have variety of models with diverse characteristics in linearity and time dependence; therefore the improved rotorcraft designs require a generalization of the analysis, i.e. being applicable to the systems having different complexity levels. Inspired by this motive, our work presents the methods of generalizing aeroservoelastic stability analysis of rotorcraft. An aeroelastic rotor tool is formulated with the scope of evaluating periodic rotor matrices. A sufficient level of modeling capacity is achieved using structural dynamics of rotating elastic blades with rod, damper and hinge elements, steady and perturbation aerodynamics and multi-blade coordinates. The aeroelastic rotor formulation is integrated to an aeroservoelastic analysis platform which is able to analyze rotorcraft with a modular approach. The capability of quantitative stability analysis is extended from eigen-solution of linear time invariant systems to linear time periodic systems using Floquet's method and to nonlinear non-autonomous systems using Lyapunov Characteristic Exponents. The rate of change of stability is also significant in robustness analysis and design of dynamical systems. For this reason, using the same methods of quantitative stability estimation, the parametric sensitivity of the stability measures is formulated analytically. The methods are verified and illustrated on rotorcraft problems.

Dedication

To mom and dad; always supportive and encouraging

Acknowledgements

I WOULD like to thank my supervisor prof. Pierangelo Masarati for his guidance, support, encouragement and patience throughout the study. He has taught me many invaluable things with his welcoming, friendly and helpful attitude. Always motivating, but never interfering; he has widen my understanding and knowledge.

I appreciate the helps prof. Giuseppe Quaranta; when I need he always welcomed me. Special thanks to Dr. Vincenzo Muscarello for helping me in comprehensive modeling of rotorcraft and discussions on the related topics. The comments of prof. Franco Mastroddi are also greatly acknowledged.

The professors, staff and other PhD students of the department have always been so kind, friendly and helpful. Thanks them all. I specially owe thanks to prof. Carlo. L. Bottasso, he spent his time to clearly inform me about the PhD program and made my start in Milano easier.

Many thanks with love to my wife, Feyza, who closely shared the final year of my PhD. She has always been patient, encouraging and supportive. Additionally, I should thank to my father and mother in law who have taken care of my wife and house when I am away from home for my studies in Milano.

Special thanks to Turkish residents in Milano with many names I cannot count but always in my heart with their support.

Finally, my friends; I have always appreciated and needed their close friendship and generous supports.

Summary

CHAPTER 1 begins with a statement of motivation. The aeroservoelastic analysis of rotorcraft is outlined by briefly explaining the major disciplines and interactions among them. The steps of generalizing rotorcraft aeroservoelastic stability analysis and strategy that is followed in this work is summarized.

Chapter 2 describes the formulation of aeroelastic rotor model including verification analysis.

Chapter 3 is devoted to the stability and analytical sensitivity analysis of linear time periodic systems using Floquet theory. Method is illustrated on a simple first order differential equation with periodic coefficients.

Chapter 4 explains the use of Lyapunov Characteristic Exponents in estimating the stability and sensitivity of non-linear non-autonomous systems. The computational aspects of discrete QR decomposition algorithm and the problems related to the application of Lyapunov Exponents to mechanical systems are addressed and illustrated on a damped oscillator.

Chapter 5 provides the numerical examples and further illustrations and verifications of the methods and tools on rotorcraft related problems. Stability and parametric sensitivity analysis of linear time invariant, linear time periodic and non-linear non-autonomous systems are performed.

Chapter 6 concludes the thesis by pointing out important aspects and addresses the possible extensions of the work.

Contents

CHAPTER 1

Introduction

This Chapter introduces the building blocks of our research and addresses the corresponding chapters and sections. Section 1.1 is a statement of motivation. Then, in Section 1.2 aeroservoelasticity of rotorcraft is introduced. Finally, Section 1.3 presents the scope of the thesis and briefly describes the strategy to achieve the objectives.

1.1 Motivation

Rotorcraft, also known as helicopters or rotary-wing aircraft, are flying vehicles that utilize rotating wings to provide lift, propulsion, and control forces, which enable the aircraft to rise vertically and hover above the ground [1]. They have an indispensable role in aviation with their capability to fly at zero or low air-speeds, sidewards and backwards maneuvering skills and being able to take-off and land vertically. Hence, rotorcraft can operate in remote areas, where there is no airstrip and even no ground contact exists. For this reason, rotorcraft are ideal and unique vehicles for search and rescue [2]. Besides, they are also frequently used for other purposes such as transportation of human and cargo, military actions, fire fighting, construction; especially under the

conditions in which fixed-wing airplanes cannot operate.

A sufficient magnitude of relative speed between lifting surfaces and air is needed to provide the required thrust levels at zero and low airspeeds. This is simply done by rotating wings with respect to the fuselage. However, since they do not operate in high speed axial flow, rotors have to be designed big enough in order to enable all essential tasks of a flying vehicle, i.e. rotor contributes to lifting, propelling and controlling the rotorcraft [3]. These essential tasks are not separable and the resulting cross couplings between the tasks lead to complexity and dominance over all the aspects of helicopter operation from aerodynamics to the safety. Result is complex flight physics as compared to fixed wing aircraft [4]. Because of the higher complexity, rotary wing operation and maintenance costs are higher than those of conventional airplanes. As a result, inflation rates in helicopter purchase prices are much higher as compared to the rates of consumer price index and air-passenger ticket prices. (See Ref. [5] for a comprehensive cost analysis). Besides cost, chronic problems exist such as proneness to instability and excess levels of vibration which remain throughout the service life. Majority of these chronic problems are mainly induced by the dominating physics of the rotor under which aerodynamics, structural dynamics and flight control systems interact.

In order to achieve competitive designs with reduction in characteristic rotary-wing problems, it should be first kept in mind that rotorcraft physics is multidisciplinary and determined by nonlinear and time dependent equations in the broadest sense. A field is given a long but comprehensive name *aeroservoelasticity* to handle the complex problem and address the interactions among the governing disciplines of flight sciences. For rotorcraft, determination of stability is an important task in aeroservoelasticity, in fact the most critical, since they are inherently unstable systems [6]. Aerodynamics, structural dynamics and control systems are involved in the stability of rotorcraft which may additionally include significant nonlinear and time-dependent effects. Analysis models are usually simplified to achieve quick results with practical cost. Although these simplifications are still valid and accurate for an important set of flight conditions, critical information about the system can be lost in many cases. Ignorance of multidisciplinary, nonlinear and time-dependent effects can cause significant consequences about stability; hence the capability of the analyses should be available and generalized for rotorcraft sytems having different levels of complexity.

This work is a result of such a motivation and focused on developing tools and methods in order to increase the effectiveness of aeroservoelastic stability analysis of rotorcraft. The nomenclature is given within the text. Although some symbols may be used for more than one parameter or variable for independent topics, maximum care has been taken in each subject to clearly state the symbols at each section and what they refer to. In this work, there is no separate section for literature survey; however the bibliographic notes that are the basis of our research and the advised references for further reading are provided in this chapter and throughout the text.

1.2 Rotorcraft Aeroservoelasticity

"Aeroservoelasticity is a multidisciplinary technology dealing with the interaction of the aircraft's flexible structure, the steady and unsteady aerodynamic forces resulting from the aircraft motion, and the flight control systems" as designated in Ref. [7]. This definition is valid for any structure including rotorcraft; which significantly interacts with air through streamlined surfaces, have non-negligible elasticity and require a human or an artificial system for stabilization, control and guidance. In fact, the subject is an extension of aeroelasticity by including the interaction with flight control systems; as modern aircrafts started using fly by wire systems more frequently in order to improve the handling qualities and stability, flight performance and ride quality, and also to reduce loads and improve service life [8]. The building blocks of aeroservoelasticity are structural dynamics, aerodynamics and flight control systems. These blocks are briefly explained in following sections for their importance in rotorcraft and possible sources of aeroservoelastic couplings are addressed.

1.2.1 Aerodynamics

Aerodynamics is the core branch of flight physics that is concerned with the flow of the air [9]. Rotorcraft involve almost all of the complex aerodynamics phenomena except supersonic flow. Fig. 1.1 gives a complete picture of the complicated aeromechanics of a typical helicopter. Although, an adequate description is still missing [10], successful attempts has been made to make vertical flight possible and to understand significant aspects.

The main complexity arises form the rotation. When forward flight speed is non-zero, blades traveling at one half of the rotor disk ad-

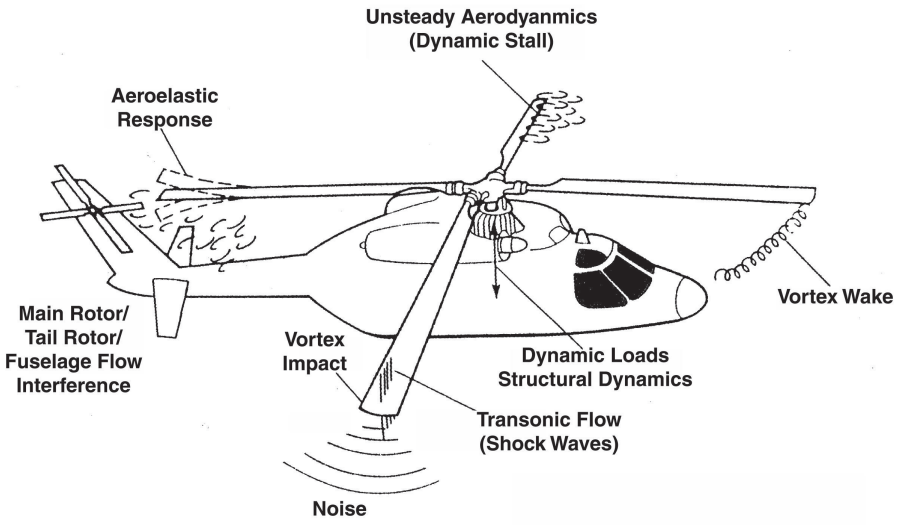

Figure 1.1: *Complex aeromechanical phenomena induced by helicopter rotor (from Ref. [11]).*

vance the speed of the vehicle. When this is summed with the speed due to rotation, blade tips experience more serious compressibility effects as the vehicle accelerates. Then, the major drawback is reduced maximum forward flight speed, which is typically about 200 knots in limit. On the other hand, the other half of the rotor disk operates in the opposite direction of the vehicle heading. When the speed due to rotation is subtracted from the vehicle's speed, reverse flow conditions occur near the blade root, which in turn causes blade sections operate in stall and resulting in high levels of drag. Due to this differential loading, forward flight operation cause alternating loads; a source of excitation at frequencies multiple (n) of the rotor angular speed $n\Omega$; where Ω being rotor angular speed.

The rotor wakes are dominated by the strong blade tip vortices and their geometry is quite complex due to rotation. Flying under their own wake is not rare for rotorcraft and more severely, the interaction of the wake with the body and other components results in noise and vibration. Moreover, the periodicity of the wake is spoiled under unsteady effects such as control inputs or maneuvering conditions, which can lead to instabilities [10].

The motion and elastic deformation of the blades, which can be

steady or vibratory, affect the airloads significantly [12]. Depending on the geometry, flexibility and inertial characteristics of the control system and blades, blade sections respond to the time dependent aerodynamic loads. The response, characterized by bending and twisting of the blade sections, modifies the effective angle of attack of blade sections, which in turn alter the loads.

1.2.2 Structural Dynamics

In aeronautics, the basic functions of an aircraft's structures is to transmit and resist applied loads, to maintain the aerodynamic shape and to protect the interiors from environmental conditions [13]. In rotorcraft, while the fuselage is not so different than that of a fixed wing, the existence of rotor results in additional complexity.

First of all, the connection of the blade to the rotor hub should allow motion in order to ease the handling by relieving the blade root moments and transmit control inputs to the blades. The solution is to link the blades to the hub via mechanical hinges and bearings or elastic structures that have high flexibility. This motion is described by the equilibrium of centrifugal and aerodynamic loads. Because of this reason, the rotor blades behave like a mechanism to some extent, which in turn make them intrinsically dynamical structures.

The elasticity of helicopter blades is mainly a result of their geometry. The span of the rotor blades should be large for the sake of hover efficiency [14], which is a basic measure of the utility of rotorcraft [15]. Moreover, low solidity (ratio of the total area of the blades to the area of the rotor) is also essential for reduced power required to hover at the same thrust level; hence chord length should be kept as low as possible, as long as the stall margin of the blade cross section allows [10]. Then, large radius and small chord length lead to slender rotor blades, meaning very flexible structures. This is especially critical in their thin directions, which also carries most of the blade thrust; and also significant in twisting direction which has direct impact on airloads. In fact, the main rotor blades have such a low stiffness that they can hardly carry their own weight without rotation. The centrifugal loads stiffen the blade; therefore flexibility is not a problem from strength point of view. However, for frequencies higher than the rotor angular speed, the blade elasticity should be considered; since the aerodynamic damping reduces its effectiveness as frequency increases. Elastic couplings between flapping, lagging and pitching motions are also common due

to material distribution over the cross section. Especially due to the use of composite materials in modern helicopter blades, anisotropy and non-homogeneity are distinctive characteristics [16].

Inertial loads plays an important role in dynamics of the rotor blade in addition to the stiffening effect of centrifugal tension. First of all, mass and inertia of the blade resists the change of momentum as in the case of any mechanical system. However, although the assumption of infinitesimal strains is still valid, the deflections and rotations can be moderate or large [17, 18]. Moreover, Coriolis forces, a specific effect due to rotation, couples flapping and lagging motions of rotor blades. Inertial couplings between centrifugal loads, blade position and orientation induce destabilization in lead-lag motion and additionally cause propeller moment in pitch direction. The chordwise center of gravity offsets from pitch and elastic axes are also among stability related issues. Static, dynamic and aerodynamic balance of blades are also critical to reduce low frequency vibrations [19]. Section 2.3 together with inertial loads given in Section 2.5.1 describe the formulation of rotor blade structural dynamics. Interested readers may also refer to Refs. [20] and [21] for a general survey and comparison on the beam theories for rotor blades.

Even in the absence of excitation forces, the dynamics of the rotor and fuselage may couple. One very critical condition is ground resonance, which is defined as the dynamical coupling of the rotor in-plane degrees of freedom with the fuselage and undercarriage system when rotorcraft contacts with the ground. Section 5.3 presents a detailed analyses with periodic and nonlinear effects. Similar resonant condition may also occur on air for hingeless rotors (See Ref. [22] for a detailed description of both ground and air resonance).

Rotor blades are excited by oscillatory aerodynamic forcing, which reduce the service life of the blades and other components. Vibration amplitude amplifies if natural frequencies of the blades are close to harmonics of rotor frequency [23]. Moreover, the vibrations are transmitted to the fuselage through mechanical and aerodynamic load-paths [24]. The frequency interval of the rotor induced oscillatory loads are wide and include many low and high frequency rotor and fuselage elastic modes (See for example Ref. [25]). Hence, it is very likely that a resonant condition occur even for high frequency elastic modes, which in turn dramatically degrades flight safety and comfort. Helicopter vibrations are generally considered to limit several factors like safety, reliability, comfort and maximum speed. Additionally, an excessive

level of vibrations leads to an increase in maintenance stops which in turn increase the operational costs (See Ref. [26] for a detailed cost analysis). Another important effect is the degradation in the cabin comfort, more severely chronic pain can be felt by the pilots in long term [27]. More severe vibrations may cause failure and instability during flight. As a consequence, vibrations are directly related to the acceptance in commercial market [28].

1.2.3 Control

An aircraft can achieve and maintain its trimmed flight or maneuver via a pilot or flight control system (FCS) or both, which mainly require forces and moments to control the attitude of the body [29]. For rotorcraft, due to the operation at lower speeds, the airspeed over the control surfaces are not always high enough (except high speed forward flight). This is opposed to the higher operation speed and well separated functions of lift, propulsion and control in fixed wing aircraft; in which slight deflections are enough to control a conventional airplane. Therefore, classical control surfaces of fixed-wing aircraft are not very useful in rotorcraft and the main sources of control forces and moments are rotors and their differential thrust [4]. The swash plate of the main rotor can change the orientation of the blades collectively or sinusoidally, which is linked to the control sticks in the cockpit. Thus, the magnitude and direction of the thrust force can be adjusted to provide the required forces and moments. The side effect of the change of thrust is the induced drag on the rotor hence the power output from the engine should be controlled by means of a throttle. The directional control is achieved generally using pedals in the cockpit which collectively changes the angle of attack of the tail rotor blades, thus a torque is generated around the vehicle center of gravity. There also exist some other means of directional control than a tail rotor but they are out of the scope of this work (See for example Ref. [6]).

Modern aircrafts are donated by FCSs in order to improve stability and ease the handling of pilot, which also have gained importance and the number of applications in rotorcraft industry [30] (Also see Ref. [31] for historical aspects). These systems mainly control the rigid body attitudes of the aircraft; besides, they also evolved to improve flight safety and ride comfort by suppressing vibrations (See Refs. [32–35] for active and passive vibration suppression analysis). In the case of a FCS application, the sensors measure the rates of the body and

controller processes the feedback information to maintain the required orientation. However the signals, owing to aircraft flexibility, carry contributions caused by such flexibility. As a result, the gains and filters of the FCS would also operate on signals coming from the flexible aircraft, if they were not appropriately corrected (Refs. [36] and [37]). Thus, the controls about the frequencies of aeroelastic system is driven, possibly leading to aeroelastic instabilities. This is more critical in rotorcraft since the level of vibration is much higher as compared to the fixed-wing airplanes.

In addition to FCSs, the vehicle can also interact with the pilot and cause unintended oscillations and low stability margins. Depending on the frequency of the interaction, the phenomena is referred to as rigid body or aeroelastic rotorcraft-pilot coupling (RPC) [38]. Rigid body RPC occurs at low frequencies and hence the problem is directly related to flight dynamics. Aeroelastic interactions are more related to involuntary pilot behavior [39, 40], which is a significant source of degradation in handling qualities and safety [41]. The source of this phenomenon is the interaction of vibratory loads with the biodynamics of the pilot, which is inherently uncertain. In practice, the inceptor motion involuntarily produced by the pilot is often associated to the acceleration experienced by the pilot through the seat, which is a result of the transmitted vibratory loads. (See for example Ref. [42] on the involuntary collective motion associated to motion along the vertical axis, and Ref. [43] on the lateral axis, and a recent study in Ref. [44]). The motion of the involuntary pilot feeds the systems through control chain and the resulting closed-loop system can lose stability even if the open loop system is stable (See Refs. [45, 46] for robust stability analysis of involuntary pilot coupling).

1.3 Generalizing Rotorcraft Aeroservoelastic Stability Analysis

The discussion above shows that there is no central discipline in the design of rotorcraft. At elementary levels, the problems can be solved assuming independent disciplines; however, the multidisciplinary nature should be carefully preserved with possible nonlinear and time variant effects in order to foresee significant problems such as instabilities, vibrations, limit cycles oscillations and other problems related to the aeroservoelasticity of the system. For example, Fig. 1.2 visualizes an example of a problem in rotorcraft aeroservoelasticity. The vehicle involving aeroelastic couplings presents time oscillatory loads; thus

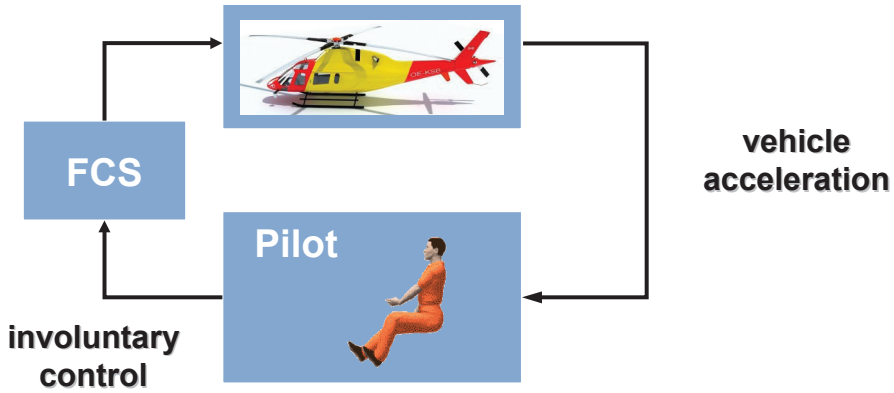

Figure 1.2: *An aeroservoelastic rotorcraft problem: The aeroelastic vehicle generating oscillatory loads and vibration, flight control system characterized by gains and phases and an involuntary pilot closing the loop.*

induces vibrations on the pilot through elastic fuselage. The involuntary pilot inputs, caused by the vibrations on the pilot, activate the flight control systems, which is characterized by gains and phases. The resulting system is highly multidisciplinary with inherently nonlinear sub-systems and feedback through FCS and human pilot.

Considering that rotorcraft cost much more than their fixed-wing propeller driven counterparts as stated in Ref. [5], which is due to higher levels of complexity, the decisions made in the design process are then more critical and the aeroservoelasticity concept should be more involved. In this work, we are interested in developing tools and methods in order to increase the effectiveness and capability of aeroservoelastic stability analysis of rotorcraft; hence the need of simplifications and the level of uncertainty can be minimized. The capability of aeroservoelastic stability estimation can be increased by following two paths. The first way is to focus on the multi-disciplinary nature of aeroservoelasticity by increasing the number of disciplines and developing detailed comprehensive models of rotorcraft and its subcomponents. The second path is to increase the capability of mathematical and numerical tools to quantify the stability, such that the systems having different levels of complexity can be analyzed without requiring simplifications in multi-discipliner, nonlinear and time-variant nature of rotorcraft.

The first path is well-known in rotorcraft industry. In fact, from

commercial to academic purposes, many comprehensive tools have been developed for multi-disciplinary analysis of rotorcraft and many helicopters in service verify the capacity and success of these tools. Among them the pioneer is CAMRAD series [47–49], started in 70s and still an active project. Then, as computers speed up, flexible multibody dynamics codes emerged in almost every field of mechanics. Since rotorcraft possesses components having quite different behaviors from hinges to slender elastic blades, the philosophy of multibody dynamics fits well for rotorcraft simulation purposes. The two multibody dynamics codes mainly dedicated to rotorcraft research and development are DYMORE [50] and MBDyn [51]. A state of art idea is to develop a numerical platform which is capable of representing elastic and rigid boundary conditions between the components of a rotorcraft that can come from independent sources. For this reason, a simulation tool called MASST (Modern Aeroservoelastic State Space Tools) was developed at Politecnico di Milano prior to this work, for the aeroservoelastic and aeromechanical analysis of aircraft and rotorcraft (See Refs. [52], [53] while a brief description is also available in Section 2.1). The philosophy of MASST is being the platform of coupling the mathematical models of the rotorcraft components originating from independent sources. Nevertheless, a valuable extension to MASST and hence increase the capability of aeroservoelastic analysis is to develop an in-house aeroelastic rotor code. The benefits of such a work is: flexibility can be supplied to MASST for performing stability analysis of rotorcraft with different levels of complexity; MASST can be better used as a design code by allowing optimization and parametric analysis; and freedom from commercial comprehensive tools is achieved. This part of our research is extensively explained in Chapter 2 including the theoretical background and some examples for verification.

The second path that we have followed is to extend the capability of stability and sensitivity analysis without requiring simplifications in the system nonlinearity and time dependence. Stability is defined as the study of the nearby solutions of an equilibrium [54]. In other words, we are interested in the behavior of the solution of an equilibrium under the presence of a perturbation [55]. Although the definition is the same for any system, the methods that estimates stability differ depending on the complexity. A straightforward method is perturbing one input or disturbance channel of the system and measuring decaying characteristic of the output by experimenting on a real system or simulating its mathematical model. Fortunately, there exist

spectral methods which quantify the decaying characteristic of independent components of solution, i.e. the system's exponential multipliers or characteristic exponents. Having determined the stability measures that quantify stability, it is easier to interpret and compare the results. Besides, spectral methods are also suitable for analytical estimation of sensitivity of stability estimates. In this work, spectral methods of estimating stability is preferred and developed for systems having different levels of complexity. Whatever the flight conditions, multi-disciplinary interactions and characteristics of sub-components are; rotorcraft aeroservoelastic stability problems can be handled following the theory of dynamical systems. Mathematically speaking, the general form of a dynamical system is,

$$\dot{\mathbf{x}} = \mathbf{f}\left(\mathbf{x}, t\right), \qquad \mathbf{x}(t_0) = \mathbf{x}_0 \tag{1.1}$$

where, $\mathbf{x}$ is the state variable vector and $\mathbf{f}$ is the function that governs the system; such that the knowledge of $\mathbf{x}(t_0)$ at initial time t_0 and $\mathbf{f}$ provides the future state vector $\mathbf{x}(t)$, with $t > t_0$ [56]. In the most general version, $\mathbf{f}$ is nonlinear and also non-autonomous, i.e. time variant. Special cases occur when the problem is linear, i.e. $\mathbf{f}(\mathbf{x}, t) = \mathbf{A}(t)\mathbf{x}(t)$, or even periodic, i.e. linear with $\mathbf{A}(t + T) = \mathbf{A}(t)$ for a given constant T, $\forall t$. Autonomous problems arise when $\mathbf{f}(\mathbf{x})$ does not explicitly depend on time t; a special case occurs when the problem is linear, i.e. $\mathbf{f}(\mathbf{x}) = \mathbf{A}\mathbf{x}$. Although, irrespective of the complexity and the structure of the mathematical representation, the decaying characteristics of state variables after a perturbation determine stability, the techniques of estimating the measures of stability properties differ.

Evaluating the stability of linear time invariant (LTI) systems is straightforward and can be simply computed using the well-known eigenvalue decomposition. In its current state, MASST can already extract the eigenvalues of a systems; in addition to that analytical sensitivity of LTI systems is formulated and explained in Section 2.8. On the other hand, as a next step, the stability of linear time periodic (LTP) systems can be added in order to increase this capacity of stability and sensitivity analysis. Floquet Theory is very convenient for this purpose, as it is a natural extension of eigenvalue analysis for LTP systems [57]. Then, stability of LTP systems are formulated based on the spectral analysis of LTP systems using Floquet Theory and described in Chapter 3. Although the eigenvalue method of LTI systems and Floquet solution of LTP systems are widely used in rotorcraft stability estimation and can represent the dynamics of many rotorcraft

problems; they imply simplifications when the system is nonlinear and a-periodic. Then, in order to further improve and generalize the stability analysis of rotorcraft; a method that can indicate the stability of solutions of nonlinear non-autonomous systems is required. Further expectations from this method should be: not to require simplifications, reference solutions and assumption of a period; and additionally to give the same results and interpretation with eigen-solution and Floquet method, when implied on LTI and LTP systems respectively. For this reason, quantitative stability of linear time periodic and nonlinear non-autonomous systems are formulated using Lyapunov Characteristic Exponents (LCEs) which are the indicators of the stability properties of solutions of differential equations [58]. Discrete QR decomposition is used to estimate these LCEs. Chapter 4 is dedicated to explain the mathematical backgrounds, addresses some of the issues and difficulties on a simple illustrative example.

In a dynamical system, especially in the design phase, the rate of change of stability estimates with respect to a parameter also plays a significant role if that parameter is expected to change or there is uncertainty in it. Such sensitivity is useful to gain insight into the dependence of stability indicators on system parameters, or can be integrated into gradient-based (or gradient-aware) optimization procedures [59] and continuation algorithms [60], or into uncertainty evaluation problems (See for example Refs. [61, 62] for rotorcraft related optimization problems and Ref. [63] for an aeroelastic tailoring example of a helicopter blade). A novel contribution of this work is the development of analytical sensitivity estimations instead of finite-differences to avoid issues related to sharp changes in sensitivity parameters and to gain the possibility to detect such changes, in order to detect topology changes of the solution and track them using continuation algorithms. Detecting Hopf bifurcation is an example to such a topology change in which the real part of the critical characteristic exponents, have non-zero sensitivity at critical parameter [64]. Estimation of stability properties for LTI, LTP and nonlinear non-autonomous systems are described and formulated in the relevant sections of Chapters 2, 3 and 4 respectively.

In order to verify and illustrate the tools and methods, numerical examples are provided in Chapter 5. The analyses include parametric stability and sensitivity of LTP and nonlinear non-autonomous rotorcraft systems. Finally, Chapter 6 states the concluding remarks and addresses possible extensions to this work.

CHAPTER 2

Aeroelastic Rotor Model

2.1 Introduction

A linear time invariant (LTI) aeroelastic rotor model is the fundamental tool in the stability analysis of rotorcraft and provides a basis for the generalized aeroservoelastic stability analysis. Strictly speaking, the equations of motions governing the rotorcraft aeroelasticity is nonlinear [65]. However, linearizing a system is sometimes necessary and can be advantageous if properly done. First of all, there is great literature and vast number of linear tools in structural dynamics, aerodynamics and control fields, which are more robust, easy to implement and cost efficient as compared to nonlinear formulations. Second, sometimes nonlinear effects may not be mathematically representable or globally significant to some extent. Third, there cannot be enough information about the exact nonlinear behavior. Moreover, nonlinearity can be isolated from the rest of the linear model, hence the linear subcomponents may not require more sophisticated models. Under these circumstances, depending on the characteristics of the nonlinearity, the nonlinear terms are either completely ignored as usually done in stability analysis or that system is considered as a linear

but uncertain system [66].

The methods that widens the aeroservoelastic stability analysis are presented in next chapters. Stability and sensitivity of periodic systems is described in Chapter 3 while stability and sensitivity of nonlinear non-autonomous rotorcraft systems is investigated Chapter 4. The rotorcraft related illustrations are given in Chapter 5. This chapter is devoted completely to the linear time periodic aeroelastic rotor model. Integration with an aeroservoelastic tool MASST is an important objective; hence, current MASST version is briefly presented in Section 2.2 first. Section 2.3 formulates the elastic blade behavior. Boundary conditions, hinge connection and one dimensional rod and damper elements are presented in Section 2.4. The external loads are described in Section 2.5 which includes inertial and aerodynamic forces and moments, their integration and transformation. Section 2.6 summarizes the steady state solution of equations of motion. The transformation between rotating and non-rotating reference frames is described in Section 2.7. The analytical estimation of the sensitivity of LTI systems is formulated in Section 2.8. Finally, the verification problems are provided in Section 2.9 in order to present the soundness of the approach.

2.2 MASST Aeroservoelastic Analysis Platform

Prior to this work, a simulation tool named MASST (Modern Aeroservoelastic State Space Tools) was developed at Politecnico di Milano for the aeroservoelastic and aeromechanical analysis of aircraft and rotorcraft (Refs. [52], [53]). MASST analyzes compact yet complete modular models of complex linearized aeroservoelastic systems. Models are composed of subcomponents collected from well-known, reliable and possibly state-of-the-art sources and blended together in a mathematical environment. The problem is formulated in state-space form. This approach is often termed modern in the automatic control community. The equations of motion of the system are cast as first order time differential equations. As a consequence, generic state-space approaches can be used to analyze aeroelastic systems. MASST has been designed to be modular and to incorporate heterogeneous subcomponents from different sources to model:

- deformable aircraft structural dynamics
- airframe unsteady aerodynamics
- rotor aeroelasticity

- drive train dynamics
- servoactuators dynamics
- sensors and filters dynamics
- (Automatic) Flight Control System (FCS)
- pilot biomechanics

When these elements are combined, they provide a powerful and flexible closed loop aeroservoelastic modeling capability. Each component is modeled in its most natural and appropriate modeling environment and then cast into state-space form. Substructures are connected using the Craig- Bampton Component Mode Synthesis (CMS) approach [67].

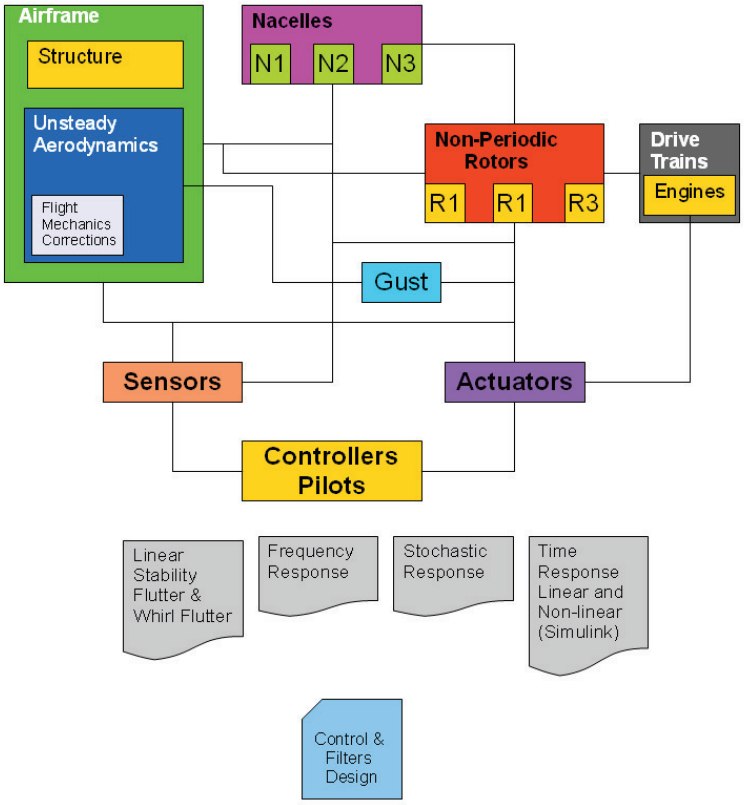

Figure 2.1: *Block diagram of the different elements that can participate in a MASST model.*

Fig. 2.1 gives the analysis boundaries of current version of MASST. The rotor matrices are obtained from external sources and they are expected to be non-periodic. However, rotor is the most critical and complicated part of a rotorcraft; very few tools are available with some of them are completely nonlinear thus too complicated for stability analysis while very few of them have free licenses. Then, in order to free MASST from external rotor sources with the flexibility to extend the modeling capability from linear time invariant to nonlinear non-autonomous system and perform parametric sensitivity analysis; an aeroelastic rotor model is essential. This is done by formulating the aeroelastic model of a rotating beam with hub motion, describing the necessary transformations from aerodynamic to structural domains and from rotating to non-rotating frames, adding flexibility in aerodynamic modeling and developing linear time periodic and nonlinear non-autonomous stability and sensitivity formulations.

2.3 Formulation of Elastic Rotor Blades

The elastic behavior of helicopter rotor blades has been formulated in literature for different levels of complexities. For example, see Ref. [68–70] for the derivation of linear and nonlinear equations. Analytical solution is not possible unless the problem is reduced to its simplest form, which is usually inaccurate for most of the problems. Among numerical methods, Finite Element Method has been extensively used (See Refs. [71–73]). A modern approach is Finite Volume concept, which is based on the direct balance of forces and moments on a finite volume of solid rather than using the weak formulation of strain energy. One can find an analogy with finite volume method in CFD, specifically the node-centered form. The finite volume formulation of Ref. [74] is implemented in this work to obtain the structural dynamics representation of linearized rotating C^0 beams, which is also proven to be shear-lock free. This method is also used in MBDyn[1] Multibody Dynamics Code with its nonlinear version.

The beam is discretized using 3 node elements, each node possessing 3 translational 3 rotational degrees of freedom. For a rotating beam

[1]MBDyn is a general purpose Multibody Dynamics analysis software. It was developed at the "Dipartimento di Scienze e Tecnologie Aerospaziali of the University Politecnico di Milano, Italy". MBDyn features the integrated multidisciplinary simulation of multibody, multiphysics systems, including nonlinear mechanics of rigid and flexible bodies subjected to kinematic constraints, along with smart materials, electric networks, active control, hydraulic networks, and essential fixed-wing and rotorcraft aerodynamics. See Ref [51] for more details, theory and illustrations.

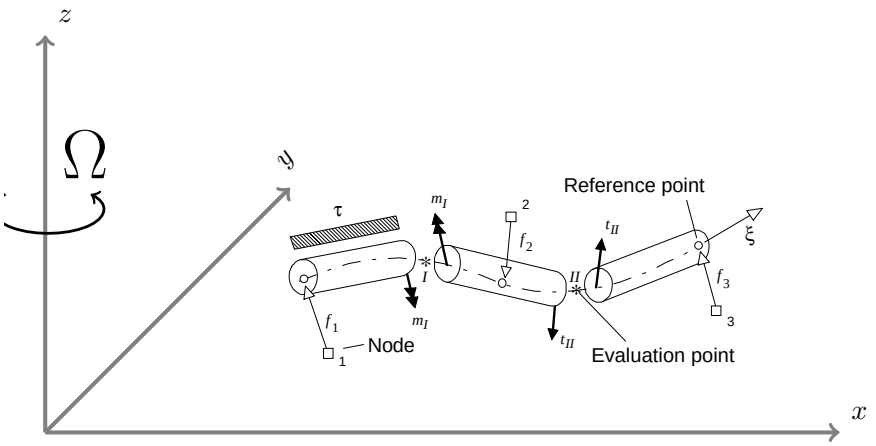

Figure 2.2: *3-node Beam element in blade reference frame : The degrees of freedom of the blade element is defined and external loads are applied at its 3 nodes, whereas strains and internal loads are evaluated at 2 evaluation points*

element, the equilibrium of internal forces at 2 internal points and external forces at the 3 nodes are written and linearized. The internal loads are related to the internal strains using a 6×6 stiffness matrix. Then, the linearized strain terms are written as a function of node degrees of freedom using interpolation polynomials.

2.3.1 Beam Discretization

The 3-node beam element is given in Fig. 2.2. The longitudinal axis is the blade axis extending radially outward, the vertical axis (z axis) is parallel to the rotation axis of the rotor and lateral axis y lies on the rotor plane perpendicular to radial and vertical axes. In this chapter, this reference frame is referred to as *blade reference frame*. The nodes, with arab footers ($i = 1, 2, 3$), are the locations on the blade reference frame, where position ($\mathbf{p}$) and curvature ($\boldsymbol{\kappa}$) about three orthogonal axes are represented and external loads are applied; in other words they are the degrees of freedom of the mathematical model.

The reference plane, at which beam element lies and elastic properties are defined is named as *material reference frame* and lies on a dimensionless coordinate ξ, given an orientation $\mathbf{R}$ and offset $\mathbf{f} = \mathbf{R}\tilde{\mathbf{f}}$ with respect to the blade reference frame; where the variables having an over-tilde ($\tilde{\bullet}$) represent a variable defined in a relative frame of reference, i.e the material reference frame. The strains and internal loads are computed at the evaluation points along the material

reference frame, which are represented by roman footers ($k = I, II$), as shown in Fig. 2.2. For this beam model, the evaluation points are located at material frame coordinates $\xi_I = -1/\sqrt{3}$ and $\xi_{II} = 1/\sqrt{3}$. These points are Gauss quadrature points for polynomials up to third order and they are proven to provide exact behavior for end applied nodes [74]. The position and the spatial derivative of a point on the beam reference line (ξ) as a function of the node variables are defined using second order polynomials ($N_j(\xi)$),

$$N_1(\xi) = \frac{\xi(\xi-1)}{2} \qquad N_2(\xi) = 1-\xi^2 \qquad N_3(\xi) = \frac{\xi(\xi+1)}{2} \tag{2.1}$$

where $\xi = -1, 0, 1$ are the points on local coordinate (ξ) corresponding to 3 nodes. Then, the position $\mathbf{p}(\xi)$ and curvature $\boldsymbol{\varphi}(\xi)$ and their derivatives along the line passing through the material reference frame (ξ) can be expressed as a linear combination of the corresponding values at the nodes, namely $\mathbf{p}_i$ and $\boldsymbol{\kappa}_i$:

$$\mathbf{p}(\xi) = N_i(\xi)\mathbf{p}_i \ , \ \mathbf{p}'(\xi) = N_i'(\xi)\mathbf{p}_i; \ \ i = 1,3 \tag{2.2a}$$
$$\boldsymbol{\kappa}(\xi) = N_i(\xi)\boldsymbol{\kappa}_i \ , \ \boldsymbol{\kappa}'(\xi) = N_i'(\xi)\boldsymbol{\varphi}_i; \ \ i = 1,3 \tag{2.2b}$$

2.3.2 Equilibrium Equation and Linearization

The rotating blade is discretized based on a C^0, i.e. Timoshenko, beam formulation, meaning that displacement and rotation are two separate fields [75]. The equation of beam can be stated as an equilibrium between the internal forces and moment ($\boldsymbol{\vartheta}$) and the distributed forces and moments ($\boldsymbol{\tau}$);

$$\boldsymbol{\vartheta}' - \mathbf{T}^T\boldsymbol{\vartheta} + \boldsymbol{\tau} = 0 \tag{2.3}$$

where derivative is evaluated with respect to beam reference line ξ and $\mathbf{T}^T$ is the arm matrix of internal forces:

$$\mathbf{T} = \begin{bmatrix} 0 & \mathbf{p}'\times \\ 0 & 0 \end{bmatrix} \tag{2.4}$$

The internal loads ($\boldsymbol{\vartheta} = [\boldsymbol{\vartheta}_I^T \ \boldsymbol{\vartheta}_{II}^T]^T$) evaluated at the evaluation points and the external loads ($\mathbf{F} = [\mathbf{F}_1^T \ \mathbf{F}_2^T \ \mathbf{F}_3^T]^T$) applied at node points are in equilibrium according to the formulation [74];

$$\mathbf{A}\boldsymbol{\vartheta} = \mathbf{F} \tag{2.5}$$

where $\mathbf{A}$ is the referred to as arms matrix obtained by integrating Eq. 2.3, which guarantees equilibrium between the external loads at the

nodes (marked with arab footers) and internal loads at the evaluation points (marked with roman footers):

$$\mathbf{A} = \begin{bmatrix} \mathbf{I} & \mathbf{0} & \mathbf{0} & \mathbf{0} \\ (\mathbf{p}_I - \mathbf{p}_1)\times & -\mathbf{I} & \mathbf{0} & \mathbf{0} \\ \mathbf{I} & \mathbf{0} & -\mathbf{I} & \mathbf{0} \\ -(\mathbf{p}_I - \mathbf{p}_2)\times & \mathbf{I} & (\mathbf{p}_{II} - \mathbf{p}_1)\times & -\mathbf{I} \\ \mathbf{0} & \mathbf{0} & \mathbf{I} & \mathbf{0} \\ \mathbf{0} & \mathbf{0} & -(\mathbf{p}_{II} - \mathbf{p}_3)\times & \mathbf{I} \end{bmatrix} \tag{2.6}$$

If perturbation is applied to Eq. 2.5,

$$\cancel{\mathbf{A}_0\boldsymbol{\vartheta}_0} + \mathbf{A}_0\delta\boldsymbol{\vartheta} + \delta\mathbf{A}\boldsymbol{\vartheta}_0 + \cancel{\delta\mathbf{A}\delta\boldsymbol{\vartheta}} = \cancel{\mathbf{F}_0} + \delta\mathbf{F} \tag{2.7}$$

leading to the linearized form,

$$\mathbf{A}_0\delta\boldsymbol{\vartheta} + \delta\mathbf{A}\boldsymbol{\vartheta}_0 = \delta\mathbf{F} \tag{2.8}$$

where terms with 0 subscript are reference conditions. Eq. 2.8 is the linearized equilibrium equation around a reference condition after neglecting higher order terms and canceling the reference condition. The term $\mathbf{A}_0\delta\boldsymbol{\vartheta}$ gives the perturbation of internal loads with an arms matrix at reference configuration whereas $\delta\mathbf{A}\boldsymbol{\vartheta}_0$ term is responsible for the stiffness contribution due to pre-stress of the beam element under reference centrifugal loads.

2.3.3 Linearization of Strain

In C^0 beam formulation, the strain vector $\boldsymbol{\psi}$ is composed of linear strain $\boldsymbol{\varepsilon}$ and angular strain $\boldsymbol{\kappa}$ which corresponds to the translation and rotation of the cross section respectively. In this study, the linearized forms for initially zero curvature beams are used.

Linear Strain

The linear strain in blade frame for a point with location $\mathbf{p}$ is the difference between the final and initial states:

$$\boldsymbol{\varepsilon} = \mathbf{p}' - \mathbf{R}\mathbf{p}_0' \tag{2.9}$$

where $\mathbf{R}$ is the rotation matrix from initial configuration to the final one, $\mathbf{p}_0$ is the strain in reference condition and $()'$ indicates spatial derivative with respect to reference line. The zero index $()_0$, from now

on, is used for reference condition unless otherwise stated. Linearizing the strain relation gives:

$$\delta\boldsymbol{\varepsilon} = \delta\mathbf{p}' - \delta\mathbf{R}\mathbf{p}_0' \tag{2.10}$$

On the other hand, for any matrix satisfying orthogonal rotation property, it can be proved that:

$$\delta\mathbf{R} = \delta\boldsymbol{\theta} \times \mathbf{R}_0 \;\; \delta\mathbf{R}^T = -\mathbf{R}_0^T \delta\boldsymbol{\theta}\times \tag{2.11}$$

where $\delta\boldsymbol{\theta}$ represents the vector of the perturbation angles of the node. Then dropping δ by replacing $\delta\mathbf{p}$ and $\delta\boldsymbol{\theta}$ with variables $\mathbf{x}$ and $\boldsymbol{\varphi}$, the linearized strain is obtained as:

$$\delta\boldsymbol{\varepsilon} = \mathbf{x}' + \mathbf{p}_0' \times \boldsymbol{\varphi} \tag{2.12}$$

Angular strain

Similarly the curvature ($\boldsymbol{\kappa}$) in the node frame can be stated as the difference between final and initial curvatures,

$$\boldsymbol{\kappa} = \boldsymbol{\rho} - \mathbf{R}\boldsymbol{\rho}_0 \tag{2.13}$$

where $\boldsymbol{\rho} = \mathbf{R}'\mathbf{R}^T$ is the actual curvature for the rotation matrix from initial configuration to the final one, namely $\mathbf{R}$. Considering that $\delta\boldsymbol{\rho}_0$ is by definition zero, linearizing gives,

$$\delta\boldsymbol{\kappa} = \delta\boldsymbol{\rho} - \delta\mathbf{R}\boldsymbol{\rho}_0 = \delta\boldsymbol{\rho} - \boldsymbol{\varphi} \times \boldsymbol{\rho}_0 \tag{2.14}$$

since $\mathbf{R}_0\boldsymbol{\rho}_0 = \boldsymbol{\rho}_0$. The linearization of $\delta\boldsymbol{\rho}$ is not trivial. First linearize $\mathbf{R}'\mathbf{R}^T$:

$$\delta\boldsymbol{\rho}\times = \delta(\mathbf{R}'\mathbf{R}^T) = \delta\mathbf{R}'\mathbf{R}_0^T + \mathbf{R}_0'\delta\mathbf{R}^T \tag{2.15}$$

$\delta\mathbf{R}'$ needs to be explicitly written. Schwartz's Theorem is applicable to rotation matrix, then the sequence of perturbation and derivative can be altered which leads to;

$$\delta\mathbf{R}' = (\delta\mathbf{R})' = (\boldsymbol{\varphi} \times \mathbf{R}_0)' = \boldsymbol{\varphi}' \times \mathbf{R}_0' + \boldsymbol{\varphi} \times \mathbf{R}_0' \tag{2.16}$$

Considering that $\mathbf{R}_0\mathbf{R}_0^T = \mathbf{I}$ and $\mathbf{R}_0'\mathbf{R}_0^T = \boldsymbol{\rho}\times_0$, the term $\delta\boldsymbol{\rho}\times$ can be written as

$$\begin{aligned}\delta\boldsymbol{\rho}\times &= \boldsymbol{\varphi}' \times \mathbf{R}_0\mathbf{R}_0^T + \boldsymbol{\varphi} \times \mathbf{R}_0'\mathbf{R}_0^T - \mathbf{R}_0'\mathbf{R}_0^T\boldsymbol{\varphi}\times \\ &= \boldsymbol{\varphi}' \times + \boldsymbol{\varphi} \times \boldsymbol{\rho}_0 \times - \boldsymbol{\rho}_0 \times \boldsymbol{\varphi}\times\end{aligned} \tag{2.17}$$

The terms with double cross product should be treated to achieve further simplification, which can be done using Jacobi identity:

$$\mathbf{a} \times (\mathbf{b} \times \mathbf{c}) + \mathbf{b} \times (\mathbf{c} \times \mathbf{a}) + \mathbf{c} \times (\mathbf{a} \times \mathbf{b}) = 0 \tag{2.18}$$

Applying Jacobi identity to terms with double cross product term of Eq. 2.17 needs right multiplication with a dummy vector $\mathbf{w}$. Then, using anti-commutative property of cross product and Jacobi identity with $\mathbf{a} = \boldsymbol{\varphi}$, $\mathbf{b} = \boldsymbol{\rho}$, $\mathbf{a} = \mathbf{v}$:

$$\begin{aligned}
&(\delta\boldsymbol{\rho} \times -\boldsymbol{\varphi}'\times)\mathbf{w} = \boldsymbol{\varphi} \times \boldsymbol{\rho}_0 \times \mathbf{w} - \boldsymbol{\rho}_0 \times \boldsymbol{\varphi} \times \mathbf{w} \\
&(\delta\boldsymbol{\rho} - \boldsymbol{\varphi}') \times \mathbf{w} = \boldsymbol{\varphi} \times \boldsymbol{\rho}_0 \times \mathbf{w} + \boldsymbol{\rho}_0 \times \mathbf{w} \times \boldsymbol{\varphi} = -\mathbf{w} \times (\boldsymbol{\varphi} \times \boldsymbol{\rho}_0) \\
&(\delta\boldsymbol{\rho} - \boldsymbol{\varphi}') \times \mathbf{w} = (\boldsymbol{\varphi} \times \boldsymbol{\rho}_0) \times \mathbf{w}
\end{aligned} \tag{2.19}$$

Then the dummy vector $\mathbf{w}$ and cross product operation can be dropped:

$$\delta\boldsymbol{\rho} = \boldsymbol{\varphi}' + \boldsymbol{\varphi} \times \boldsymbol{\rho}_0 \tag{2.20}$$

Inserting Eq. 2.20 into Eq. 2.14, terms with cross products cancel:

$$\delta\boldsymbol{\kappa} = \boldsymbol{\varphi}' + \cancel{\boldsymbol{\varphi} \times \boldsymbol{\rho}_0} - \cancel{\boldsymbol{\varphi} \times \boldsymbol{\rho}_0} \tag{2.21}$$

Finally the linearized form of angular strain can be stated as a first order derivative of perturbation angle:

$$\delta\boldsymbol{\kappa} = \boldsymbol{\varphi}' \tag{2.22}$$

2.3.4 Perturbation of Internal Loads

It is more convenient to represent constitutive law in the material reference frame. Then, a transformation between blade and material reference frames is required. The internal forces can be expressed in blade frame as;

$$\boldsymbol{\vartheta} = \boldsymbol{\mathcal{D}}\boldsymbol{\psi} = \boldsymbol{\mathcal{R}}\tilde{\boldsymbol{\mathcal{D}}}\boldsymbol{\mathcal{R}}^T\boldsymbol{\psi} \tag{2.23}$$

where $\boldsymbol{\mathcal{R}}$ and $\tilde{\boldsymbol{\mathcal{D}}}$ are the rotation and constitutive law matrices having the contributions from two evaluation points and similarly $\boldsymbol{\vartheta}$ and $\boldsymbol{\psi}$ are the internal load and strain vectors at the evaluation points,

$$\boldsymbol{\mathcal{R}} = diag([\mathbf{R}_I \;\; \mathbf{R}_I \;\; \mathbf{R}_{II} \;\; \mathbf{R}_{II}]) \;\; , \;\; \tilde{\boldsymbol{\mathcal{D}}} = diag([\tilde{\mathbf{D}}_I \;\; \tilde{\mathbf{D}}_{II}]) \tag{2.24a}$$

$$\boldsymbol{\vartheta} = [\boldsymbol{\vartheta}_I^T \;\; \boldsymbol{\vartheta}_{II}^T]^T \;\; , \;\; \boldsymbol{\psi} = [\boldsymbol{\psi}_I^T \;\; \boldsymbol{\psi}_{II}^T]^T \tag{2.24b}$$

which enables to input the constitutive law in using an arbitrary set of coordinates with prescribed rotation matrices. Using updated Lagrangian approach, i.e. preserving reference loads, the perturbation of

internal loads $\boldsymbol{\vartheta}$ is;

$$\delta\boldsymbol{\vartheta} = \delta\boldsymbol{\mathcal{R}}\tilde{\boldsymbol{\mathcal{D}}}\boldsymbol{\mathcal{R}}_0^T\boldsymbol{\psi}_0 + \boldsymbol{\mathcal{R}}_0\tilde{\boldsymbol{\mathcal{D}}}\boldsymbol{\mathcal{R}}^T\delta\boldsymbol{\psi} \tag{2.25}$$

where terms with 0 index represents reference conditions. Remembering that $\delta\mathbf{R} = \boldsymbol{\varphi}\times\mathbf{R}_0$ and $\delta\mathbf{R}^T = \mathbf{R}_0^T\boldsymbol{\varphi}\times$, for a rotation matrix $\mathbf{R}$ and corresponding linearized rotation angle $\boldsymbol{\varphi}$, Eq. 2.25 is rearranged as,

$$\delta\boldsymbol{\vartheta} = -\boldsymbol{\vartheta}_0\times\boldsymbol{\varphi} + \boldsymbol{\mathcal{R}}_0\boldsymbol{\mathcal{D}}\boldsymbol{\mathcal{R}}_0^T\delta\boldsymbol{\psi} \tag{2.26}$$

where $\boldsymbol{\vartheta}_0$ and $\boldsymbol{\psi_0}$ are the reference internal forces and strains and $\times$ represents the matrix from of a vector product operation as before. Considering that the magnitude of centrifugal loads are significantly higher then that of other forms of external loads in a typical rotor blade; only tension forces due to rotation ($\mathbf{t_0}$) at evaluation points are considered as reference internal loads. Finally, $\delta\boldsymbol{\psi}$ can be written as a summation over node variables ($i = 1, 3$) using shape functions and linearized strain for the perturbation variables $\mathbf{x}_i$ and $\boldsymbol{\varphi}_i$,

$$\delta\boldsymbol{\psi} = \begin{bmatrix}\delta\boldsymbol{\varepsilon}_I\\ \delta\boldsymbol{\kappa}_I\\ \delta\boldsymbol{\varepsilon}_{II}\\ \delta\boldsymbol{\kappa}_{II}\end{bmatrix} = \sum_{i=1}^{3}\begin{bmatrix} N'_{Ii}\mathbf{I} & \mathbf{p}'_{0I}\times N_{Ii} - N'_{Ii}\mathbf{f}_i\times\\ 0 & N'_{I,i}\mathbf{I}\\ N'_{IIi}\mathbf{I} & \mathbf{p}'_{0I}\times N_{IIi} - N'_{IIi}\mathbf{f}_i\\ 0 & N'_{IIi}\mathbf{I}\end{bmatrix}\begin{bmatrix}\mathbf{x}_i\\ \boldsymbol{\varphi}_i\end{bmatrix} \tag{2.27}$$

with $\mathbf{f} = \mathbf{R}\tilde{\mathbf{f}}$, where $\tilde{\mathbf{f}}$ is the offset of the material frame from blade reference frame.

2.3.5 Constitutive Law

The internal loads $\tilde{\boldsymbol{\vartheta}}$ are related to strains $\tilde{\boldsymbol{\psi}}$ by a linear elastic constitutive law in material reference frame $\tilde{\boldsymbol{\vartheta}}_k = \tilde{\mathbf{D}}_k\tilde{\boldsymbol{\psi}}_k$ at two evaluation points $\xi_{I,II} = -1/\sqrt{3}, 1/\sqrt{3}$. For example, the 6×6 material matrix $\tilde{\mathbf{D}}$ for an isotropic cross section with double symmetry about its principal axis has the following form;

$$\tilde{\mathbf{D}} = \begin{bmatrix} EA & 0 & 0 & 0 & 0 & 0\\ 0 & GA_y & 0 & 0 & 0 & 0\\ 0 & 0 & GA_z & 0 & 0 & 0\\ 0 & 0 & 0 & GJ & 0 & 0\\ 0 & 0 & 0 & 0 & EI_y & 0\\ 0 & 0 & 0 & 0 & 0 & EI_z\end{bmatrix} \tag{2.28}$$

where EA is the axial stiffness, GA_y and GA_z are the shear stiffness about principal axes, GJ is the torsional stiffness, EJ_y and EJ_z are the bending stiffnesses about bending principal axes. For an orthotropic cross section, $\tilde{\mathbf{D}}$ can be fully populated. In general, accurate beam constitutive properties for non-homogeneous and anisotropic sections can be formulated using the approach originally proposed in Ref. [76].

2.3.6 Stiffness contribution due to pre-stress

The $\delta\mathbf{A}\boldsymbol{\vartheta}_\mathbf{0}$ term in Eq. 2.8 represent the geometric effect of reference loads on the response of the beam. In the case of a rotor blade, significant tension field results from the rotation at high speed and dominates the dynamics. The linearization of arms matrix $\mathbf{A}$ comes from Eq. 2.6 by perturbing the variables $\mathbf{p}$. This matrix is multiplied by tension due to centrifugal loads. Without going into detail, collecting the variables as a right hand side vector, the stiffness contribution due to pre-stress can be obtained as a summation over the perturbation node variables $\mathbf{x}_i$ and $\boldsymbol{\varphi}_i$ $(i = 1, 3)$ as;

$$\delta\mathbf{A}\boldsymbol{\vartheta}_0 = \sum_{i=1}^{3} \begin{bmatrix} \mathbf{0} & \mathbf{0} \\ \mathbf{t}_{I0} \times (N_{Ii} - \delta_{i1}) & -\mathbf{t}_{I0} \times N_{Ii}\mathbf{f}_i\times \\ \mathbf{0} & \mathbf{0} \\ \begin{pmatrix} -\mathbf{t}_{I0} \times (N_{Ii} - \delta_{i2}) \\ +\mathbf{t}_{II0} \times (N_{IIi} - \delta_{i2}) \end{pmatrix} & \begin{pmatrix} \mathbf{t}_{I0} \times N_{Ii}\mathbf{f}_i\times \\ -\mathbf{t}_{II0} \times N_{IIi}\mathbf{f}_i\times \end{pmatrix} \\ \mathbf{0} & \mathbf{0} \\ -\mathbf{t}_{II0} \times (N_{IIi} - \delta_{i3}) & \mathbf{t}_{II0} \times N_{IIi}\mathbf{f}_i\times \end{bmatrix} \begin{bmatrix} \mathbf{x}_i \\ \boldsymbol{\varphi}_i \end{bmatrix} \tag{2.29}$$

where δ_{ij} is the Kronecker delta operator.

2.4 Additional Elements

This section presents the elements that are frequently used in helicopter rotors. Within the scope of this work, displacement boundary conditions, a rod element and hinge connection is presented while the element library can be extended as a future work.

2.4.1 Displacement Boundary Conditions

The Boundary Conditions are required when the blade or rotor connected to a ground support and translation and/or rotation is constraint at its some of the degrees of freedom. For this purpose, the

classical way of representing displacement boundary conditions of Finite Elements Method is used, by removing the constrained degrees of freedom from the matrices those govern the system. Possible types are clamped and hinged connections; the former prevents both translational and rotational degrees of freedom whereas the latter only constraints translation. This is a well-known concept in finite element analysis, thus skipped here. The details can be found in any finite element method book (For example see Refs. [77] and [78]) .

2.4.2 Rod with Offset

Rod is a one dimensional element that can be used in modeling control system links, springs and dampers. A rod is represented by two nodes and can carry load on its axial direction. Following the formulation given in Theory Manuel of MBDyn [51], the vector between nodes with position vectors $\mathbf{p}_1, \mathbf{p}_2$ and having offset from nodes $\mathbf{f}_1, \mathbf{f}_2$ can be defined as;

$$\mathbf{l} = \mathbf{p}_2 + \mathbf{f}_2 - \mathbf{p}_1 - \mathbf{f}_1 \tag{2.30}$$

with the scalar distance $l = \sqrt{\mathbf{l}^T \mathbf{l}}$. The strain and strain rate are:

$$\varepsilon = \frac{l}{l_0} - 1 \quad , \quad \dot{\varepsilon} = \frac{\dot{l}}{l_0} \tag{2.31}$$

where l_0 is the unstrained length of the rod. The time derivative of the distance vector can be written as;

$$\dot{\mathbf{l}} = \dot{\mathbf{p}}_2 + \boldsymbol{\omega}_2 \times \mathbf{f}_2 - \dot{\mathbf{p}}_1 - \boldsymbol{\omega}_1 \times \mathbf{f}_1 \tag{2.32}$$

where $\boldsymbol{\omega}$ is the angular velocity of the node. The axial force on rod is a function of strain and strain rate $f = f(\varepsilon, \dot{\varepsilon})$, which can also be converted into a function of displacement and displacement rate, $f = f(\mathbf{l}, \dot{\mathbf{l}})$. The force vector and distance vector should have the same direction for one dimensional rod element, then:

$$\mathbf{F} = \frac{\mathbf{l}}{l_0} f \tag{2.33}$$

Since no force field is assumed within the element, the forces at the two ends of the rod are equal in magnitude with opposite directions and

the moments are simply cross product of the forces with the offsets,

$$\begin{bmatrix} \mathbf{F}_1 \\ \mathbf{M}_1 \\ \mathbf{F}_2 \\ \mathbf{M}_2 \end{bmatrix} = \begin{bmatrix} -\mathbf{F} \\ -\mathbf{f}_1 \times \mathbf{F} \\ \mathbf{F} \\ \mathbf{f}_2 \times \mathbf{F} \end{bmatrix} \tag{2.34}$$

with their linearizations:

$$\begin{bmatrix} \delta\mathbf{F}_1 \\ \delta\mathbf{M}_1 \\ \delta\mathbf{F}_2 \\ \delta\mathbf{M}_2 \end{bmatrix} = \begin{bmatrix} -\delta\mathbf{F} \\ -\mathbf{f}_1 \times \delta\mathbf{F} \\ \delta\mathbf{F} \\ \mathbf{f}_2 \times \delta\mathbf{F} \end{bmatrix} \tag{2.35}$$

Linearizing the force vector acting on the rod gives;

$$\delta\mathbf{F} = \frac{f}{l}\left(\mathbf{I} - \frac{\mathbf{l}\mathbf{l}^T}{l^2}\right)\delta\mathbf{l} + \frac{\mathbf{l}}{l}\delta f \tag{2.36}$$

where the linearized axial force is determined as,

$$\delta f = \frac{\partial f}{\partial \varepsilon}\delta\varepsilon + \frac{\partial f}{\partial \dot{\varepsilon}}\delta\dot{\varepsilon} \tag{2.37}$$

with the linearization of strain and strain rate:

$$\delta\varepsilon = \frac{\delta l}{l_0} \quad \delta\dot{\varepsilon} = \frac{\delta \dot{l}}{l_0} \tag{2.38}$$

Then, the perturbation of the length of the rod and its rate of change are obtained as;

$$\delta l = \frac{1}{l}\mathbf{l}^T\delta\mathbf{l} \tag{2.39a}$$

$$\delta \dot{l} = \frac{\mathbf{l}^T}{l}\delta\dot{\mathbf{l}} + \frac{\dot{\mathbf{l}}^T}{l}\left(\mathbf{I} - \frac{\mathbf{l}\mathbf{l}^T}{l^2}\right)\delta\mathbf{l} \tag{2.39b}$$

Using the perturbation displacement $\mathbf{x}$ and rotation $\boldsymbol{\varphi}$ as before, the perturbation of distance and distance rate vectors are:

$$\delta\mathbf{l} = \mathbf{x}_2 + \mathbf{f}_2 \times \boldsymbol{\varphi}_2 - \mathbf{x}_1 - \mathbf{f}_1 \times \boldsymbol{\varphi}_1 \tag{2.40a}$$

$$\delta\dot{\mathbf{l}} = \dot{\mathbf{x}}_2 - \mathbf{f}_2 \times \boldsymbol{\omega}_2 - \boldsymbol{\omega}_2 \times \mathbf{f}_2 \times \boldsymbol{\varphi}_1 - \dot{\mathbf{x}}_1 - \mathbf{f}_1 \times \boldsymbol{\omega}_1 - \boldsymbol{\omega}_1 \times \mathbf{f}_1 \times \boldsymbol{\varphi}_1 \tag{2.40b}$$

If Eqs. 2.36 to 2.40 are combined, the perturbation force on the rod can be stated as;

$$\delta\mathbf{F} = \mathbf{K}_l\delta\mathbf{l} + \mathbf{K}_{\dot{l}}\delta\dot{\mathbf{l}} \tag{2.41}$$

where

$$\mathbf{K}_l = \frac{f}{l}\mathbf{I} + \left(\frac{1}{l^2 l_0}\frac{\partial f}{\partial \epsilon} - \frac{\dot{\epsilon}}{l^3}\frac{\partial f}{\partial \dot{\epsilon}} - \frac{f}{l^3}\right)\mathbf{l}^T\mathbf{l} + \frac{1}{l^2 l_0}\frac{\partial f}{\partial \dot{\epsilon}}\mathbf{l}^T\mathbf{l} \tag{2.42a}$$

$$\mathbf{K}_{\dot{l}} = \frac{1}{l^2 l_0}\frac{\partial f}{\partial \dot{\epsilon}}\mathbf{l}^T\mathbf{l} \tag{2.42b}$$

which can be used in Eq. 2.35 to represent forces and moments at the two nodes of the rod. The classical spring damper constants are given as:

$$k = \frac{1}{l_0}\frac{\partial f}{\partial \epsilon}, \quad c = \frac{1}{l_0}\frac{\partial f}{\partial \dot{\epsilon}} \tag{2.43}$$

2.4.3 Revolute Hinge

Hinges are widely used at the roots of blade: they allow flap, lead-lag motion to relieve moments at blade roots, thus rolling of the rotorcraft in forward flight is prevented; and provide rotation of the blade around pitch axis for inputting control commands. In order to represent free rotation around one axis, revolute hinge is formulated. In this study they are modeled by assigning a hinge in between two adjacent nodes and then canceling the common degrees of freedom while retaining the independent one. Now, supposing that a hinge is located between two beam elements, with indices n and m, then the equation for the relative motion can be stated as,

$$x_{m,i} = x_{n,i} \;\; i = 1, 3 \tag{2.44a}$$

$$\varphi_{m,i} = \varphi_{n,i} \;\; i \neq n_{rel} \tag{2.44b}$$

$$\varphi_{m,i} = \Delta\varphi_{n,i} + \varphi_{n,i} \;\; i = n_{rel} \tag{2.44c}$$

where n_{rel} is the relative rotation degree of freedom and i is the degrees of freedom of the nodes of two beams at the hinge connection. This means that, the three displacement and two rotation degrees of freedom at the hinge are equal, thus dependent, whereas there exist one independent rotation degree of freedom allowed by the hinge. In a regular connection of two nodes, the degrees of freedom of one node is equal to that of the other node, i.e. there are 6 independent degrees

of freedom out of 12 (2×6 from two nodes at the connecting node). However, when hinge is present between two nodes, relative motion should be guaranteed by preserving one additional rotation degree of freedom, thus there exist 7 independent degrees of freedom. If the degrees of freedom of the first node is preserved, the vector including independent variables can be written as:

$$\mathbf{q} = \begin{bmatrix} x_{m,1} & x_{m,2} & x_{m3} & \varphi_{m,1} & \varphi_{m,2} & \varphi_{m,3} & \varphi_{n,n_{rel}} \end{bmatrix}^T \tag{2.45}$$

When forming the global matrices, this relative degree of freedom can be preserved by multiplying the degrees of freedom with a reduction matrix. Assuming that the relative degree of freedom is around third axis and the degrees of freedom of node m is preserved, this procedure can be illustrated for the nodes (m) and (n) as;

$$\mathbf{q}_m = \boldsymbol{\mu}_{red,m}\mathbf{q} = \begin{bmatrix} x_{m,1} \\ x_{m,2} \\ x_{m,3} \\ \varphi_{m,1} \\ \varphi_{m,2} \\ \varphi_{m,3} \end{bmatrix} = \begin{bmatrix} 1 & 0 & 0 & 0 & 0 & 0 & 0 \\ 0 & 1 & 0 & 0 & 0 & 0 & 0 \\ 0 & 0 & 1 & 0 & 0 & 0 & 0 \\ 0 & 0 & 0 & 1 & 0 & 0 & 0 \\ 0 & 0 & 0 & 0 & 1 & 0 & 0 \\ 0 & 0 & 0 & 0 & 0 & 1 & 0 \end{bmatrix} \begin{bmatrix} x_{m,1} \\ x_{m,2} \\ x_{m,3} \\ \varphi_{m,1} \\ \varphi_{m,2} \\ \varphi_{m,3} \\ \varphi_{n,3} \end{bmatrix} \tag{2.46a}$$

$$\mathbf{q}_n = \boldsymbol{\mu}_{red,n}\mathbf{q} = \begin{bmatrix} x_{n,1} \\ x_{n,2} \\ x_{n,1} \\ \varphi_{n,1} \\ \varphi_{n,2} \\ \varphi_{n,3} \end{bmatrix} = \begin{bmatrix} 1 & 0 & 0 & 0 & 0 & 0 & 0 \\ 0 & 1 & 0 & 0 & 0 & 0 & 0 \\ 0 & 0 & 1 & 0 & 0 & 0 & 0 \\ 0 & 0 & 0 & 1 & 0 & 0 & 0 \\ 0 & 0 & 0 & 0 & 1 & 0 & 0 \\ 0 & 0 & 0 & 0 & 0 & 0 & 1 \end{bmatrix} \begin{bmatrix} x_{m,1} \\ x_{m,2} \\ x_{m,3} \\ \varphi_{m,1} \\ \varphi_{m,2} \\ \varphi_{m,3} \\ \varphi_{n,3} \end{bmatrix} \tag{2.46b}$$

where $\boldsymbol{\mu}_{red,m}$ and $\boldsymbol{\mu}_{red,n}$ are reduction matrices for the connecting nodes and can be modified according to the allowed rotation degree of freedom. Then the local mass and stiffness matrices, which are developed for each node, can be post-multiplied by these matrices to provide the additional independent degree of freedom while removing the depen-

dent ones:

$$\mathbf{K}_{red,m} = \mathbf{K}_m \boldsymbol{\mu}_{red,m} \quad \mathbf{M}_{red,m} = \mathbf{M}_m \boldsymbol{\mu}_{red,m} \tag{2.47a}$$

$$\mathbf{K}_{red,n} = \mathbf{K}_n \boldsymbol{\mu}_{red,n} \quad \mathbf{M}_{red,n} = \mathbf{M}_n \boldsymbol{\mu}_{red,n} \tag{2.47b}$$

and the stiffness matrices can be assembled in their locations in the global stiffness matrix.

2.5 External Loads

Recall Eq. 2.5, the equilibrium equation between internal and external loads:

$$\mathbf{A}\boldsymbol{\vartheta} = \mathbf{F} \tag{2.48}$$

The external loads are taken into account under the node applied forces and moments ($\mathbf{F}$). The application of inertial loads is presented in Section 2.5.1. The steady and perturbation aerodynamics are described in Section 2.5.2. The hub induced effects are explained in Section 2.5.3. The integration of section forces and moment is presented in Section 2.5.4. Finally, a formulation of aeroelastic coupling is provided in Section 2.5.5.

2.5.1 Inertial Loads

An exact representation of inertial loads requires integration over the beam element. However, using lumped mass and inertia gives enough accuracy without increasing computational work and preferred for this reason.

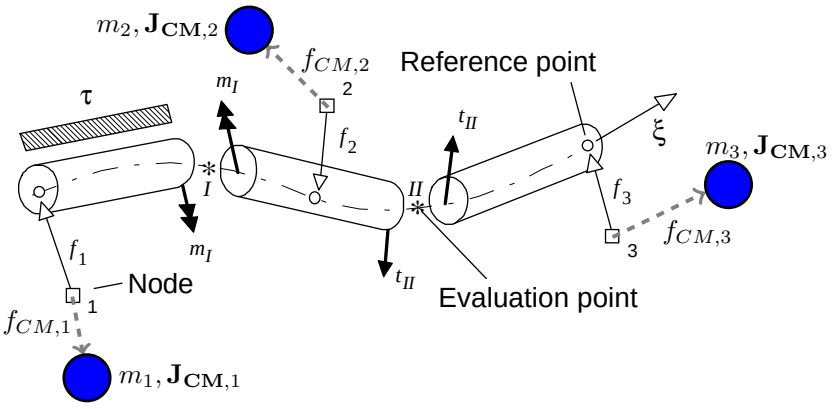

Figure 2.3: *Lumped mass and inertia*

Lumped Mass and Inertia in Rotating Frame

The mass and inertia distribution of the blade is discretized similar to that of elastic beam elements. As given in Fig. 2.3, the lumped mass m having a 3×3 inertia matrix $\mathbf{J_{CM}}$ are assigned to nodes with offsets $\mathbf{f_{CM}}$, which represents the inertial characteristics of the volume in the vicinity of the corresponding node. Then, the inertial force acting on a node can be represented as;

$$\mathbf{F_{in}} = -m\frac{d^2}{dt^2}(\mathbf{x} + \mathbf{f_{CM}}) \tag{2.49}$$

where the center of mass in blade reference frame is given as $\mathbf{f}_{CM} = \mathbf{R}\tilde{\mathbf{f}}_{\mathbf{CM}}$, with center of mass offset $\tilde{\mathbf{f}}_{\mathbf{CM}}$ given in material reference frame. The load in rotating reference frame can be expressed after differentiation as;

$$\mathbf{F_{in}} = -m(\ddot{\mathbf{x}} + \dot{\boldsymbol{\omega}} \times \mathbf{f_{CM}} + \boldsymbol{\omega} \times \boldsymbol{\omega} \times \mathbf{f_{CM}}) \tag{2.50}$$

where the term $\ddot{\mathbf{x}}$ and $\dot{\boldsymbol{\omega}} = \ddot{\boldsymbol{\varphi}}$ are the translational and rotational accelerations of the node represented in rotating reference frame. The higher order term $(\boldsymbol{\omega} \times \boldsymbol{\omega}\times)$ can be neglected since we deal with the perturbation displacement and rotations. For constant RPM, the inertial loads formula becomes:

$$\mathbf{F_{in}} = -m(\ddot{\mathbf{x}} - \mathbf{f_{CM}} \times \dot{\boldsymbol{\omega}}) = -m(\ddot{\mathbf{x}} + \mathbf{f_{CM}} \times^T \dot{\boldsymbol{\omega}}) \tag{2.51}$$

The moment at the node comes from two contributions. The first one is the derivative of angular momentum; the other one is the force contribution that originates from offset of center of mass, which can be written as,

$$\mathbf{M_{in}} = -\mathbf{J_{CM}}\dot{\boldsymbol{\omega}} - \boldsymbol{\omega} \times \mathbf{J_{CM}}\boldsymbol{\omega} + \mathbf{f_{CM}} \times \mathbf{F_{in}} \tag{2.52}$$

where $\mathbf{J_{CM}}$ is the inertia matrix at the center of mass. Inserting inertial force into above equation gives:

$$\mathbf{M_{in}} = -\mathbf{J_{CM}}\dot{\boldsymbol{\omega}} - \boldsymbol{\omega} \times \mathbf{J_{CM}}\boldsymbol{\omega} - m(\mathbf{f_{CM}} \times \ddot{\mathbf{x}} - \mathbf{f_{CM}} \times \mathbf{f_{CM}} \times \dot{\boldsymbol{\omega}}) \tag{2.53}$$

Following the same procedure that was applied to inertial force, neglecting higher order terms and defining inertia about node $\mathbf{J_n}$ as $\mathbf{J_n} = \mathbf{J_{CM}} + m\mathbf{f_{CM}} \times \mathbf{f_{CM}}\times^T$ leads to compact moment equation:

$$\mathbf{M_{in}} = -\mathbf{J_n}\dot{\boldsymbol{\omega}} - m\mathbf{f_{CM}} \times \ddot{\mathbf{x}} = -\mathbf{J_n}\dot{\omega} + m\mathbf{f_{CM}} \times^T \ddot{\mathbf{x}} \tag{2.54}$$

Remembering that for perturbation scales, the angular velocity is the time derivation of the rotation angle, i.e $\boldsymbol{\omega} = \dot{\boldsymbol{\varphi}}$ and collecting in matrix form yields perturbation force and moment due to inertia:

$$\begin{bmatrix} \mathbf{F_{in}} \\ \mathbf{M_{in}} \end{bmatrix} = - \begin{bmatrix} m\mathbf{I} & m\mathbf{f_{CM}}\times^T \\ m\mathbf{f_{CM}}\times & \mathbf{J_n} \end{bmatrix} \begin{bmatrix} \ddot{\mathbf{x}} \\ \ddot{\boldsymbol{\varphi}} \end{bmatrix} \tag{2.55}$$

Effect of Rotation

The lumped mass formulation in previous chapter is given for a mass in rotating reference frame, where $\ddot{\mathbf{x}}$ should be decomposed into its constituents. The transformation matrix from non-rotating reference frame variable $\mathbf{x}_{nr}$ to rotating reference frame variable $\mathbf{x}_r$ can be written as,

$$\mathbf{x}_{nr} = \mathbf{R}_\Omega \mathbf{x}_r \tag{2.56}$$

where $\mathbf{R_\Omega}$ is the transformation matrix from rotating to non-rotating reference frame. Differentiating once gives velocity in non rotating frame,

$$\dot{\mathbf{x}}_{nr} = \boldsymbol{\Omega} \times \mathbf{R}_\Omega \mathbf{x}_r + \mathbf{R_\Omega} \dot{\mathbf{x}}_r \tag{2.57}$$

where derivative of orientation vector for a rotating frame is $\dot{\mathbf{R}} = \boldsymbol{\Omega} \times \mathbf{R}$. Differentiating once more gives acceleration in non rotating frame:

$$\ddot{\mathbf{x}}_{nr} = (\dot{\boldsymbol{\Omega}} + \boldsymbol{\Omega} \times \boldsymbol{\Omega}\times)\mathbf{R}_\Omega \mathbf{x}_r + 2\boldsymbol{\Omega} \times \mathbf{R}_\Omega \dot{\mathbf{x}}_r + \mathbf{R}_\Omega \ddot{\mathbf{x}}_r \tag{2.58}$$

The acceleration in non-rotating reference frame is required to be projected on the rotating frame, in which loads acting on beam elements are expressed. Considering the orthogonality of the rotation matrix, i.e. $\mathbf{R}\mathbf{R}^T = \mathbf{I}$; when Eq. 2.58 is pre-multiplied by $\mathbf{R}_\Omega^T$, the acceleration projected to rotating reference frame becomes:

$$\mathbf{R}_\Omega^T \ddot{\mathbf{x}}_{nr} = (\mathbf{R}_\Omega^T \dot{\boldsymbol{\Omega}} \times \mathbf{R}_\Omega + \mathbf{R}_\Omega^T \boldsymbol{\Omega} \times \boldsymbol{\Omega} \times \mathbf{R}_\Omega)\mathbf{x}_r + 2\mathbf{R}_\Omega^T \boldsymbol{\Omega} \times \mathbf{R}_\Omega \dot{\mathbf{x}}_r + \mathbf{R}_\Omega^T \mathbf{R}_\Omega \ddot{\mathbf{x}}_r \tag{2.59}$$

Since $\mathbf{R}_\Omega$ is the rotation matrix caused by the angular velocity $\boldsymbol{\Omega}$ about a single axis: $\mathbf{R}_\Omega \boldsymbol{\Omega} = \boldsymbol{\Omega}$, $\mathbf{R}_\Omega^T \boldsymbol{\Omega} = \boldsymbol{\Omega}$ and $\mathbf{R}_\Omega^T \boldsymbol{\Omega} \times \mathbf{R}_\Omega = (\mathbf{R}_\Omega^T \boldsymbol{\Omega})\times$. Then the acceleration projected on rotating reference frame can be simplified as,

$$\mathbf{R}_\Omega^T \ddot{\mathbf{x}}_{nr} = (\dot{\boldsymbol{\Omega}} \times + \boldsymbol{\Omega} \times \boldsymbol{\Omega}\times)\mathbf{x}_r + 2\boldsymbol{\Omega} \times \dot{\mathbf{x}}_r + \ddot{\mathbf{x}}_r \tag{2.60}$$

which gives the explicit form of $\ddot{\mathbf{x}}$ term in Eq. 2.55.

The $\mathbf{\Omega} \times \mathbf{\Omega} \times \mathbf{x}$ term in Eq. 2.60 is the perturbation of the centrifugal force acting on the blade sections. The perturbation due to this term gives additional important term in rotor dynamics:

$$\mathbf{F_{ds}} = -m\mathbf{\Omega} \times \mathbf{\Omega} \times \mathbf{x} \tag{2.61}$$

In order to show the effect, assume that the rotor is rotating around z axis, i.e. $\mathbf{\Omega} = [0 \;\; 0 \;\; \Omega_z]^T$, and the perturbations of node in x, y and z directions, given in the rotating reference frame, can be stated as $\mathbf{x} = [\delta u \;\; \delta v \;\; \delta w]^T$ in radial, chordwise and flapwise directions. The perturbation in radial direction direction δu can be neglected since external perturbation loads in that direction is negligible as compared to the other two directions. Then the simplified form of the equation can be written as:

$$\mathbf{F_{ds}} = [0 \;\; m\Omega_z^2 \delta v \;\; 0]^T \tag{2.62}$$

The effect of this force, which is mainly in the lead lag direction, is referred to as destabilization force since as opposed to Eq. 2.55, the sign is positive therefore adds energy into the system.

The $2\mathbf{\Omega} \times \dot{\mathbf{x}}_r$ term in Eq. 2.60 represents a characteristic term of rotor dynamics. The perturbation force due to this term is named as Coriolis Forces and causes coupling between flapping and lead-lag motions:

$$\mathbf{F_{cor}} = -m2\mathbf{\Omega} \times \dot{\mathbf{x}} \tag{2.63}$$

2.5.2 Aerodynamics

In this section the way of representing aerodynamics on a rotating blade is described. Since, the content is broadly available in literature, details are skipped; the explanations related to aerodynamic loading is brief and interested reader can find more in any rotorcraft aerodynamics book such as Refs. [79, 80]. Moreover, it should also be noted that aerodynamics is formulated to provide a basis for the aerodynamic terms for the stability analysis and is open to development.

Blade Element Momentum Theory is used in order to formulate steady aerodynamic loads with addition of some basic inflow models. The steady and perturbation aerodynamic matrices are obtained. The transformation between aerodynamic and structural reference frames are described.

Steady Aerodynamics

The blade tangential (U_T), perpendicular (U_P) and radial (U_R) velocity components, considering the sign convention of this study, can be written as,

$$\frac{U_T}{\Omega R} = (r + \mu \sin\psi) \tag{2.64a}$$

$$\frac{U_P}{\Omega R} = (\lambda + \frac{r\dot{\beta}}{\Omega} + \mu\beta\cos\psi) = (\lambda + \frac{\dot{x}_p(r)}{\Omega R\cos\beta} + \mu\frac{x_p(r)}{rR}\cos\psi) \tag{2.64b}$$

$$\frac{U_R}{\Omega R} = \mu\cos\psi \tag{2.64c}$$

where λ is the non-dimensional inflow, r is the non-dimensional radial coordinate and μ is the ratio between the helicopter forward velocity and the blade tip velocity in hover, so called the advance ratio. β is the flapping angle which can also be replaced by $x_p(r)/rR\cos\beta$ considering sign convention of the blade structural dynamics formulation as given in Fig. 2.2, where here x_p being the component of blade motion that is perpendicular to rotor plane. Since, β is close to zero under normal rotor operation, $\cos\beta$ can be set to 1. For 2D aerodynamics the section lift (dL), drag (dD) and moment (dM) per unit span are written as,

$$dL = \frac{1}{2}\rho U^2 c C_l(\alpha) \tag{2.65a}$$

$$dD = \frac{1}{2}\rho U^2 c C_d(\alpha) \tag{2.65b}$$

$$dM = \frac{1}{2}\rho U^2 c C_m(\alpha) \tag{2.65c}$$

with $U = \sqrt{U_T^2 + U_P^2}$ is the magnitude of the speed of the flow advanced by the leading edge of the section, c is the chord length and α is the angle of attack. The angle of attack is a function of section geometric angle, θ, and induced angle: ϕ,

$$\alpha = \theta - \phi = \theta - \tan^{-1}(U_p/U_T) \tag{2.66}$$

The angles θ and ϕ are defined as,

$$\theta = \theta_{control} + \theta_{twist} + \theta_{elastic} \tag{2.67a}$$

$$\phi = \tan^{-1}(U_p/U_T) \tag{2.67b}$$

where $\theta_{control}$ is the control input to the blade, θ_{twist} is the geometric twist angle and $\theta_{elastic}$ is the elastic rotation of the blade around its

pitch axis due to the blade and control systems stiffness. Then the section forces and moments in rotor plane can be expressed as:

$$dF_z = dL\cos\phi - dD\sin\phi \tag{2.68a}$$
$$dF_y = dL\sin\phi + dD\cos\phi \tag{2.68b}$$
$$dM = dM \tag{2.68c}$$

These loads are expressed over the span of the blade and transformed to structural reference frame using the method proposed in Section 2.5.5.

Inflow Models

In this study, some basic inflow models are used. Here the formulas are provided for non-dimensional inflow ratio λ.

Hover Inflow Model: For hover, inflow distribution is modeled using Prandtl's tip-loss function as given in Ref. [10], which can be expressed using a correction factor F;

$$F = (2/\pi)\cos^{-1}(\mathrm{e}^{-f}) \tag{2.69}$$

where f is a function of radial coordinate r and number of blades N_b;

$$f = N_b(1-r)/2r\phi \tag{2.70}$$

and $\phi = \lambda(r)/r$ is the induced inflow angle at station r. Then, the quadratic equation is written as;

$$\lambda(r) = \frac{\sigma Cl_\alpha}{16F}\left(\sqrt{1+\frac{32F}{\sigma Cl_\alpha}\theta r}-1\right) \tag{2.71}$$

where Cl_α is the lift curve slope and θ is the blade pitch angle, $\sigma = N_b c_{mean}/\pi R$ is the rotor solidity for mean chord length c_{mean}. Fixed point iteration usually converges after few steps.

Forward Flight Uniform Inflow Model: The expression for the uniform inflow in forward flight is;

$$\lambda = \mu_x\tan\alpha_d + \frac{C_T}{2\sqrt{\mu_x+\lambda^2}} \tag{2.72}$$

where α_d is the rotor disc angle relative to the forward flight speed and $\mu_x = V_\infty\cos\alpha/\Omega R$ is the advance ratio parallel to the rotor disc. Again the solution is iterative,

$$\lambda_{n+1} = \mu_x\tan\alpha_d + \frac{C_T}{2\sqrt{\mu_x+\lambda_n^2}} \tag{2.73}$$

which can be solved using fixed point iteration or Newton-Raphson procedure. For the latter, the equation and its derivative with respect to the inflow λ are arranged as:

$$f(\lambda) = \lambda - \mu_x \tan\alpha_d - \frac{C_T}{2\sqrt{\mu_x + \lambda^2}} \tag{2.74a}$$

$$f'(\lambda) = 1 + \frac{C_T}{2}\sqrt{\mu_x + \lambda_n^2}^{-3/2}\lambda \tag{2.74b}$$

Then unknown λ can be iterated using:

$$\lambda_{n+1} = \lambda_n - \left[\frac{f(\lambda)}{f'(\lambda)}\right]_n \tag{2.75}$$

Forward Flight Linear Inflow Models: Using uniform inflow model as obtained in previous section, the inflow over rotor disc can be approximated using linear functions. For a forward variation;

$$\lambda_i = \lambda_0(1 + k_x \cos\psi) \tag{2.76}$$

where $k_x = 1.2$ is suggested by Glauert. A variation to Glauert is proposed by Drees which also include lateral variation;

$$\lambda_i = \lambda_0(1 + k_x \cos\psi + k_y \sin\psi) \tag{2.77}$$

where coefficients are given as;

$$k_x = \frac{4}{3}\left(\frac{1 - \cos X - 1.8\mu^2}{\sin X}\right) \;,\; k_y = -2\mu \tag{2.78}$$

with the wake skew angle X, defined as: $X = \tan^{-1}(\mu_x/(\mu_z + \lambda_i))$.

Forward Flight Mangler Squire Inflow Model: The inflow distribution is stated in Ref. [10] as;

$$\lambda_i = \frac{2C_T}{\mu}\left[\frac{c_0}{2} - \sum_{n=1}^{\infty} c_n(r, \alpha_d)\cos n\psi\right] \tag{2.79}$$

where ψ is the azimuthal angle, α_d id the rotor disc angle and r is the radial coordinate. Similar version is also proposed by Bramwell [22]:

$$\lambda_i = 4\lambda_0\left[\frac{c_0}{2} - \sum_{n=1}^{\infty} c_n(r, \alpha_d)\cos n\psi\right] \tag{2.80}$$

Bramwell version is preferred with only Type III loading. In Type III loading, the constants c_n are expressed in terms of non-dimensional radial coordinate r, disc flow angle α_d and a function of it $\eta = \sqrt{1-r^2}$. For $n = 0$;

$$c_0 = \frac{15}{8}\eta(1-\eta^2) \tag{2.81}$$

and for n is odd,

$$\begin{aligned} c_1 &= -\frac{15\pi}{256}(5-9\eta^2)\left[(1-\eta^2)\left(\frac{1-\sin\alpha_d}{1+\sin\alpha_d}\right)\right]^{1/2} \\ c_3 &= -\frac{45\pi}{256}\left[(1-\eta^2)\left(\frac{1-\sin\alpha_d}{1+\sin\alpha_d}\right)\right]^{3/2} \end{aligned} \tag{2.82}$$

where for n is odd and greater than 3, $c_n = 0$. For even values of n:

$$\begin{aligned} c_n =& (-1)^{n/2-1}\frac{15}{8}\left[\frac{\eta+n}{n^2-1}\frac{9\eta^2+n^2-6}{n^2-9}\right. \\ &\left. + \frac{3\eta}{n^2-9}\right]\left[\left(\frac{1-\eta}{1+\eta}\right)\left(\frac{1-\sin\alpha_d}{1+\sin\alpha_d}\right)\right]^{n/2} \end{aligned} \tag{2.83}$$

Perturbation Aerodynamics

The perturbation of aerodynamic forces are obtained by linearizing the nonlinear force and moment expressions given in Section 2.5.2. The motion of the blade sections are assumed to be small in magnitude and hence aerodynamic force and moment expressions are linearized for quasi-steady aerodynamics. As also noted in Section 2.5.2, this part of the work is developed to provide a sufficient level of complexity for aerodynamic stability terms and is open to improvement.

Perturbation of Lift Force: Lift force per unit span is,

$$L = \frac{1}{2}\rho c C_l(\alpha) U_T^2 \tag{2.84}$$

where all parameters have their conventional meaning as described in Section 2.5.2 and $U_T = \Omega R(r + \mu\sin\psi)$. Perturbing the equation with respect to the tangential velocity and the angle of attack gives:

$$\Delta L = \rho c U_T C_l(\alpha)\delta U_T + \frac{1}{2}\rho c C_{l\alpha} U_T^2 \delta\alpha \tag{2.85}$$

The perturbation of the tangential velocity is simply equal to the in-plane component of blade motion $\delta\dot{\mathbf{x}} = [\delta\dot{u} \;\; \delta\dot{v} \;\; \delta\dot{w}]^T$. Then:

$$\Delta U_T = \delta\dot{v} \tag{2.86}$$

The perturbation of angle of attack comes from perturbing Eq. 2.66, obtained by assuming $U_P \ll U_T$:

$$\Delta\alpha = \delta(\theta - \frac{U_P}{U_T}) = \delta\theta - \frac{\delta U_p}{U_T} \tag{2.87}$$

Neglecting the time dependency of inflow, the perturbation in vertical flow speed is obtained to be equal to the flap motion:

$$\delta U_P = \dot{w} \tag{2.88}$$

The perturbation in the section angle $\delta\theta$ is assumed to be only dependent on the elastic twist and control system flexibility. Then, perturbation lift force in terms of the rate of change of coordinates is:

$$\Delta L = \frac{1}{2}\rho c U_T^2 C_{l\alpha}\left(\frac{2C_l}{U_T C_{l\alpha}}\dot{v} + \delta\theta - \frac{\delta\dot{w}}{U_T}\right) \tag{2.89}$$

Perturbation of Drag Force: The drag force per unit span is:

$$D = \frac{1}{2}\rho c C_d(\alpha) U_T^2 \tag{2.90}$$

Perturbing the equation with respect to the tangential velocity and the angle of attack gives;

$$\Delta D = \rho c U_T C_d(\alpha)\delta U_T + \frac{1}{2}\rho c C_{d\alpha} U_T^2 \delta\alpha \tag{2.91}$$

and making use of Eqs. 2.86 and 2.87, we have:

$$\Delta D = \frac{1}{2}\rho c U_T^2 C_{d\alpha}\left(\frac{2C_d}{U_T C_{d\alpha}}\dot{v} + \delta\theta - \frac{\delta\dot{w}}{U_T}\right) \tag{2.92}$$

Perturbation of Pitching Moment: Pitching moment equation per unit span is;

$$M = \frac{1}{2}\rho c C_m(\alpha) U_T^2 + d_{AC} L \tag{2.93}$$

where d_{AC} is the distance of aerodynamic center from the reference axis of aerodynamics formulation. Perturbing the equation with respect to the tangential velocity and the angle of attack gives;

$$\Delta M = \rho c U_T C_m(\alpha)\delta U_T + \frac{1}{2}\rho c C_{m\alpha} U_T^2 \delta\alpha + d_{AC}\delta L \tag{2.94}$$

leading to:

$$\begin{aligned}\Delta M = &\frac{1}{2}\rho c U_T^2 C_{m\alpha}\left(\frac{2C_m}{U_T C_{m\alpha}}\dot{v} + \delta\theta - \frac{\delta\dot{w}}{U_T}\right)\\ &+ d_{AC}\frac{1}{2}\rho c U_T^2 C_{l\alpha}\left(\frac{2C_l}{U_T C_{l\alpha}}\dot{v} + \delta\theta - \frac{\delta\dot{w}}{U_T}\right)\end{aligned} \tag{2.95}$$

Rearranging the terms gives:

$$\begin{aligned}\Delta M = \frac{1}{2}\rho c U_T^2\Bigg(&\frac{2(C_m + d_{AC}C_l)}{U_T}\dot{v}\\ &+ (C_{m\alpha} + d_{AC}C_{l\alpha})\delta\theta - \frac{(C_{m\alpha} + d_{AC}C_{l\alpha})}{U_T}\delta\dot{w}\Bigg)\end{aligned} \tag{2.96}$$

2.5.3 Hub motion

Hub degrees of freedom in perturbation form is required to couple the motions originating from the rotor and the fuselage. The motion of the hub eventually induces motion on the blade and modifies aerodynamic and inertial matrices. The position of a point on a blade in non-rotating, i.e. stationary, reference frame $\mathbf{p}$ is a function of the hub motion $\mathbf{p}_H$ and the orientation of the blade with respect to non-rotating frame $\mathbf{R}$ times the position of that point on the blade $\tilde{\boldsymbol{\rho}}$ in rotating frame,

$$\mathbf{p} = \mathbf{p}_H + \mathbf{R}\tilde{\boldsymbol{\rho}} \tag{2.97}$$

where the variables having an over-tilde ($\tilde{\bullet}$) are defined in rotating frame. Perturbing the coordinate considering that $\delta\boldsymbol{\Theta}_H$ is the perturbation of the hub orientation, i.e. the vector including roll, pitch and yaw, gives;

$$\delta\mathbf{p} = \delta\mathbf{p}_H + \delta\mathbf{R}\tilde{\boldsymbol{\rho}} = \delta\mathbf{p}_H + \delta\boldsymbol{\Theta}_H \times \mathbf{R}\tilde{\boldsymbol{\rho}} \tag{2.98}$$

with $\delta\mathbf{R} = \delta\boldsymbol{\Theta}_H \times \mathbf{R}$. Now, let $\delta\mathbf{p} = \mathbf{x}$, $\delta\mathbf{p}_H = \mathbf{x}_H$ and $\delta\boldsymbol{\Theta} = \boldsymbol{\omega}_H$ as perturbation the variables and remove all δ in front of the vectors:

$$\mathbf{x} = \mathbf{x}_H + \delta\boldsymbol{\omega}_H \times \mathbf{R}\tilde{\boldsymbol{\rho}} \tag{2.99}$$

Since we need the motion in rotating reference frame, we need to pre-multiply by the transpose of the rotation matrix:

$$\tilde{\mathbf{x}} = \mathbf{R}^T\mathbf{x} = \mathbf{R}^T\mathbf{x}_H + \mathbf{R}^T\boldsymbol{\omega}_H \times \mathbf{R}\tilde{\boldsymbol{\rho}} \tag{2.100}$$

Remembering $\mathbf{R}^T\boldsymbol{\omega}_H \times \mathbf{R} = (\mathbf{R}^T\boldsymbol{\omega}_H)\times$ and using anti-commutative property of cross product leads to:

$$\tilde{\mathbf{x}} = \mathbf{R}^T\mathbf{x}_H - \tilde{\boldsymbol{\rho}} \times \mathbf{R}^T\boldsymbol{\omega}_H \tag{2.101}$$

Eq. 2.101 represents the perturbation of the degrees of freedom on the rotating blade as a function of perturbation of the translational and rotational motion of the hub. We need first and second order time derivatives in order to completely represent the induced effect of the hub motion on blade. Taking first order time derivative gives:

$$\dot{\tilde{\mathbf{x}}} = \dot{\mathbf{R}}^T\mathbf{x}_H + \mathbf{R}^T\dot{\mathbf{x}}_H - \tilde{\boldsymbol{\rho}} \times \dot{\mathbf{R}}^T\boldsymbol{\omega}_H - \tilde{\boldsymbol{\rho}} \times \mathbf{R}^T\dot{\boldsymbol{\omega}}_H \tag{2.102}$$

Using the equality $\dot{\mathbf{R}}^T = -\mathbf{R}^T\Omega\times$, Ω being the angular velocity of the rotor (not to be confused with perturbation $\boldsymbol{\omega}_H$), equation can be better stated;

$$\dot{\tilde{\mathbf{x}}} = -\mathbf{R}^T\Omega \times \mathbf{x}_H + \mathbf{R}^T\dot{\mathbf{x}}_H + \tilde{\boldsymbol{\rho}} \times \mathbf{R}^T\Omega \times \boldsymbol{\omega}_H - \tilde{\boldsymbol{\rho}} \times \mathbf{R}^T\dot{\boldsymbol{\omega}}_H \tag{2.103}$$

which represents the induced velocity of the hub motion on the blade. Differentiating Eq 2.103 once more with a constant Ω assumption gives the acceleration term:

$$\begin{aligned}\ddot{\tilde{\mathbf{x}}} =& \mathbf{R}^T\Omega \times \mathbf{R}^T\Omega \times \mathbf{x}_H - 2\mathbf{R}^T\Omega \times \dot{\mathbf{x}}_H + \mathbf{R}^T\ddot{\mathbf{x}}_H \\ &+ \tilde{\boldsymbol{\rho}} \times \mathbf{R}^T\Omega \times \boldsymbol{\omega}_H + 2\tilde{\boldsymbol{\rho}} \times \mathbf{R}^T\Omega \times \dot{\boldsymbol{\omega}}_H - \tilde{\boldsymbol{\rho}} \times \mathbf{R}^T\ddot{\boldsymbol{\omega}}_H\end{aligned} \tag{2.104}$$

Similarly for the rotation of the cross section as a function of hub perturbation degrees of freedom can be obtained as:

$$\tilde{\boldsymbol{\varphi}} = \mathbf{R}^T\boldsymbol{\omega}_H \tag{2.105a}$$

$$\dot{\tilde{\boldsymbol{\varphi}}} = -\mathbf{R}^T\Omega \times \boldsymbol{\omega}_H + \mathbf{R}^T\dot{\boldsymbol{\omega}}_H \tag{2.105b}$$

$$\ddot{\tilde{\boldsymbol{\varphi}}} = \mathbf{R}^T\Omega \times \mathbf{R}^T\Omega \times \boldsymbol{\omega}_H - 2\mathbf{R}^T\Omega \times \dot{\boldsymbol{\omega}}_H + \mathbf{R}^T\ddot{\boldsymbol{\omega}}_H \tag{2.105c}$$

Results are used to represent the contribution of hub motion on multi-blade coordinates and on hub forces and moments.

2.5.4 Integrated Forces and Moments

As explained, the perturbation matrices at the shaft axis is required to couple the dynamics of the fuselage and rotor. Then, the forces and moments over the blade should be integrated at the blade root and then transformed into non-rotating frame. The aerodynamics (subscript *aero*) and inertial loads (subscript *in*) at an azimuth angle ψ and the coordinate of the blade cross section $\tilde{\boldsymbol{\rho}}$ can be written as:

$$\mathbf{L}(\psi,\tilde{\boldsymbol{\rho}}) = \begin{bmatrix}\mathbf{f}(\psi,\tilde{\boldsymbol{\rho}})\\ \mathbf{m}(\psi,\tilde{\boldsymbol{\rho}})\end{bmatrix} = \begin{bmatrix}\mathbf{f}_{in}(\psi,\tilde{\boldsymbol{\rho}})\\ \mathbf{m}_{in}(\psi,\tilde{\boldsymbol{\rho}})\end{bmatrix} + \begin{bmatrix}\mathbf{f}_{aero}(\psi,\tilde{\boldsymbol{\rho}})\\ \mathbf{m}_{aero}(\psi,\tilde{\boldsymbol{\rho}})\end{bmatrix} \tag{2.106}$$

In order to produce stability matrices, the inertial and aerodynamic loads should be written in perturbation form. Remembering δ is removed for simplicity and $\mathbf{x}$ and $\boldsymbol{\varphi}$ represents perturbation displacement and rotations:

$$\begin{aligned}\mathbf{L}(\psi,\tilde{\boldsymbol{\rho}}) = \begin{bmatrix}\mathbf{f}(\psi,\tilde{\boldsymbol{\rho}})\\ \mathbf{m}(\psi,\tilde{\boldsymbol{\rho}})\end{bmatrix} &= \begin{bmatrix}\mathbf{f}_{/\ddot{\mathbf{x}}} & \mathbf{f}_{/\ddot{\boldsymbol{\varphi}}}\\ \mathbf{m}_{/\ddot{\mathbf{x}}} & \mathbf{m}_{/\ddot{\boldsymbol{\varphi}}}\end{bmatrix}\begin{bmatrix}\ddot{\mathbf{x}}\\ \ddot{\boldsymbol{\varphi}}\end{bmatrix}\\ &+ \begin{bmatrix}\mathbf{f}_{/\dot{\mathbf{x}}} & \mathbf{f}_{/\dot{\boldsymbol{\varphi}}}\\ \mathbf{m}_{/\dot{\mathbf{x}}} & \mathbf{m}_{/\dot{\boldsymbol{\varphi}}}\end{bmatrix}\begin{bmatrix}\dot{\mathbf{x}}\\ \dot{\boldsymbol{\varphi}}\end{bmatrix} + \begin{bmatrix}\mathbf{f}_{/\mathbf{x}} & \mathbf{f}_{/\boldsymbol{\varphi}}\\ \mathbf{m}_{/\mathbf{x}} & \mathbf{m}_{/\boldsymbol{\varphi}}\end{bmatrix}\begin{bmatrix}\mathbf{x}\\ \boldsymbol{\varphi}\end{bmatrix}\end{aligned} \tag{2.107}$$

The matrices $\mathbf{f}_{/}$ and $\mathbf{m}_{/}$ are functions of time t and cross section coordinate $\tilde{\boldsymbol{\rho}}$ and they are linearized matrices with respect to the blade degrees of freedom and its time derivatives at one node. Here only closed form of loads is given to show the integration where the details of their derivation can be found in Sections 2.5.1 and 2.5.2. Then, equivalent forces and moments at the blade root, $\mathbf{L}_r$, can be written as:

$$\mathbf{L}_r(\psi,r) = \begin{bmatrix}\mathbf{I} & \mathbf{0}\\ \tilde{\boldsymbol{\rho}}\times & \mathbf{I}\end{bmatrix}\begin{bmatrix}\mathbf{f}(\psi,r)\\ \mathbf{m}(\psi,r)\end{bmatrix}$$

Note that, the result is a 6×6 matrix times the perturbation of degrees of freedom and their first and second order time derivatives. This is the force and moment contribution of that node and integrating from tip to root gives the resultant loads at the blade root or these matrices can be assembled to form the perturbation rotor matrices. After this point, the loads at the blade root are transformed to the non-rotating frame using multi-blade coordinate transformation of Section 2.7.

2.5.5 Aeroelastic Coupling

In order to have freedom in aerodynamic modeling, a transformation is necessary which can handle from simple $1D$ aerodynamic discretization to complex $3D$ meshes. The method presented in Refs. [81] and [82] provides a powerful method for such a necessity based on conservation of work principle. The transformations between the displacements and forces are made with a linear matrix $\mathbf{H}$ given as;

$$\mathbf{x}_a = \mathbf{H}\mathbf{x}_s \ , \ \mathbf{F}_s = \mathbf{H}^T\mathbf{F}_a \tag{2.108}$$

where $\mathbf{x}_a$ and $\mathbf{x}_s$ are the displacement of aerodynamic and structural nodes and $\mathbf{f}_a$ and $\mathbf{f}_s$ are the forces on the aerodynamic and structural nodes. Obviously, equations also hold for the time derivatives and perturbations. The method uses moving least square in order to find the optimal mapping such that the corresponding aerodynamic nodes for each structural node is matched with a weighing constant.

Transformation of Forces and Moments

The force transformation matrix given in Eq. 2.108 is applicable to the transformation of forces between 2D and/or 3D aerodynamic and structural dynamics meshes and does not include transformation of moment. Hence, in order the method to be able to used for 1D aerodynamic formulations such as Blade Element Momentum Theory, the formula needs to be modified; so that the moment, which is a result of integrated forces over the chord, is included in the analysis. This can be defined by considering the relation between the force $\mathbf{F}_{s,n}$, defined at a single structural node (n), and the aerodynamic force and moment, $\mathbf{F}_{a,p}$ and $\mathbf{M}_{a,p}$, acting at corresponding aerodynamic nodes (p) with a distance $\mathbf{f}_{np}$ from the structural node, such that;

$$\mathbf{F}_{s,n} = \sum_p c_{np}\mathbf{F}_{a,p} \ , \ \mathbf{M}_{s,n} = \sum_p c_{np}\mathbf{f}_{np} \times \mathbf{F}_{a,p} + c_{np}\mathbf{M}_{a,p} \tag{2.109}$$

where c_{np} is the element of $\mathbf{H}^T$ matrix weighing the contribution of the loads at aerodynamic point p at the structural node n and is already formulated in Ref. [82]. This leads to the general transformation matrix for loads $\mathbf{H}_L$ between structural and aerodynamic loads;

$$\left\{ \begin{array}{c} \mathbf{F}_s \\ \mathbf{M}_s \end{array} \right\} = \left[\begin{array}{c} \\ \mathbf{H_L} \\ \\ \end{array} \right] \left\{ \begin{array}{c} \mathbf{F}_a \\ \mathbf{M}_a \end{array} \right\} \tag{2.110}$$

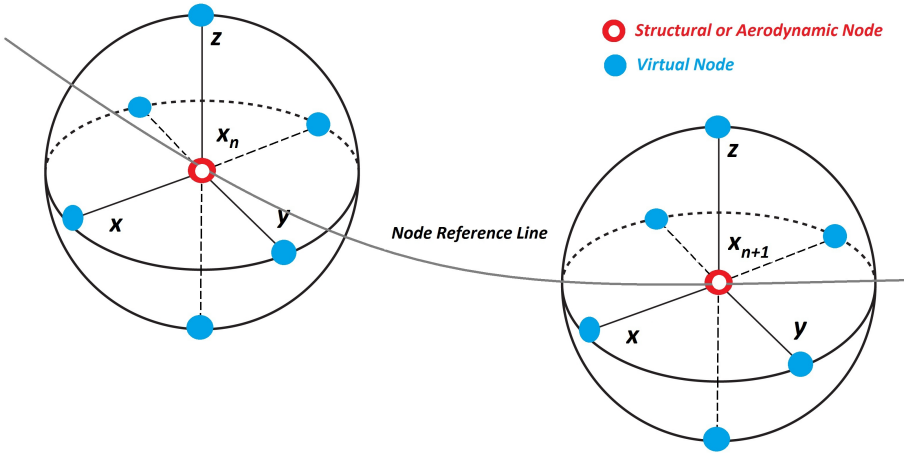

Figure 2.4: *The virtual points form a sphere around the nodes in order to provide the necessary resolution to evaluate curl and rigid body motion*

Transformation of Displacement and Rotations

Although the formulation of this work has the capability to analyze multiple load path structures, 1D sequence of beam elements is sufficient to represent the structural dynamics of the blades for many aeromechanical problems. In 1D formulations, the warping of the cross section is described by a rotation perturbation; hence orientation of a structural node needs to be taken into account. Then, the solution is to adopt the $\mathbf{H}$ matrix already available from Ref. [82] and develop the transformation matrices for the 1D structural model. Transformation for node displacement $\mathbf{H}_d$, including rotations, can be stated as,

$$\left\{ \begin{array}{c} \mathbf{x}_a \\ \boldsymbol{\psi}_a \end{array} \right\} = \left[\begin{array}{c} \mathbf{H_d} \end{array} \right] \left\{ \begin{array}{c} \mathbf{x}_s \\ \boldsymbol{\psi}_s \end{array} \right\} = \left[\begin{array}{cc} \mathbf{H}_{x_a/x_s} & \mathbf{H}_{x_a/\psi_s} \\ \mathbf{H}_{\psi_a/x_s} & \mathbf{H}_{\psi_a/\psi_s} \end{array} \right] \left\{ \begin{array}{c} \mathbf{x}_s \\ \boldsymbol{\psi}_s \end{array} \right\} \tag{2.111}$$

where $\mathbf{H}_{x_a/x_s}$ is the transformation given in Eq. 2.108 which is already available and provides a basis for the rest. In order to use the same method with rotation degrees of freedom of structural and aerodynamic nodes, 6 virtual nodes are defined. These 6 nodes, as shown in Fig. 2.4 and represented by a superscript $*$, are along the positive and negative directions of three perpendicular axis such that they form a sphere having a center at each structural node with radius r. This allows to evaluate the rigid rotation as a function of these 6 virtual nodes in a discrete manner which leads to,

$$\mathbf{x}_s^* = \mathbf{N}_s^* \boldsymbol{\psi}_s \tag{2.112}$$

where $\mathbf{x}_s^*$ is the displacements at the virtual nodes. Then matrix $\mathbf{N}_s^*$ can be defined as a cross multiplication of the distance $\mathbf{l}_i$ between the virtual nodes and the corresponding structural node such that the result gives the perturbation displacements due to the perturbation rigid body rotation:

$$\mathbf{N}_s^{*T} = \begin{bmatrix} \mathbf{l}_1\times & \mathbf{l}_2\times & \mathbf{l}_3\times & \mathbf{l}_4\times & \mathbf{l}_5\times & \mathbf{l}_6\times \end{bmatrix} \tag{2.113}$$

Thanks to the validity of the method of Ref. [82] between two separate displacement fields, the relation in Eq. 2.108 is valid. The mapping matrix $\mathbf{H}_{x_a/x_s^*}$ from these virtual nodes to aerodynamic nodes can be estimated. Then, the mapping matrix from structural node rotations to aerodynamic node displacement is stated as:

$$\mathbf{H}_{x_a/\psi_s} = \mathbf{H}_{x_a/x_s^*}\mathbf{N}_s^* \tag{2.114}$$

The next term $\mathbf{H}_{\psi_a/x_s}$ of Eq. 2.111 defines the transformation from structural node displacement to the rotation of aerodynamic node. The procedure is similar to the previous transformation, but this time the sphere nodes are formed around aerodynamic nodes and transformation matrix $\mathbf{H}_{x_a^*/x_s}$ is evaluated where $\mathbf{x}_a^*$ is the perturbation displacement at these virtual aerodynamic nodes. The displacement can be transformed into rotations by curl operator;

$$\boldsymbol{\psi}_a = \frac{1}{2} \bigtriangledown \times \mathbf{x}_a^* \tag{2.115}$$

where derivatives arising from the curl operator for the perturbation rotations and displacements are evaluated in a discrete manner by calculating the finite differences using the sphere nodes. Then, the result of the curl operation is the shape matrix $\mathbf{N}_a^*$ providing the function from the virtual node perturbation displacements $\mathbf{x}_a^*$ to aerodynamic node rotations. With the shape matrix, aerodynamic node rotation $\boldsymbol{\psi}_a$ can be written as;

$$\boldsymbol{\psi}_a = \mathbf{N}_a^*\mathbf{x}_a^* \tag{2.116}$$

which leads to the required transformation:

$$\mathbf{H}_{\boldsymbol{\psi}_a/\ \mathbf{x}_s} = \mathbf{N}_a^*\mathbf{H}_{x_a^*/x_s} \tag{2.117}$$

Last term of of Eq. 2.111 defines the transformation between structural and aerodynamic rotations. It is straightforward to obtain it by fallowing the procedures of $\mathbf{H}_{x_a/\psi_s}$ and $\mathbf{H}_{\psi_a/\ x_s}$ since two necessary shape matrices are already defined except for the transformation from

the sphere nodes around structural nodes to the sphere nodes around aerodynamic nodes namely $\mathbf{H}_{x_a^*/\ x_s^*}$. This transformation matrix can be computed by using the same method given in Eq. 2.108 for the properly defined sphere nodes. The relation is:

$$\mathbf{H}_{\psi_a/\ \psi_s} = \mathbf{N}_a^* H_{x_a^*/\ x_s^*} \mathbf{N}_s^* \tag{2.118}$$

The global transformation for node displacement and rotations $\mathbf{H}_d$ can be stated as:

$$\begin{bmatrix} \mathbf{H_d} \end{bmatrix} = \begin{bmatrix} \mathbf{H}_{x_a/x_s} & \mathbf{H}_{x_a/x_s^*}\mathbf{N}_s^* \\ \mathbf{N}_a^*\mathbf{H}_{x_a^*/x_s} & \mathbf{N}_a^*\mathbf{H}_{\mathbf{x}_a^*/\ \mathbf{x}_s^*}\mathbf{N}_s^* \end{bmatrix} \tag{2.119}$$

The intermediate transformations of Eq. 2.119, i.e. all $\mathbf{H}$, are performed between the locations of the nodes and all can be evaluated by using method given in Ref. [82] by implementing proper sphere nodes around the actual nodes. The shape matrices, all $\mathbf{N}^*$, are nothing but geometric functions as defined above. Depending on the aerodynamic model, the unnecessary transformations can be suppressed. One remark should be made here is that the distance of the virtual nodes from their corresponding real nodes, in other words radius r, is important since the method finds the closest points between aerodynamic and structural meshes to define the transformation. Since each virtual sphere has its own assigned real node, inappropriate choice may cause overlapping nodes and as a result inaccurate transformation.

Transformation of Aerodynamic Perturbation Matrices

Regardless of the aerodynamic method used, the aerodynamic perturbation forces and moments can be expressed as fallows:

$$\mathbf{F}_a = \mathbf{F}_{a/x_a}\mathbf{x}_a + \mathbf{F}_{a/\psi_a}\boldsymbol{\psi}_a \tag{2.120a}$$
$$\mathbf{M}_a = \mathbf{M}_{a/x_a}\mathbf{x}_a + \mathbf{M}_{a/\psi_a}\boldsymbol{\psi}_a \tag{2.120b}$$

Combining with Eq. 2.110 and writing in matrix form, the load vector at structural nodes can be written as:

$$\begin{Bmatrix} \mathbf{F}_s \\ \mathbf{M}_s \end{Bmatrix} = \begin{bmatrix} \mathbf{H_L} \end{bmatrix} \begin{bmatrix} \mathbf{F}_{a/x_a} & \mathbf{F}_{a/\psi_a} \\ \mathbf{M}_{a/x_a} & \mathbf{M}_{a/\psi_a} \end{bmatrix} \begin{Bmatrix} \mathbf{x}_a \\ \boldsymbol{\psi}_a \end{Bmatrix} \tag{2.121}$$

The aerodynamic degrees of freedom should also be transformed in order to solve the problem in the structural degrees of freedom. This can be done by using $\mathbf{H_d}$ given in Eq. 2.119. Then, Eq. 2.121 can be

written in the reference frame of structural loads and including the aerodynamic perturbation matrices as well:

$$\left\{ \begin{array}{c} \mathbf{F}_s \\ \mathbf{M}_s \end{array} \right\} = \left[\begin{array}{c} \mathbf{H_L} \end{array} \right] \left[\begin{array}{cc} \mathbf{F}_{a/x_a} & \mathbf{F}_{a/\psi_a} \\ \mathbf{M}_{a/x_a} & \mathbf{M}_{a/\psi_a} \end{array} \right] \left[\begin{array}{c} \mathbf{H_d} \end{array} \right] \left\{ \begin{array}{c} \mathbf{x}_s \\ \boldsymbol{\psi}_s \end{array} \right\} \tag{2.122}$$

Finally any aerodynamic perturbation is represented as a structural perturbation as:

$$\left[\begin{array}{cc} \mathbf{F}_{s/x_s} & \mathbf{F}_{s/\psi_s} \\ \mathbf{M}_{s/x_s} & \mathbf{M}_{s/\psi_s} \end{array} \right]_{aero} = \left[\begin{array}{c} \mathbf{H_L} \end{array} \right] \left[\begin{array}{cc} \mathbf{F}_{a/x_a} & \mathbf{F}_{a/\psi_a} \\ \mathbf{M}_{a/x_a} & \mathbf{M}_{a/\psi_a} \end{array} \right] \left[\begin{array}{c} \mathbf{H_d} \end{array} \right] \tag{2.123}$$

Although the formulas are given for displacement, the same $\mathbf{H_L}$ and $\mathbf{H_d}$ matrices are valid for the time derivatives. This method makes it possible to formulate aerodynamic perturbation in aerodynamic domain which is more favorable and provides freedom. And then it can be transformed into structural domain in which the structural dynamics is formulated for the contribution of aerodynamic perturbation matrices.

2.6 Steady State Solution

The perturbation matrices are defined as the linearization around a reference condition hence for most of the problems a reference steady solution is required. The system of equations can be written as,

$$\mathbf{M}\ddot{\mathbf{x}} + \mathbf{C}\dot{\mathbf{x}} + \mathbf{K}\mathbf{x} = \mathbf{f}(\mathbf{x}, t) \tag{2.124}$$

where $\mathbf{M}$ is the global mass matrix $\mathbf{C}$ is the damping matrix $\mathbf{K}$ is the stiffness matrix and $\mathbf{q}$ is the degree of freedom vector. The vector $\mathbf{f}(\mathbf{x}, t)$ represents the forcing function aerodynamic or any source of external excitation. First, integration in time is briefly explained than harmonic balance method for periodic problems is described.

2.6.1 Integration of Equations of Motion

There is vast of literature on the integration of equations of motion (See for example Ref. [78] for application in structural dynamics and Ref. [3] for rotorcraft applications) hence here only important steps are provided. Generally the algorithms use the state space form, $\dot{\mathbf{q}} = \mathbf{A}\mathbf{x} + \mathbf{f}$, then Eq. 2.124 is converted to the state space form;

$$\left[\begin{array}{c} \dot{\mathbf{x}} \\ \ddot{\mathbf{x}} \end{array} \right] = \left[\begin{array}{cc} \mathbf{O} & \mathbf{I} \\ -\mathbf{M}^{-1}\mathbf{K} & -\mathbf{M}^{-1}\mathbf{C} \end{array} \right] \left[\begin{array}{c} \mathbf{x} \\ \dot{\mathbf{x}} \end{array} \right] + \left[\begin{array}{c} \mathbf{0} \\ \mathbf{M}^{-1}\mathbf{f}(\dot{\mathbf{x}}, \mathbf{x}, t) \end{array} \right] \tag{2.125}$$

and then can be integrated for the states $\dot{\mathbf{x}}$ and $\mathbf{x}$ using a suitable integration method.

2.6.2 Harmonic Balance

For linear time periodic systems, the steady steady solution under external forces can be obtained faster using Harmonic Balance (See Ref. [83] for a general discussion). Using the azimuth angle ψ instead of time t to emphasize the periodicity gives:

$$\mathbf{M}(\psi)\ddot{\mathbf{x}}(\psi) + \mathbf{C}(\psi)\dot{\mathbf{x}}(\psi) + \mathbf{K}(\psi)\mathbf{x}(\psi) = \mathbf{f}(\dot{\mathbf{x}}, \mathbf{x}, \psi) \tag{2.126}$$

Due to periodicity, the external loads $\mathbf{f}$, response $\mathbf{x}$ and any of the mass, damping and stiffness matrices, say $\mathbf{G}$, can be written as a Fourier series with a fundamental frequency of rotor angular speed Ω [84];

$$\mathbf{f}(\psi) = \mathbf{f}_0 + \sum_{n=1}^{N_h} \mathbf{f}_n \mathrm{e}^{\mathrm{j}n\Omega} \tag{2.127a}$$

$$\mathbf{x}(\psi) = \mathbf{x}_0 + \sum_{n=1}^{N_h} \mathbf{x}_n \mathrm{e}^{\mathrm{j}n\Omega} \tag{2.127b}$$

$$\mathbf{G}(\psi) = \mathbf{G}_0 + \sum_{n=1}^{N_h} \mathbf{G}_n \mathrm{e}^{\mathrm{j}n\Omega} \tag{2.127c}$$

where N_h is the number of harmonics in the analysis and $\mathrm{j} = \sqrt{-1}$. Then, all the matrices related to structural dynamics are kept on left hand side and aerodynamic forces are located on right hand side;

$$\big[-n^2\Omega^2\mathbf{M}_n + \mathrm{j}n\Omega\mathbf{C}_n + \mathbf{K}_n \big]\mathbf{x}_n = \mathbf{f}_n \tag{2.128}$$

and solved for steady solution $\mathbf{x}_0$ and harmonic solutions $\mathbf{x}_n$ for a sufficient number of n depending on the problem. Due to the dependence of aerodynamic forces on blade motion, iteration is needed. Moreover, in rotor aerodynamics frequencies of excitation forces can be very close to blade frequencies, especially to first flap mode. Therefore in order to prevent resonance and obtain a converged solution, aerodynamic damping is added to both sides of equation as proposed in Ref. [3]. The aerodynamic damping matrix, which is developed in Section 2.5.2, can be used. Since the same value is added on both sides, only divergence of the solution is prevented without changing the steady state solution.

2.7 MULTI-BLADE COORDINATES

The three essential reference frames in rotorcraft analysis are given in Fig. 2.5. All of them are useful for specific purposes. First one is named as helicopter reference frame attached to the body of the vehicle and mainly used for flight mechanics analysis. Second one is referred to as the shaft axis around which blades rotate and suitable to represent rotor forces and motion hence links the body dynamics to the blade dynamics. Both helicopter and shaft reference frames are inertial except the shaft axis can have offset, rotation and tilt with respect to the helicopter axis. The third one is the blade reference frame which is attached to each blade and rotating with it. This is a relative frame and very convenient to represent the blade loads and motion.

In order to analyze rotorcraft all together with its rotating and non-rotating components, the perturbation matrices in rotating reference frame should be transformed to an inertial reference frame. For this reason, the multiblade coordinate transformation developed for 3 bladed wind turbines in Ref. [85] is generalized for a rotor having number of N equally spaced blades. For the b^{th} blade, the azimuth angle is written as:

$$\psi_b = \psi + (b-1)\frac{2\pi}{N} \tag{2.129}$$

If q_b is a degree of freedom of the blade b in rotating frame, the transformation to the non rotating blade is done as follows,

$$q_0 = \frac{1}{N}\sum_{b=1}^{N} q_b \tag{2.130a}$$

$$q_{nc} = \frac{2}{N}\sum_{b=1}^{N} q_b \cos n\psi_b \tag{2.130b}$$

$$q_{ns} = \frac{2}{N}\sum_{b=1}^{N} q_b \sin n\psi_b \tag{2.130c}$$

$$q_{N/2} = \frac{1}{N}\sum_{b=1}^{N} q_b(-1)^b \tag{2.130d}$$

where q_0 is the collective mode, q_{nc} and q_{ns} are the n^{th} cyclic modes and $q_{N/2}$ is the differential modes all of which are in non-rotating frame.

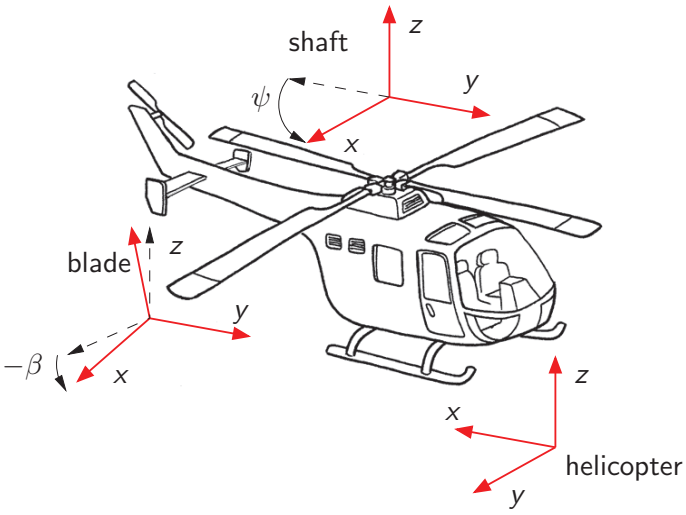

Figure 2.5: *Three reference frames of helicopter dynamics*

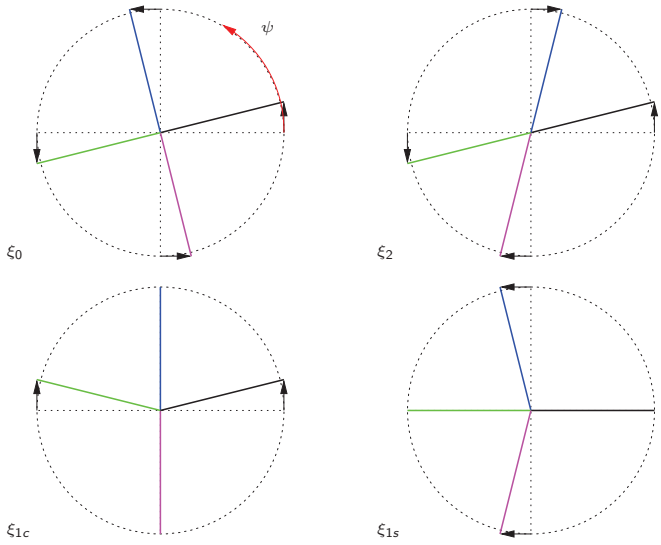

Figure 2.6: *Example of multi-blade coordinates, lead-lag motion of the blades.*

Collective and cyclic modes exist for any rotor having 3 or more blades whereas the differential mode is active only for the rotors having an even number of blades but does not contribute to the coupled fuselage-rotor dynamics for isotropic, i.e. equally spaced identical blades, rotors. The total number of n is $(N-1)/2$ if N is odd and $(N-2)/2$ if N is even. An example is given in Fig. 2.6 for the lead lag motion of a four bladed rotor including collective ζ_0, cyclic ζ_{1c} and ζ_{1s} and reactionless ζ_2 modes. In general, equations of motion of the system in rotating reference frame for a rotor is written as:

$$\mathbf{M}\ddot{\mathbf{x}} + \mathbf{C}\dot{\mathbf{x}} + \mathbf{K}\mathbf{x} = \mathbf{F}\mathbf{u} + \mathbf{F}_d\mathbf{w} \tag{2.131}$$

$\mathbf{M}$, $\mathbf{C}$, $\mathbf{K}$, $\mathbf{F}$ and $\mathbf{F}_d$ are mass, damping (including gyroscopic effects), stiffness, control and disturbance matrices having contribution from each blade at any instant of time according to the rotor degree of freedom vector written in rotating frame,

$$\mathbf{x} = \begin{bmatrix} \mathbf{x}_H^T & q_1^1 & q_2^1 & .. & q_N^1 & \dots & q_1^j & q_2^j & . & q_N^j & \dots & q_1^m & q_2^m & .. & q_{N/2}^m \end{bmatrix}^T \tag{2.132}$$

which includes the 6×1 column vector representing the hub fixed-frame-referenced degrees of freedom $\mathbf{X}_H$ and j^{th} rotating degree of freedom for the b^{th} blade q_b^j for a number of rotating degrees of freedom m. Similarly, the degrees of freedom vector in non-rotating frame is written as:

$$\mathbf{x}_{NR} = \begin{bmatrix} \mathbf{x}_H^T & q_0^1 & q_c^1 & q_s^1 & q_{N/2}^1 & \dots & q_0^j & q_c^j & q_s^j & q_{N/2}^j & \dots & q_0^m & q_c^m & q_s^m & q_{N/2}^m \end{bmatrix}^T \tag{2.133}$$

Equations of motion are also needed to be transformed to the non-rotating frame. Analytical from of transformation has limited usage so as proposed in Ref. [85] a more generic transformation is preferred. Starting from a single mode, it can be written that

$$\begin{bmatrix} q_1^j \\ q_2^j \\ q_3^j \\ \vdots \\ q_N^j \end{bmatrix} = \tilde{\mathbf{t}} \begin{bmatrix} q_0^j \\ q_c^j \\ q_c^j \\ \vdots \\ q_{N/2}^j \end{bmatrix} \tag{2.134}$$

where the transformation $\tilde{\mathbf{t}}$ matrix for even number of blades, N, is;

$$\tilde{\mathbf{t}} = \begin{bmatrix} 1 & \cos\psi_1 & \sin\psi_1 & \dots & \cos\frac{(N-2)}{2}\psi_1 & \sin\frac{(N-2)}{2}\psi_1 & (-1)^1 \\ 1 & \cos\psi_2 & \sin\psi_2 & \dots & \cos\frac{(N-2)}{2}\psi_2 & \sin\frac{(N-2)}{2}\psi_2 & (-1)^2 \\ & & & & \vdots & & \\ 1 & \cos\psi_b & \sin\psi_b & \dots & \cos\frac{(N-2)}{2}\psi_b & \sin\frac{(N-2)}{2}\psi_2 & (-1)^b \\ & & & & \vdots & & \\ 1 & \cos\psi_N & \sin\psi_N & \dots & \cos\frac{(N-2)}{2}\psi_N & \sin\frac{(N-2)}{2}\psi_N & (-1)^N \end{bmatrix} \tag{2.135}$$

and for an odd N;

$$\tilde{\mathbf{t}} = \begin{bmatrix} 1 & \cos\psi_1 & \sin\psi_1 & \dots & \cos\frac{(N-1)}{2}\psi_1 & \sin\frac{(N-1)}{2}\psi_1 \\ 1 & \cos\psi_2 & \sin\psi_2 & \dots & \cos\frac{(N-1)}{2}\psi_2 & \sin\frac{(N-1)}{2}\psi_2 \\ & & & \vdots & & \\ 1 & \cos\psi_b & \sin\psi_b & \dots & \cos\frac{(N-1)}{2}\psi_b & \sin\frac{(N-1)}{2}\psi_b \\ & & & \vdots & & \\ 1 & \cos\psi_N & \sin\psi_N & \dots & \cos\frac{(N-1)}{2}\psi_N & \sin\frac{(N-1)}{2}\psi_N \end{bmatrix} \tag{2.136}$$

Now, the global degrees of freedom including all modes can be written as;

$$\mathbf{X}_R = \mathbf{T}_1\mathbf{X}_{NR} \tag{2.137}$$

where $\mathbf{T}_1$ is a block diagonal matrix;

$$\mathbf{T}_1 = \begin{bmatrix} \mathbf{I}_{6\times6} & & & & \\ & \tilde{\mathbf{t}} & & & \\ & & \tilde{\mathbf{t}} & & \\ & & & \ddots & \\ & & & & \tilde{\mathbf{t}} \end{bmatrix} \tag{2.138}$$

which have blocks of $\mathbf{t}$ matrices with the number of degrees of freedom. Differentiating Eq. 2.137 once and twice with respect to time gives;

$$\dot{\mathbf{X}}_R = \mathbf{T}_1\dot{\mathbf{X}}_{NR} + \Omega\mathbf{T}_2\mathbf{X}_{NR} \tag{2.139a}$$

$$\ddot{\mathbf{X}}_R = \mathbf{T}_1\ddot{\mathbf{X}}_{NR} + 2\Omega\mathbf{T}_2\dot{\mathbf{X}}_{NR} + (\Omega^2\mathbf{T}_2 + \dot{\Omega}\mathbf{T}_2)\mathbf{X}_{NR} \tag{2.139b}$$

where Ω and $\dot{\Omega}$ are the angular speed and acceleration of the rotor. The two additional transformation matrices are obtained by differentiating $\mathbf{T}_1$ once and twice with respect to azimuthal angle ψ,

$$\mathbf{T}_2 = \begin{bmatrix} \mathbf{0}_{6\times6} & & & & \\ & \tilde{\mathbf{t}}_2 & & & \\ & & \tilde{\mathbf{t}}_2 & & \\ & & & \ddots & \\ & & & & \tilde{\mathbf{t}}_2 \end{bmatrix} \tag{2.140a}$$

$$\mathbf{T}_3 = \begin{bmatrix} \mathbf{0}_{6\times6} & & & & \\ & \tilde{\mathbf{t}}_3 & & & \\ & & \tilde{\mathbf{t}}_3 & & \\ & & & \ddots & \\ & & & & \tilde{\mathbf{t}}_3 \end{bmatrix} \tag{2.140b}$$

where for N is even:

$$\tilde{\mathbf{t}}_2 = \begin{bmatrix} 0 & -\sin\psi_1 & \cos\psi_1 & \dots & -\frac{(N-2)}{2}\sin\frac{(N-2)}{2}\psi_1 & \frac{(N-2)}{2}\cos\frac{(N-2)}{2}\psi_1 & 0 \\ 0 & -\sin\psi_2 & \cos\psi_2 & \dots & -\frac{(N-2)}{2}\sin\frac{(N-2)}{2}\psi_2 & \frac{(N-2)}{2}\cos\frac{(N-2)}{2}\psi_2 & 0 \\ & & & & \vdots & & \\ 0 & -\sin\psi_b & \cos\psi_b & \dots & -\frac{(N-2)}{2}\sin\frac{(N-2)}{2}\psi_b & \frac{(N-2)}{2}\cos\frac{(N-2)}{2}\psi_b & 0 \\ & & & & \vdots & & \\ 0 & -\sin\psi_N & \cos\psi_N & \dots & -\frac{(N-2)}{2}\sin\frac{(N-2)}{2}\psi_N & \frac{(N-2)}{2}\cos\frac{(N-2)}{2}\psi_N & 0 \end{bmatrix} \tag{2.141a}$$

$$\tilde{\mathbf{t}}_3 = \begin{bmatrix} 0 & -\cos\psi_1 & -\sin\psi_1 & \dots & -\frac{(N-2)^2}{4}\cos\frac{(N-2)}{2}\psi_1 & -\frac{(N-2)^2}{4}\sin\frac{(N-2)}{2}\psi_1 & 0 \\ 0 & -\cos\psi_2 & -\sin\psi_2 & \dots & -\frac{(N-2)^2}{4}\cos\frac{(N-2)}{2}\psi_2 & -\frac{(N-2)^2}{4}\sin\frac{(N-2)}{2}\psi_2 & 0 \\ & & & & \vdots & & \\ 0 & -\cos\psi_b & -\sin\psi_b & \dots & -\frac{(N-2)^2}{4}\cos\frac{(N-2)}{2}\psi_b & -\frac{(N-2)^2}{4}\sin\frac{(N-2)}{2}\psi_b & 0 \\ & & & & \vdots & & \\ 0 & -\cos\psi_N & -\sin\psi_N & \dots & -\frac{(N-2)^2}{4}\cos\frac{(N-2)}{2}\psi_N & -\frac{(N-2)^2}{4}\sin\frac{(N-2)}{2}\psi_N & 0 \end{bmatrix} \tag{2.141b}$$

And for number of blades N being odd:

$$\tilde{\mathbf{t}}_2 = \begin{bmatrix} 0 & -\sin\psi_1 & \cos\psi_1 & \dots & -\frac{(N-1)}{2}\sin\frac{(N-1)}{2}\psi_1 & \frac{(N-1)}{2}\cos\frac{(N-1)}{2}\psi_1 \\ 0 & -\sin\psi_2 & \cos\psi_2 & \dots & -\frac{(N-1)}{2}\sin\frac{(N-1)}{2}\psi_2 & \frac{(N-1)}{2}\cos\frac{(N-1)}{2}\psi_2 \\ & & & \vdots & & \\ 0 & -\sin\psi_b & \cos\psi_b & \dots & -\frac{(N-1)}{2}\sin\frac{(N-1)}{2}\psi_b & \frac{(N-1)}{2}\cos\frac{(N-1)}{2}\psi_b \\ & & & \vdots & & \\ 0 & -\sin\psi_N & \cos\psi_N & \dots & -\frac{(N-1)}{2}\sin\frac{(N-1)}{2}\psi_N & \frac{(N-1)}{2}\cos\frac{(N-1)}{2}\psi_N \end{bmatrix} \tag{2.142a}$$

$$\tilde{\mathbf{t}}_3 = \begin{bmatrix} 0 & -\cos\psi_1 & -\sin\psi_1 & \dots & -\frac{(N-1)^2}{4}\cos\frac{(N-1)}{2}\psi_1 & -\frac{(N-1)^2}{4}\sin\frac{(N-1)}{2}\psi_1 \\ 0 & -\cos\psi_2 & -\sin\psi_2 & \dots & -\frac{(N-1)^2}{4}\cos\frac{(N-1)}{2}\psi_2 & -\frac{(N-1)^2}{4}\sin\frac{(N-1)}{2}\psi_2 \\ & & & \vdots & & \\ 0 & -\cos\psi_b & -\sin\psi_b & \dots & -\frac{(N-1)^2}{4}\cos\frac{(N-1)}{2}\psi_b & -\frac{(N-1)^2}{4}\sin\frac{(N-1)}{2}\psi_b \\ & & & \vdots & & \\ 0 & -\cos\psi_N & -\sin\psi_N & \dots & -\frac{(N-1)^2}{4}\cos\frac{(N-1)}{2}\psi_N & -\frac{(N-1)^2}{4}\sin\frac{(N-1)}{2}\psi_N \end{bmatrix} \tag{2.142b}$$

Now, substituting derivatives into Eq. 2.131, the equation in non-rotating frame can be obtained as,

$$\mathbf{M}_{NR}\ddot{\mathbf{X}}_{NR} + \mathbf{C}_{NR}\dot{\mathbf{X}}_{NR} + \mathbf{K}_{NR}\mathbf{X}_{NR} = \mathbf{F}_{NR}\mathbf{u}_{NR} + \mathbf{F}_{d,NR}\mathbf{w} \tag{2.143}$$

where matrices in non-rotating reference frame are defined as:

$$\mathbf{M}_{NR} = \mathbf{M}\mathbf{T}_1 \tag{2.144a}$$

$$\mathbf{C}_{NR} = 2\Omega\mathbf{M}\mathbf{T}_2 + \mathbf{C}\mathbf{T}_1 \tag{2.144b}$$

$$\mathbf{K}_{NR} = \Omega^2\mathbf{M}\mathbf{T}_3 + \dot{\Omega}\mathbf{M}\mathbf{T}_2 + \Omega\mathbf{C}\mathbf{T}_2 + \mathbf{K}\mathbf{T}_1 \tag{2.144c}$$

The Nc control inputs in rotating frame are connected to controls in non-rotating frame via $\mathbf{u} = \mathbf{T}_{1c}\mathbf{u}_{NR}$, then;

$$\mathbf{F}_{NR} = \mathbf{F}\mathbf{T}_{1c} \tag{2.145}$$

where,

$$\mathbf{T}_{1c} = \begin{bmatrix} \mathbf{I}_{Nc\times Nc} & & & \\ & \tilde{\mathbf{t}} & & \\ & & \tilde{\mathbf{t}} & \\ & & & \ddots \\ & & & \tilde{\mathbf{t}} \end{bmatrix} \tag{2.146}$$

Finally, the disturbance vector is already defined in non-rotating frame:

$$\mathbf{F}_{d,NR} = \mathbf{F}_d$$

2.8 Sensitivity of Stability Properties for LTI Systems

One of the main motivation of the thesis is to be able to evaluate the analytical sensitivity matrices for rotor blade design variables. This part covers the sensitivity of the eigenvalues of a linear time invariant (LTI) problem following the method of Ref. [86]. The sensitivity formulations of stability properties for more complex systems are presented in Chapter 3 for linear time periodic systems and in Chapter 4 for a general nonlinear non-autonomous problem.

A general aeroelastic eigenvalue problem for eigenvalue (s) and eigenvector $x(s)$ is;

$$\left[s^2\mathbf{M}(p) + s\mathbf{C}(p) + [\mathbf{K}(p) - \mathbf{H}(s,p)]\right]x(s) = 0 \tag{2.147}$$

where the matrices $\mathbf{M}$, $\mathbf{C}$, $\mathbf{K}$ and $\mathbf{H}$ are the global mass, damping, stiffness and complex aerodynamic matrices parametrized with parameter p. The aerodynamic matrix $\mathbf{H}$ can be a function of the complex eigenvalue s, then using a second order Taylor Series expansion around zero frequency $s = 0$, matrix $\mathbf{H}$ can be approximated as:

$$\mathbf{H}(s) = s^2\mathbf{H}''(0) + s\mathbf{H}'(0) + \mathbf{H}(0) \tag{2.148}$$

The rate of change the eigenvalues with respect to a parameter p, i.e. the first order derivative, is what is looked for. Then, differentiating Eq. 2.147 with respect to a scalar parameter p;

$$\begin{aligned}
&2s\mathbf{M}\mathbf{x}s_{/p} + s^2\mathbf{M}_{/p}\mathbf{x} + s^2\mathbf{M}\mathbf{x}_{/p} + \mathbf{C}\mathbf{x}s_{/p} + s^2\mathbf{M}_{/p}\mathbf{x} + s\mathbf{C}\mathbf{x}_{/p} + \mathbf{K}_{/p}\mathbf{x} \\
&+\mathbf{K}\mathbf{x}_{/p} - [2s\mathbf{H}''(0)\mathbf{x}s_{/p} + s^2\mathbf{H}''_{/p}(0)\mathbf{x} + s^2\mathbf{H}''(0)\mathbf{x}_{/p} + \mathbf{H}'(0)\mathbf{x}s_{/p} \\
&+s\mathbf{H}'_{/p}(0)x + s\mathbf{H}'(0)\mathbf{x}_{/p} + \mathbf{H}_{/p}(0)\mathbf{x} + \mathbf{H}(0)\mathbf{x}_{/p}] = 0
\end{aligned} \tag{2.149}$$

where the sensitivities of the matrices are simply the derivatives of the matrix elements with respect to that parameter.

If the number of degrees of freedom is n, Eq. 2.149 provides n equations whereas there are $n+1$ unknowns since both of $s_{/p}$ (1 unknown) and $\mathbf{x}_{/p}$ (n unknowns) are needed to be evaluated. One more equation is required and it comes from the orthogonality of the normalized eigenvector;

$$\mathbf{x}^T\mathbf{x} = 1 \tag{2.150}$$

where $\mathbf{x}^T$ is the complex conjugate transpose of $\mathbf{x}$. The derivative with respect to parameter p leads to:

$$\mathbf{x}^T \mathbf{x}_{/p} = 0 \tag{2.151}$$

Now the equation is full rank and the stability derivatives of the eigenvalue and eigenvector can be evaluated. Combining Eq. 2.149 and Eq. 2.150 in matrix form gives;

$$\begin{bmatrix} \mathbf{S}_0 \end{bmatrix} \begin{bmatrix} \mathbf{x}_{/p} \\ s_{/p} \end{bmatrix} = \begin{bmatrix} \mathbf{S}_{/p} \end{bmatrix} \tag{2.152}$$

where the sub-matrices of left hand side matrix $\mathbf{S}_0$ are ;

$$\begin{aligned}
\mathbf{S}_0(1,1) &= s^2(\mathbf{M} + \mathbf{H}''(0)) + s(\mathbf{C} + \mathbf{H}'(0)) + (\mathbf{K} + \mathbf{H}(0))) \\
\mathbf{S}_0(2,1) &= 2\mathbf{x}^T \\
\mathbf{S}_0(1,2) &= 2s(\mathbf{M} + \mathbf{H}''(0))\mathbf{x} + (\mathbf{C} + \mathbf{H}'(0))\mathbf{x} \\
\mathbf{S}_0(2,2) &= \mathbf{0}
\end{aligned}$$

with the sub-matrices of right hand side matrix $\mathbf{S}_{/p}$:

$$\begin{aligned}
\mathbf{S}_{/p}(1) &= -[s^2(\mathbf{M}_{/p} - \mathbf{H}''_{/p}(0)) + s(\mathbf{C}_{/p} - \mathbf{H}'_{/p}(0)) + (\mathbf{K}_{/p} - \mathbf{H}_{/p}(0))]\mathbf{x} \\
\mathbf{S}_{/p}(2) &= 0
\end{aligned}$$

Then, the solution of Eq. 2.152 gives the first order derivatives of eigenvalue ($s_{/p}$) and eigenvector ($\mathbf{x}_{/p}$) at a solution point s and $\mathbf{x}$. If the interested frequencies are the damped natural frequencies or quasi-static aerodynamics is preferred, the system of equations can be reduced to;

$$\begin{bmatrix} s^2\mathbf{M} + s\mathbf{C} + \mathbf{K} & 2s\mathbf{M} + \mathbf{C} \\ 2\mathbf{x}^T & 0 \end{bmatrix} \begin{bmatrix} \mathbf{x}_{/p} \\ s_{/p} \end{bmatrix} = \begin{bmatrix} -(s^2\mathbf{M}_{/p} + s\mathbf{C}_{/p} + \mathbf{K}_{/p})] \\ 0 \end{bmatrix} \tag{2.153}$$

2.9 Examples and Verification

This section includes the examples and verification of the tool. *LARotor: Linearized Aeroelastic Rotor* is the name given to the tool discussed in this chapter, whereas the name of other references are given in related figures and sections. In Chapter 5, more advanced problems related to rotorcraft aeroservoelastic stability and sensitivity can be found.

2.9.1 Natural Frequencies of a Rotating blade

A rotating blade, which is provided in Ref. [87], is analyzed to verify the structural dynamics formulation of linearized blade model for the estimation of natural frequencies. The blade is subjected to a range of rotor angular speed values between 0 RPM and 660 RPM. First five natural frequencies, composed of 4 bending and 1 torsional modes, are compared with the estimates using NASTRAN and MBDyn. In the fan-plot diagram of Fig. 2.7, it can be observed that all three numerical tools give very close results.

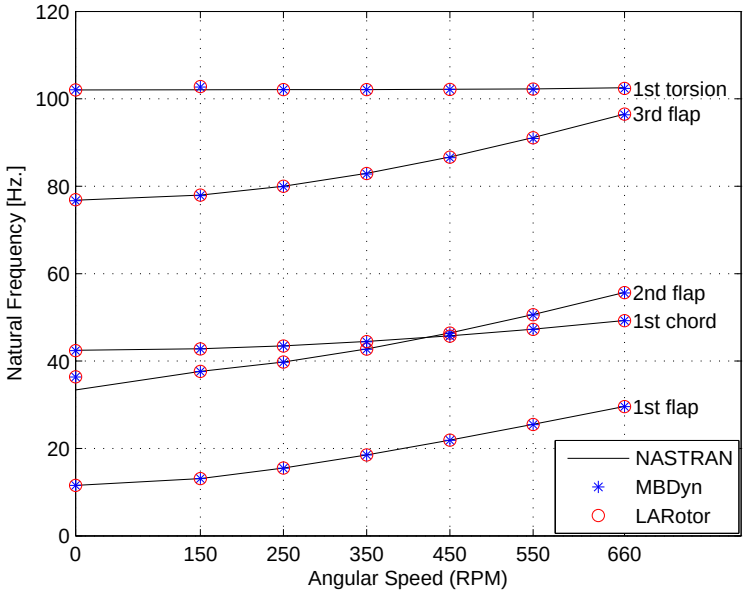

Figure 2.7: *Natural Frequencies of a rotating blade: Comparison of first 5 rotating blade modes on a fan-plot diagram for a range of rotor angular speed values from* 0 *RPM to* 660 *RPM.*

2.9.2 Steady flap response

Steady flap responses are compared using the model developed for a helicopter rotor blade operating at forward flight. The model is prepared using the data given in Ref. [51]. Results are compared with MBDyn Multibody Dynamics Code. Both models use Mangler Squire Inflow Model. The steady state flap response as a function of azimuth angle is given in Fig. 2.8 and provides good correlation.

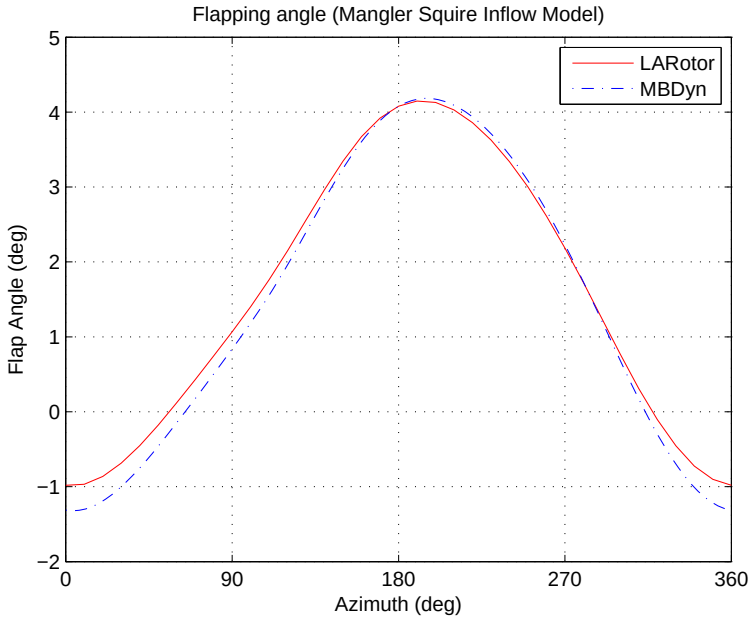

Figure 2.8: *Steady response: Comparison of steady-state flapping angles of a helicopter blade over the rotor disc, with Mangler-Squire inflow model*

2.9.3 PUMA Rotor Blade

This section presents the verification of linearized aeroelastic blade model for the natural frequencies and steady aerodynamics. The aeroelastic blade is prepared using the formulation described in this chapter so far and based on the data given in Ref. [88]. First, blade modes in vacuo is compared with MBDyn [51] in a fanplot diagram given in Fig. 2.9. The fanplot diagram shows good correlation with the results obtained by MBDyn [89] and results taken from Ref. [88].

Second set of verification is the steady aerodynamics and again compared with MBDyn multibody dynamics code and with the data taken from Ref. [89]. Fig. 2.10 and Fig. 2.11 present the thrust coefficient C_T and power coefficient C_P, which are scaled with rotor solidity σ, as a function of collective pitch angle of the blade. Moreover, polar curve is given in Fig. 2.12, in which horizontal and vertical axes represent the thrust and drag coefficients respectively. Results show good agreement. See also Section 5.4 for additional helicopter aeroservoelastic stability analysis using the same rotor with additional fuselage and control system couplings.

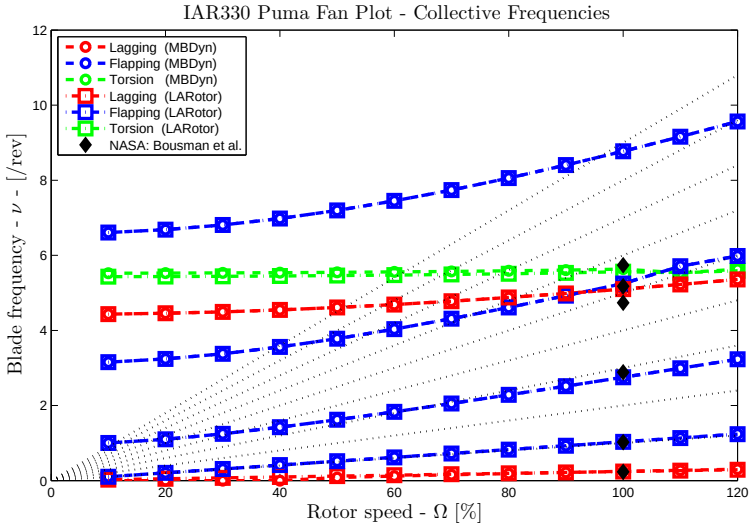

Figure 2.9: *PUMA Rotor Blade: Rotating blade modes for PUMA Helicopter, Comparison with MBDyn Multibody Dynamics Code.*

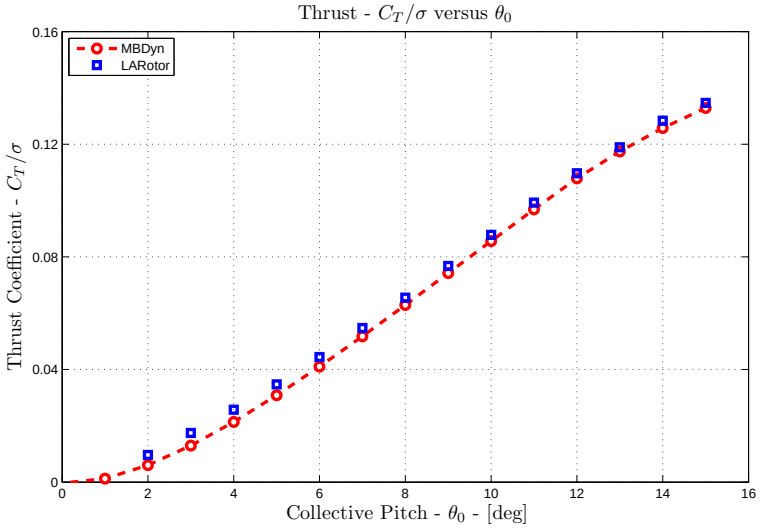

Figure 2.10: *PUMA Rotor Blade: Thrust Coefficient vs Collective pitch, Comparison with MBDyn Multibody Dynamics Code.*

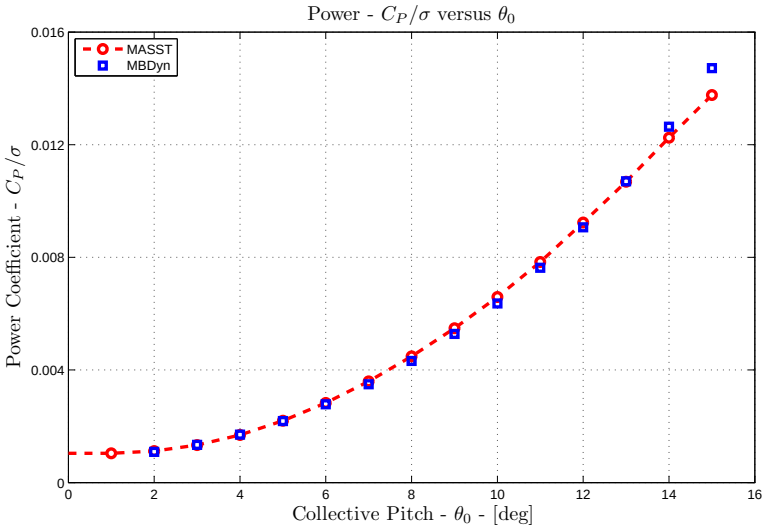

Figure 2.11: *PUMA Rotor Blade: Power Coefficient vs Collective pitch, Comparison with MBDyn Multibody Dynamics Code.*

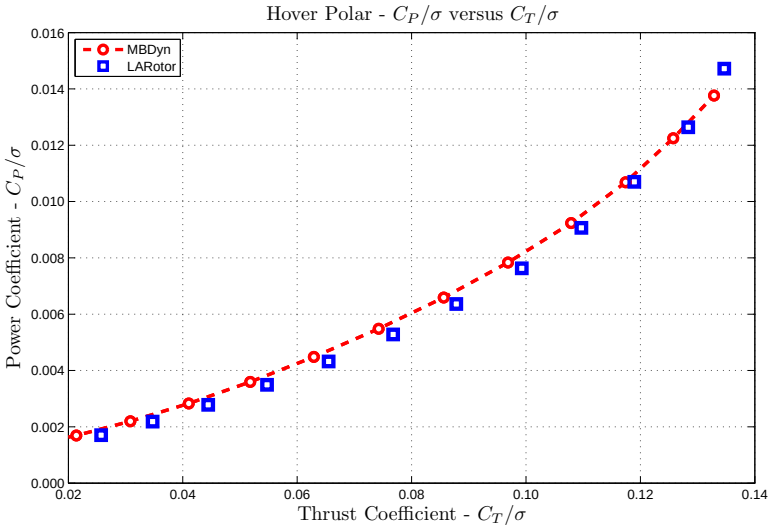

Figure 2.12: *PUMA Rotor Blade: Power Coefficient vs Thrust Coefficient, Comparison with MBDyn Multibody Dynamics Code.*

CHAPTER 3

Linear Time Periodic Systems

3.1 Introduction

Within the usual concept of flight mechanics, in a steady flight aircraft's linear and angular velocity are constant in a body-fixed reference frame. Horizontal flight, turns, and climbs can be considered as steady flight conditions. On the other hand, in a periodic flight condition, some or all of the aircraft's linear and angular velocity components change periodically with a prescribed period. Some types of maneuvers or operation under significant imbalances can be considered in this class.

However, the boundary between being steady and periodic is ambiguous for rotorcraft. Even under the absence of any periodic maneuver or imbalance in the system, rotorcraft are inherently periodic systems due to the dominant characteristic of rotor operation with significant time-periodic effects and thus the system repeats itself after each fundamental period T. There are many problems in which steadiness is spoiled, even if the flight condition or maneuver can be considered as steady. For example, a typical steady flight condition of a fixed-wing aircraft is given in Fig. 3.1. If a rotorcraft performs the

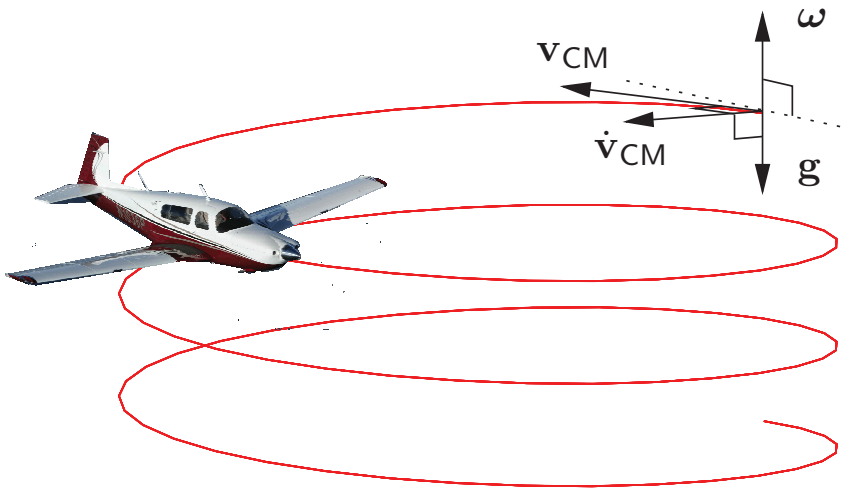

Figure 3.1: *Representation of steady flight.*

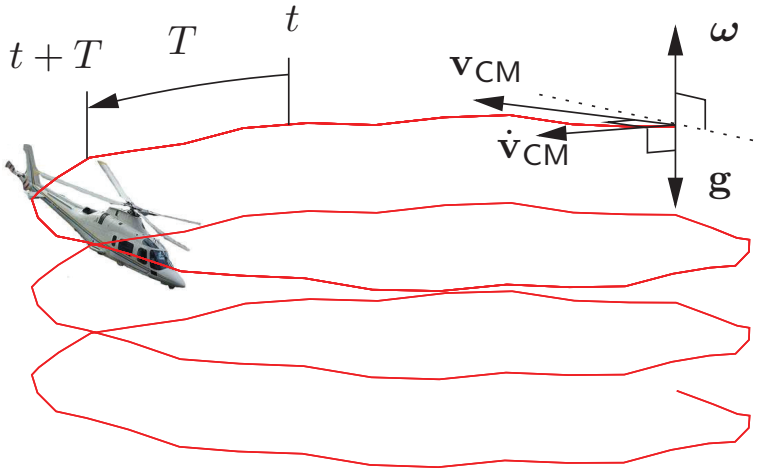

Figure 3.2: *Representation of periodic flight.*

same maneuver as visualized in Fig. 3.2, the trajectory would be wavy and is composed of sub-trajectories those are repeating themselves after each period T. Then, the assumption of steady flight for rotorcraft can imply important simplifications within the periodic nature of rotorcraft. For this reason, stability and sensitivity analyses of such time-periodic systems require additional care and effort as compared to those of constant coefficient systems and specific methodologies have been developed (See Ref. [90] for an overview of the periodic systems and analysis methods for a wide range of problems).

In Chapter 2, an aeroelastic rotor with time-periodic equations of motion is presented together with the sensitivity of the stability parameters for linear time invariant (LTI) systems. Since rotorcraft cannot be not limited to LTI systems; the methods for stability and sensitivity of stability estimates need to be extended for more general cases. The most general case is nonlinear non-autonomous systems and its formulation is given in Chapter 4 whereas linear time periodic systems (LTP) is a significant subset.

This chapter covers the evaluation of periodic stability and the sensitivity of stability parameters of LTP systems. The stability criterion is based on the characteristic exponents or more generally the real part of the eigenvalues of the monodromy matrix of the periodic system following the Floquet's Theory and described in Section 3.2. Parametric sensitivity of the stability properties is formulated in Section 3.3 for a generic rotating dynamical system having periodic coefficients. A demonstration is presented in Section 3.4 using a simple example that has analytical solution. Numerical examples of more complicated problems related to rotorcraft aeroservoelastic stability and sensitivity can be found in Chapter 5.

3.2 Stability of Periodic Structures

One of the most frequently used methods for the stability analysis of linear time periodic (LTP) systems is Floquet's theory, which is also proven to be beneficial in rotorcraft problem. [91]. The theory is based on an extension of the notion of state transition matrix to a transition matrix for periodic orbits, referred to as 'monodromy matrix'. Floquet Theory is a well-know tool in rotorcraft literature; however, we find it beneficial to include here to show the basis of sensitivity formulation.

3.2.1 State Transition Matrix

Considering a dynamical system written in state space from; the equation of motion at any instant of time can be stated with its initial conditions as,

$$\dot{\mathbf{x}} = \mathbf{A}\mathbf{x} \ , \ \mathbf{x}(t_0) = \mathbf{x}_0 \tag{3.1}$$

where the 'dot' operator computes the time derivative, $\mathbf{A}$ is the state space matrix of the dynamical system, $\mathbf{x}$ is the vector of states and $\mathbf{x}_0$, the state at time t_0, is the initial condition. In LTP systems, matrix $\mathbf{A}$ is a periodic function of time, with period T:

$$\mathbf{A}(T + t) = \mathbf{A}(t). \tag{3.2}$$

Given its periodicity, it is necessary and sufficient to determine the relationship between the state of the system at two time values separated by one period T. To formulate the concept, first the state transition matrix $\mathbf{Y}$, which is an integral function of matrix $\mathbf{A}$, is defined for any two states at times t and initial time t_0,

$$\mathbf{x}(t) = \mathbf{Y}(t, t_0)\mathbf{x}(t_0) \tag{3.3}$$

where $\mathbf{Y}(t_0, t_0) = \mathbf{I}$ is the identity matrix by definition. Inserting Eq. 3.3 into Eq. 3.1,

$$\dot{\mathbf{Y}}(t, t_0)\mathbf{x}(t_0) = \mathbf{A}(t)\mathbf{Y}(t, t_0)\mathbf{x}(t_0) \tag{3.4}$$

and thus, for the arbitrariness of the initial state $\mathbf{x}(t_0)$,

$$\dot{\mathbf{Y}}(t, t_0) = \mathbf{A}(t)\mathbf{Y}(t, t_0) \tag{3.5}$$

Integration from the initial time t_0 to a generic time t yields:

$$\mathbf{Y}(t, t_0) = \mathrm{e}^{\int_{t_0}^{t} \mathbf{A}(\tau)\mathrm{d}\tau} \tag{3.6}$$

3.2.2 Monodromy Matrix and Stability

The monodromy matrix $\mathbf{H}$ is defined as the state transition matrix given in Eq. 3.3, evaluated between a reference start time $t = t_0$ and an end time $t = t_0 + T$, corresponding to exactly one period T after the start time, namely:

$$\mathbf{x}(t_0 + T) = \mathbf{Y}(t_0 + T, t_0)\mathbf{x}(t_0) = \mathbf{H}\mathbf{x}_0. \tag{3.7}$$

In the following, $t_0 = 0$ is used without loss of generality, since eigenvalues of the monodromy matrix is independent of the initial time as long as the period is preserved [57]. Once such relationship is defined, as stated in Ref. [84], there is no need to further analyze the system in time, since the evolution of the system between multiples of the period occurs according to the same monodromy matrix. Expressing the state as the product of a vector $\mathbf{q}(t)$ of generalized coordinates and a matrix of orthogonal, time-dependent vectors $\mathbf{U}(t)$, namely $\mathbf{x}(t) = \mathbf{U}(t)\mathbf{q}(t)$, Eq. 3.7 can be written as:

$$\mathbf{U}(T)\mathbf{q}(T) = \mathbf{H}\mathbf{U}(0)\mathbf{q}(0). \tag{3.8}$$

Since the vectors $\mathbf{U}(t)$ are periodic, $\mathbf{U}(T) = \mathbf{U}(0)$, thus:

$$\mathbf{q}(T) = \mathbf{U}(0)^{-1}\mathbf{H}\mathbf{U}(0)\mathbf{q}(0). \tag{3.9}$$

Considering a spectral decomposition[1] of the monodromy matrix, $\mathbf{H} = \mathbf{V}\mathbf{\Theta}\mathbf{V}^{-1}$, and choosing $\mathbf{U}(0) = \mathbf{V}$, one obtains;

$$\mathbf{q}(T) = \mathbf{\Theta}\mathbf{q}(0) \tag{3.10}$$

i.e. the evolution factor of each generalized coordinate over a period is given by the corresponding diagonal element θ_i of the diagonal matrix $\mathbf{\Theta}$. Interpreting it as an exponential evolution over the time T, one obtains $\theta_i = \mathrm{e}^{\lambda_i T}$, with:

$$\lambda_i = \frac{1}{T}\log(\theta_i) = \frac{1}{T}\log(\rho_i \mathrm{e}^{\mathrm{j}\alpha_i}) = \frac{1}{T}\log(\rho_i) + \frac{1}{T}\mathrm{j}\alpha_i \tag{3.11}$$

The periodic system is stable if all the eigenvalues λ_i have negative real part (i.e. when the motion that characterizes each generalized coordinates contracts with time after a period) as in the case of linear time invariant (LTI) dynamical systems [57]. The interpretation of the imaginary part of the periodic eigenvalues may be misleading, as discussed for example in Refs. [92] and [93], since $\alpha_i \pm 2n\pi$ for integer n satisfies Eq. 3.11 as well. However, this work focuses on the stability of the system, which only depends on the value of the real part of the eigenvalues, i.e. the $\log(\rho_i)/T$ term, and thus it is single valued, no further interpretation is required.

[1] Under the assumption that matrix $\mathbf{H}$ can be diagonalized; otherwise, a general orthogonal decomposition, for example the Schur decomposition, can be used.

3.2.3 Computation of Monodromy Matrix

An efficient approach to evaluate the monodromy matrix is Hsu's method of Ref. [94], also reported in Ref. [95], which is followed in this work (See also [96] for other computational schemes). The calculation of the state transition matrix is presented first. Hsu's method computes the state transition matrix of linear non-autonomous (including the special case of LTP) problems in a rather compact form. The method applies to LTP problems of the form $\dot{\mathbf{x}} = \mathbf{A}(t)\mathbf{x}$ by considering a piecewise constant approximation of matrix $\mathbf{A}(t)$, namely $\mathbf{A}(t) \approx \mathbf{A}(\hat{t}) = \hat{\mathbf{A}}$, with $\hat{t}$ suitably chosen as $\hat{t} \in [t_j, t_{j+1}]$. The choice of $\hat{t}$ may influence the results. With the proposed approximation, the state transition matrix is readily obtained in analytical form as

$$\mathbf{Y}(t_{j+1}, t_j) \approx \mathrm{e}^{\hat{\mathbf{A}}(t_{j+1}-t_j)}, \tag{3.12}$$

where the matrix exponential can be evaluated using one of the methods given in Ref. [97]. It may be approximated (e.g. truncated when computed as a matrix power series) to improve the computational efficiency of the method .

To practically compute the monodromy matrix of a LTP problem, the period T can be divided into N smaller time intervals such that $t_{j+1} - t_j = T/N = \Delta t$. The monodromy matrix can be evaluated by multiplying the state transition matrices of each sub-interval,

$$\mathbf{H} = \mathbf{Y}_N \dots \mathbf{Y}_n \dots \mathbf{Y}_0 = \mathrm{e}^{\hat{\mathbf{A}}_N(\Delta t)} \dots \mathrm{e}^{\hat{\mathbf{A}}_n(\Delta t)} \dots \mathbf{I} \tag{3.13}$$

where n is the discrete time step such that $t = n\Delta t$.

3.3 Sensitivity of Characteristic Exponents

The sensitivity of the stability properties is formulated for LTP systems in order to estimate the dependence of stability indicators on system parameters. As explained, analytical formulation is preferred instead of in terms of finite-differences to avoid issues related to sharp changes in sensitivity parameters and to gain the possibility to detect such changes, in order to detect topology changes of the solution and track them using continuation algorithms.

3.3.1 Formulation of Analytical Sensitivity

The eigenvalue problem for a periodic system can be written as;

$$\mathbf{H}\mathbf{v}_i = \mathbf{v}_i\theta_i = \mathbf{v}_i\mathrm{e}^{\lambda_i T} \tag{3.14}$$

where $\mathbf{H}$ is the monodromy matrix, i is the index of the eigenvalue, $\mathbf{v}_i$ is the ith eigenvector, θ_i is the i^{th} eigenvalue of the monodromy matrix, λ_i is the i^{th} evolution parameter of the dynamical system, and T is the period. Differentiating with respect to a generic scalar parameter p gives;

$$\mathbf{H}_{/p}\mathbf{v}_i + \mathbf{H}\mathbf{v}_{i/p} = \left(\mathbf{v}_i\left(\lambda_{i/p}T + \lambda_i T_{/p}\right) + \mathbf{v}_{i/p}\right)\mathrm{e}^{\lambda_i T} \tag{3.15}$$

where, as anticipated, the derivative of period with respect to a parameter, $T_{/p}$, is non-zero if and only if the parameter is related to the angular speed (Ω) of the system, namely:

$$T_{/p} = -\frac{T}{\Omega}\Omega_{/p} \tag{3.16}$$

Rearranging Eq. 3.15 to separate the unknown terms, $\mathbf{v}_{i/p}$ and $\lambda_{i/p}$, from the prescribed ones, one obtains:

$$\left(\mathbf{H} - \mathrm{e}^{\lambda_i T}\mathbf{I}\right)\mathbf{v}_{i/p} + \mathrm{e}^{\lambda_i T}\mathbf{v}_i\lambda_{i/p} = -\left(\mathbf{H}_{/p} - \mathrm{e}^{\lambda_i T}\lambda_i T_{/p}\mathbf{I}\right)\mathbf{v}_i \tag{3.17}$$

If the number of degrees of freedom is n for a given problem, the size of the system of linear Eq. 3.17 is also n. Then, for each eigenvalue λ_i and its corresponding eigenvector $\mathbf{v}_{i/p}$ with size n, a total of $n+1$ unknowns exist. Hence, one more equation is required in addition to system of equations provided by Eq. 3.17. The necessary equation is obtained by the sensitivity of the eigenvector normalization,

$$\mathbf{v}_i^H\mathbf{v}_i = 1 \tag{3.18}$$

where $\mathbf{v}_i^H$ is the conjugate transpose, i.e Hermitian conjugate, of vector $\mathbf{v}_i$. Differentiating with respect to p provides the necessary equation:

$$\mathbf{v}_{i/p}^H\mathbf{v}_i + \mathbf{v}_i^H\mathbf{v}_{i/p} = 0 \;\; (\text{which implies } \; \mathbf{v}_i^H\mathbf{v}_{/p} = 0) \tag{3.19}$$

Now the problem is full rank (provided that the multiplicity of the eigenvalue is 1); hence, the sensitivity of the stability parameters can be evaluated. Combining Eq. 3.17 and Eq. 3.19 in matrix form provides the necessary and sufficient system of equations to estimate the derivatives of the eigenvalue $\lambda_{i/p}$ and of the corresponding eigenvector, $\mathbf{v}_{i/p}$ with respect to parameter p:

$$\begin{bmatrix} \left(\mathbf{H} - \mathrm{e}^{\lambda_i T}\mathbf{I}\right) & \mathrm{e}^{\lambda_i T}\mathbf{v}_i \\ \mathbf{v}_i^H & 0 \end{bmatrix}\begin{Bmatrix} \mathbf{v}_{i/p} \\ \lambda_{i/p} \end{Bmatrix} = \begin{Bmatrix} -\left(\mathbf{H}_{/p} - \mathrm{e}^{\lambda_i T}\lambda_i T_{/p}\mathbf{I}\right)\mathbf{v}_i \\ 0 \end{Bmatrix} \tag{3.20}$$

In this formulation right hand side is should be determined and hence we need the sensitivity of the monodromy matrix.

3.3.2 Sensitivity of the Monodromy Matrix

Recall the monodromy matrix equation:

$$\mathbf{H} = \mathbf{Y}_N \dots \mathbf{Y}_n \dots \mathbf{Y}_0 = \mathrm{e}^{\hat{\mathbf{A}}_N(\Delta t)} \dots \mathrm{e}^{\hat{\mathbf{A}}_n(\Delta t)} \dots \mathbf{I} \tag{3.21}$$

Differentiating the monodromy matrix $\mathbf{H}$ with respect to a generic scalar parameter p using the chain rule gives its sensitivity, $\mathbf{H}_{/p}$,

$$\begin{aligned} \mathbf{H}_{/p} = &\mathbf{Y}_N \mathbf{Y}_{N-1} \dots \mathbf{Y}_n \dots \mathbf{Y}_2 \mathbf{Y}_{1/p} \\ &+ \mathbf{Y}_N \mathbf{Y}_{N-1} \dots \mathbf{Y}_{n/p} \dots \mathbf{Y}_2 \mathbf{Y}_1 \\ &+ \mathbf{Y}_{N/p} \mathbf{Y}_{N-1} \dots \mathbf{Y}_n \dots \mathbf{Y}_2 \mathbf{Y}_1 \end{aligned} \tag{3.22}$$

where the state transition matrix of each sub-interval is given in Eq. 3.12. Then, the sensitivity of the monodromy matrix can be formulated recursively as:

$$\frac{\mathrm{d}}{\mathrm{d}p}\left(\Pi_{i=n}^{1} \mathbf{Y}_i\right) = \mathbf{Y}_n \frac{\mathrm{d}}{\mathrm{d}p}\left(\Pi_{i=n-1}^{1} \mathbf{Y}_i\right) + \mathbf{Y}_{n/p} \Pi_{i=n-1}^{1} \mathbf{Y}_i. \tag{3.23}$$

The sensitivity of the state transition matrix of a sub-step, which is exponential as stated in Eq. 3.12, is:

$$\mathbf{Y}(t_j, t_i)_{/p} \approx \left(\hat{\mathbf{A}}_{n/p} \Delta t + \hat{\mathbf{A}}_n (\Delta t)_{/p}\right) \mathbf{Y}(t_j, t_i) \tag{3.24}$$

Here $\hat{\mathbf{A}}_{/p}$ is the sensitivity of the state space matrix of the dynamical system, evaluated at time $\hat{t}$, with respect to the given parameter p. The derivative of incremental time $(\Delta t)_{/p}$ is zero unless the parameter p affects the size of the time step (e.g. when it is related to the rotor angular speed, $\Omega = 2\pi/T$). In such case:

$$\Delta t_{/p} = \frac{\mathrm{d}}{\mathrm{d}\Omega}\left(\frac{T}{N}\right)\Omega_{/p} = \frac{1}{N}\frac{\mathrm{d}}{\mathrm{d}\Omega}\left(\frac{2\pi}{\Omega}\right)\Omega_{/p} = -\frac{2\pi}{N\Omega^2}\Omega_{/p} = -\frac{\Delta t}{\Omega}\Omega_{/p}. \tag{3.25}$$

3.4 Illustration of the method

This section presents numerical applications of the proposed procedure and verify the stability and sensitivity analysis against an analytical solution. More complex examples related to the rotorcraft can be found in Chapter 5. Consider the homogeneous mass-damper system with a periodic damping term;

$$m\ddot{x} + (c_0 + c_p \cos^2 t)\dot{x} = 0 \tag{3.26}$$

where m is the mass, c_0 is the damping constant and c_p is the periodic damping constants. The system has a period of π radians. The stiffness is not included to achieve an analytical result for the monodromy matrix and in turn eigenvalues of the periodic system. Then, the system can be considered as a first order system with $q = \dot{x}$;

$$m\dot{q} + (c_0 + c_p \cos^2 t)q = 0, \text{ or } \dot{q} = -\frac{(c_0 + c_p \cos^2 t)}{m} q = 0 \tag{3.27}$$

The monodromy matrix (in this case a scalar) can be obtained by integrating Eq. 3.27 for one period T, from $t = 0$ to $t = T$. Let $m = 1$;

$$\frac{q_T}{q_0} = H = \mathrm{e}^{-\int_0^T [c_0 + c_p \cos^2 t] dt} \tag{3.28}$$

leads to:

$$\frac{q_T}{q_0} = H = \mathrm{e}^{-Tc_0 - \frac{T}{2}c_p} \tag{3.29}$$

For one dimensional systems, the eigenvalue is equal to the monodromy matrix. Then:

$$\theta = H = \mathrm{e}^{-Tc_0 - \frac{T}{2}c_p} \tag{3.30}$$

The eigenvalue of the system λ can be obtained from the eigenvalue of the monodromy matrix θ using Eq. 3.11,

$$\lambda = \frac{1}{T}\log(\theta) = \frac{1}{T}\log(\mathrm{e}^{-Tc_0 - \frac{T}{2}c_p}) = -c_0 - \frac{1}{2}c_p \tag{3.31}$$

which is equal to the characteristic exponent in the absence of oscillatory term. If the coefficient of the periodic term, c_p, is considered as the parameter; the sensitivity of the eigenvalue, $\lambda_{/c_p}$, can be analytically obtained as:

$$\lambda_{/c_p} = \frac{1}{2} \tag{3.32}$$

These analytical results are compared with the numerical solutions (named Floquet) obtained using the steps explained in this Chapter. In the numerical solution the only input is the state space matrix as a function of time t and its period T, as given in Eq. 3.27; whereas the rest is estimated by the algorithm following the formulations of this chapter. Fig. 3.3 presents the characteristic exponent obtained by the analytical and numerical methods and Fig. 3.4 gives the corresponding sensitivity of the characteristic exponents. Both results show good correlation.

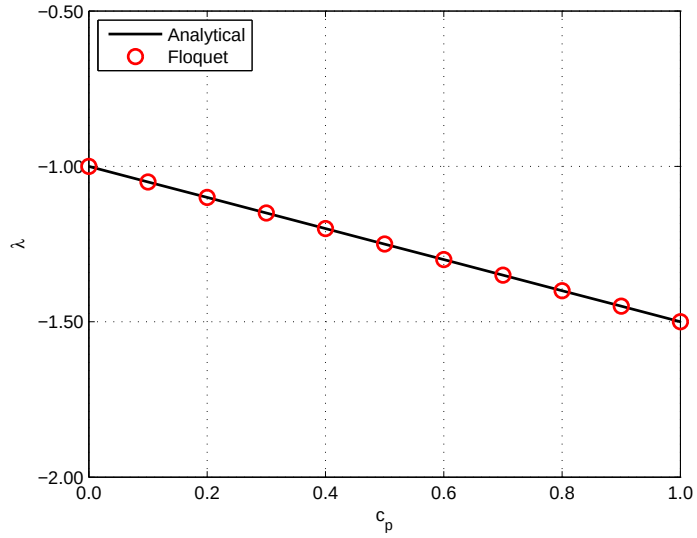

Figure 3.3: *Comparison of the characteristic exponents obtained by analytical solution and numerical method (Floquet)*

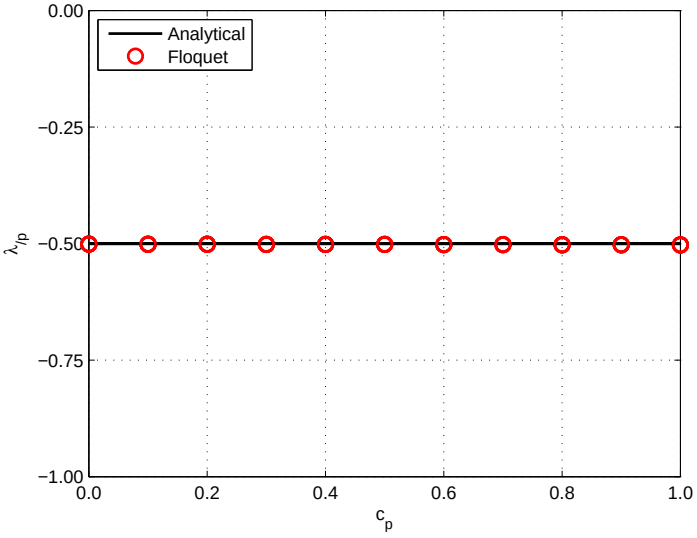

Figure 3.4: *Comparison of the sensitivity characteristic exponents obtained by analytical solution and numerical method (Floquet)*

CHAPTER 4

Nonlinear Non-Autonomous Systems

4.1 Introduction

Stability and sensitivity of stability properties for linear time invariant (LTI) systems is formulated in Chapter 2 and for linear time periodic (LTP) systems in Chapter 3. In order to extend the analysis capability and achieve a generalized aeroservoelastic stability analysis of rotorcraft, the quantitative stability and sensitivity of the stability properties of nonlinear, non-authonomous systems should not be omitted.

When a dynamical system is linear, the system of equations can be written in state space form as;

$$\dot{\mathbf{x}} = \mathbf{A}\mathbf{x}, \qquad \mathbf{x}(t_0) = \mathbf{x}_0 \tag{4.1}$$

with its states $\mathbf{x}$. If matrix $\mathbf{A}$ is non-singular, the trivial solution, $\mathbf{x} = \mathbf{0}$, is the unique equilibrium point and it can be proved that the stability of any solution of system given in Eq. 4.1, is equivalent to the stability of the trivial solution $\mathbf{x} = \mathbf{0}$ and represented by the eigenvalues of $\mathbf{A}$ in LTI systems [98]. The solution of the system either converges to zero (all eigenvalues have negative real part), diverges (all

the eigenvalues have positive real part), follows a periodic orbit (purely imaginary eigenvalues) or behaves in combination of these (some eigenvalue are positive some are negative or eigenvalues with both real and imaginary parts) [99]. The trajectories are entirely dependent on the initial conditions [100], but this does not change the stability characteristics. Same remarks are true for linear time periodic systems in which state space matrix $\mathbf{A}$ is replaced by monodromy matrix $\mathbf{H}$ (see Section 3.2).

On the other hand, the relation between the states $\mathbf{x}$ and its time derivative $\dot{\mathbf{x}}$ cannot be limited to linear functions:

$$\dot{\mathbf{x}} = \mathbf{f}\left(\mathbf{x}, t\right), \qquad \mathbf{x}(t_0) = \mathbf{x}_0 \tag{4.2}$$

where $\mathbf{f}$ is the function that governs the system and can include relations which cannot assumed to be linear. Nonlinear systems are more complicated and require deeper understanding. First of all, there can exist more than one equilibrium solution[1], and the trivial solution may or may not be one of them [99]. Therefore stability is not a global property. Moreover there are more complex behaviors such as limit cycle oscillations (LCO) which are defined as isolated closed trajectories of nonlinear dynamical systems. When an LCO develops, the system oscillates in a self-sustained manner without the need of an external input [100]. The difference between LCO and the periodic oscillations of linear systems is that the amplitude of an LCO depends entirely on the structure of the system, not to the initial conditions. Chaos is another strange behavior, an unpredictable, unstable but bounded motion [99]. Indeed, unlike linear systems, there is no correlation between boundedness and stability of a solution of a non-linear system [98]. These phenomena, which may have significant effects on the performance of the design if they occur, can be detected if the nonlinearities of the system are preserved [8, 101, 102].

Current state of art literature on rotorcraft aeroelastic stability analysis relies on LTI and LTP systems and approaches the problem by either using a constant coefficient approximation or by computing the eigenvalues of the monodromy matrix according to Floquet Theory. The former neglects periodicity and the latter is only applicable to the perturbation of the problem about a periodic orbit. Although these techniques may successfully represent the dynamics of many flight conditions, the equations of motion governing the rotorcraft dynamics are

[1] Broadly speaking, equilibrium may not exist for a nonlinear system; however, such systems are not considered within stability theory and thus out of the scope of this work

generally described by nonlinear, non-autonomous equations [65]. For these reasons, it is expected to gain great benefit in extending the rotorcraft stability analysis to capture nonlinear and time-variant effects. Being more general, Lyapunov Characteristic Exponents (LCEs) can provide a common environment in rotorcraft aeroelastic stability among both linear and nonlinear systems, and be applicable to all problems that can be proficiently analyzed by time marching analysis, including experimental data.

Analytical sensitivity of stability properties, as presented in Section 2.8 for LTI and in Section 3.3 for LTP systems, can be formulated for nonlinear non-autonomous systems using Lyapunov's theory. The parametric sensitivity of LCEs can provide a methodology for robustness analysis and design of dynamical systems with complexity level varying from LTI to nonlinear, non-autonomous. An analytical formulation of the sensitivity of the stability properties, instead of in terms of finite-differences, can help avoiding issues related to sharp changes in sensitivity parameters and to gain the possibility to detect such changes, in order to detect topology changes of the solution and track them using continuation algorithms.

Section 4.2 introduces Lyapunov Characteristic Exponents (LCEs) and presents the formulation of the evaluation of aeroservoelastic rotorcraft stability based on QR decomposition method. Some aspects of characteristic exponents estimation for problems with complex conjugate modes, which are common in aerospace systems, are discussed. Then Section 4.3 describes the analytical estimation of the sensitivity of the stability of trajectories based on Lyapunov characteristic exponents formulated using the discrete QR decomposition method. Finally, Section 4.4 presents the illustration with further discussion of LCEs on a damped oscillator problem including analytical solution. Both LCEs and sensitivity of LCEs are estimated and multiplicity of LCEs are discussed. More advanced analyses related to rotorcraft are available in Chapter 5.

4.2 Stability Estimation Using Lyapunov Characteristic Exponents

The stability of a dynamical system is related to the evolution of a solution after perturbation [103]. The practical, quantitative way of measuring stability depends on whether a system is autonomous (i.e. not explicitly dependent on time) and linear. Stability of linear, time

invariant (LTI) systems can simply be inferred from the eigenvalues of the state space matrix, namely its spectrum. The problem is more complex when the system is linear and non-autonomous, but time periodic (LTP), i.e. the state space matrix has periodic coefficients. The stability of LTP systems is evaluated by computing the eigenvalues of the monodromy matrix, namely the state transition matrix over one period as described in Chapter 3. For nonlinear, autonomous problems, the eigenvalues and eigenvectors of the linearized system computed at the coordinates of the phase plane corresponding to a steady solution provides the local information about the behavior of the system in the neighborhood of that solution. Once these points are evaluated and connected for the whole phase plane, geometric understanding of the system is possible. However, for problems having higher dimensions, geometric understanding is not so easy to interpret and quantitative way of measuring is necessary.

LTI and LTP problems typically result from linearization of nonlinear, non-autonomous problems about a steady (both LTI and LTP) or a periodic (LTP only) reference solution. LTP systems find several applications in the analysis of problems related to rotary-wing aircraft as a consequence of the intrinsic periodicity of rotor motion and LTI system analysis can usually provide sufficient approximation for LTP problems. However, broadly speaking, periodic problems only occur under strict assumptions; for example, the motion of a helicopter is periodic only during idealized steady, coordinated maneuvers. Besides, they require the existence of such solution, and the capability to define and compute it.

Obtaining a steady or periodic solution by numerical integration in time requires that solution to be stable, so the study of the stability of the solution is actually the study of *how much stable it is*, i.e. of its stability margin. A method that does not require a special reference solution (i.e. a stable point or a stable orbit) and simplifications but, on the contrary, provides indications about the existence of an *attractor*, being it a point, a periodic orbit or a higher-order solution (e.g. a multidimensional torus), while computing the evolution of the system towards it, would give valuable insight into the system properties and, at the same time, provide a viable and practical means for its analysis.

Lyapunov Characteristic Exponents (LCEs) are indicators of the nature and of the stability properties of solutions of differential equations (see for example Refs. [58, 98] and references therein). They define the spectrum of the related Cauchy (initial value) problem. Lyapunov the-

ory can be applied to nonlinear non-autonomous systems; hence, they represent a natural generalization of stability indicators that are familiar in current engineering practice. The stability of trajectories in state space can be estimated while computing their evolution. Nonlinearities are always present in any dynamical system including rotorcraft, and should be checked for stability. Hence the use of LCEs in analyzing rotorcraft stability is believed to provide a common stability analysis platform for dynamical rotorcraft systems having different levels of complexity.

4.2.1 Lyapunov Exponents for Non-Autonomous Problems

This section recalls the definition of non-autonomous problems and of the so-called Lyapunov Characteristic Exponents as a measure of its spectrum and the numerical procedure used in this study for their estimation. In engineering practice, differential problems of the form,

$$\dot{\mathbf{x}} = \mathbf{f}\left(\mathbf{x}, t\right), \qquad \mathbf{x}(t_0) = \mathbf{x}_0 \tag{4.3}$$

arise often. Special cases occur when the problem is linear, i.e. $\mathbf{f}(\mathbf{x}, t) = \mathbf{A}(t)\mathbf{x}(t)$, or even periodic, i.e. linear with $\mathbf{A}(t+T) = \mathbf{A}(t)$ for a given constant T, $\forall t$. Autonomous problems arise when $\mathbf{f}(\mathbf{x})$ does not explicitly depend on time t; a special case occurs when the problem is linear, i.e. $\mathbf{f}(\mathbf{x}) = \mathbf{A}\mathbf{x}$. In the latter case, the spectrum of the problem is clearly represented by the eigenvalues of matrix $\mathbf{A}$. In the other cases, its definition is less intuitive.

Given the problem $\dot{\mathbf{x}} = \mathbf{f}(\mathbf{x}, t)$, with the state $\mathbf{x} \in \mathbb{R}^n$, the time $t \in \mathbb{R}$, and the nonlinear non-autonomous function $\mathbf{f} \in \mathbb{R}^{n+1} \to \mathbb{R}^n$, and a solution $\mathbf{x}(t)$ for given initial conditions $\mathbf{x}(0) = \mathbf{x}_0$, the Lyapunov Characteristic Exponents λ_i are defined as:

$$\lambda_i = \lim_{t\to\infty} \frac{1}{t} \log \frac{\|{}_i\mathbf{x}(t)\|}{\|{}_i\mathbf{x}(t_0)\|} \tag{4.4}$$

where ${}_i\mathbf{x}(t)$ is the solution that describes the exponential evolution of the i-th axis of the ellipsoid that grows from an initially infinitesimal n-sphere according to the map $\mathbf{f}_{/\mathbf{x}}$ tangent to $\mathbf{f}$ along the fiducial trajectory $\mathbf{x}(t)$, i.e. the solution of the linear, non-authonomous problem ${}_i\dot{\mathbf{x}}(t) = \mathbf{f}_{/\mathbf{x}}(\mathbf{x}(t), t)\,{}_i\mathbf{x}(t)$, with ${}_i\mathbf{x}(t_0) = {}_i\mathbf{x}_0$.

Eq. 4.4 can be written in a simpler form. We can split the log

function of Eq. 4.4 as,

$$\lambda_i = \lim_{t\to\infty} \frac{1}{t}\left(\log \|_i\mathbf{x}(t)\| - \log \|_i\mathbf{x}(t_0)\| \right) \tag{4.5}$$

which is equal to:

$$\lambda_i = \lim_{t\to\infty} \frac{1}{t} \log \|_i\mathbf{x}(t)\| - \lim_{t\to\infty} \frac{1}{t} \log \|_i\mathbf{x}(t_0)\| \tag{4.6}$$

The second limit involves a constant $\|_i\mathbf{x}(t_0)\|$ divided by time t as $t \to \infty$, which is clearly zero. Then, the definition of LCEs can be reduced to a more compact form:

$$\lambda_i = \lim_{t\to\infty} \frac{1}{t} \log \|_i\mathbf{x}(t)\| \tag{4.7}$$

The definition involves the limit for $t \to \infty$; hence, in practice LCEs can only be numerically estimated for a sufficiently large value of t. In this study, unless explicitly stated, with the term "LCEs" we refer to their estimation using a large enough value of t.

LCEs represent a measure of the rate of growth of perturbed solutions. Consider infinitesimal, independent perturbations of the states with respect to a solution $\mathbf{x}(t)$ of Eq. 4.7 (the fiducial trajectory). The perturbed solution can be computed in terms of the state transition matrix $\mathbf{Y}(t, t_0)$, which is the matrix that relates two states at t_0 and t, i.e $\mathbf{x}(t) = \mathbf{Y}(t, t_0)\mathbf{x}(t_0)$. Considering $\mathbf{A}(\mathbf{x}, t) = \mathbf{f}_{/\mathbf{x}}$ gives:

$$\dot{\mathbf{Y}}(t, t_0) = \mathbf{A}(\mathbf{x}, t)\mathbf{Y}(t, t_0), \qquad \mathbf{Y}(t_0, t_0) = \mathbf{I} \tag{4.8}$$

According to the Ostrogradskiĭ-Jacobi-Liouville formula [98], the determinant of $\mathbf{Y}(t, t_0)$ (the *Wronskian determinant* of the independent solutions that constitute $\mathbf{Y}(t, t_0)$) is,

$$\det\left(\mathbf{Y}(t, t_0)\right) = \det\left(\mathbf{Y}(t_0, t_0)\right) \mathrm{e}^{\int_{t_0}^{t} \mathrm{tr}(\mathbf{A}(\tau))\ \mathrm{d}\tau} \tag{4.9}$$

where $\mathrm{tr}(\cdot)$ is the trace operator. Thus, the Wronskian never vanishes when $\mathbf{A}(t)$ is regular in $[t_0, t]$, since $\mathbf{Y}(t_0, t_0) \equiv \mathbf{I}$. The Wronskian geometrically represents the evolution in time of the volume of an infinitesimal portion of the state space.

The evolution of an arbitrary perturbation $_i\mathbf{x}(t_0) = {}_i\mathbf{x}_0$ is $_i\mathbf{x}(t) = \mathbf{Y}(t, t_0)\,{}_i\mathbf{x}_0$. As such, the contraction or expansion rate along the direction of $_i\mathbf{x}$ is estimated by considering:

$$\left(\mathrm{e}^{\chi_i t}\right)^2 = \lim_{t\to\infty} \frac{{}_i\mathbf{x}^T\,{}_i\mathbf{x}}{{}_i\mathbf{x}_0{}^T\,{}_i\mathbf{x}_0} \tag{4.10}$$

Consider now the singular value decomposition (SVD) of $\mathbf{\Phi}(t, t_0)$,

$$\mathbf{U}\mathbf{\Sigma}\mathbf{V}^T = \mathbf{\Phi}(t, t_0) \tag{4.11}$$

where $\mathbf{U} = \mathbf{U}(t)$ and $\mathbf{V} = \mathbf{V}(t)$ are orthogonal matrices. The singular values σ_i, namely the diagonal elements of $\mathbf{\Sigma} = \mathbf{\Sigma}(t)$, which are strictly greater than zero as a consequence of the above mentioned Ostrogradskiĭ-Jacobi-Liouville formula[2], express the growth of the perturbed solution along orthogonal directions in the state space.

The LCEs can also be interpreted as the limit for $t \to \infty$ of the logarithm of the singular values, σ_i, divided by the time itself[3] [58]. In fact, using the SVD to express the state transition matrix, Eq. 4.10 becomes,

$$\left(\mathrm{e}^{\chi_i t}\right)^2 = \lim_{t\to\infty} \frac{{}_i\mathbf{x}_0{}^T \mathbf{V}\mathbf{\Sigma}^2\mathbf{V}^T {}_i\mathbf{x}_0}{{}_i\mathbf{x}_0{}^T {}_i\mathbf{x}_0} \tag{4.13}$$

and independently considering perturbations ${}_i\mathbf{x}_0$ along the directions represented by the columns of $\mathbf{V}$, ${}_i\mathbf{x}_0 = \mathbf{V}_i$, one obtains

$$\chi_i = \lim_{t\to\infty} \frac{\log(\sigma_i)}{t} = \lambda_i. \tag{4.14}$$

So-called continuous formulas for the estimation of the LCEs can be derived from the definition based on the SVD, as well as on the QR decomposition (see for example [104]).

4.2.2 Numerical Estimation of LCEs

The definitions of Eqs. 4.7 and 4.14 can hardly be applied to the practical estimation of LCEs, because orthogonalization is needed to prevent the solution for each axis of the ellipsoid from interfering with the others. Numerical methods have been devised for this purpose. One of the most popular algorithm is QR decomposition and both continuous and discrete versions are available. The continuous QR method is not competitive with the discrete version [104], however it is also covered briefly for the sake of completeness.

[2] After choosing $\mathbf{Y}(t_0, t_0) = \mathbf{I}$, its determinant is 1; the integral of matrix $\mathbf{A}(t)$ is finite, and thus its exponential is a strictly positive number.

[3] In Ref. [58], the actual definition is

$$\lambda_i = \lim_{t\to\infty} \frac{\log(\sigma_i^2)}{2t}, \tag{4.12}$$

where σ_i^2 are the eigenvalues of $\mathbf{\Phi}^T(t, t_0)\mathbf{\Phi}(t, t_0) = \mathbf{V}\mathbf{\Sigma}^2\mathbf{V}^T$.

Continuous QR Method

The continuous method follows QR decomposition of Eq. 4.8. $\mathbf{Y} = \mathbf{QR}$ leads to,

$$\dot{\mathbf{Q}}(t)\mathbf{R}(t) + \mathbf{Q}(t)\dot{\mathbf{R}}(t) = \mathbf{A}(t)\mathbf{Q}(t)\mathbf{R}(t), \qquad \mathbf{Q}(0)\mathbf{R}(0) = \mathbf{I} \tag{4.15}$$

where columns of $\mathbf{Y}$ are the branches of solutions, $\mathbf{Q}$ is orthonormal matrix and $\mathbf{R}$ is an upper triangular matrix with positive diagonal elements. Skipping the details of matrix manipulations together with the properties of triangular matrices (see for example Ref. [105] for details) leads to:

$$\lambda_i = \lim_{t\to\infty} \frac{1}{t} \log \mathbf{R}_{ii}(t) = \lim_{t\to\infty} \frac{1}{t} \int_0^t \mathbf{H}_{ii}(s)ds, \quad \mathbf{H}_{ii} = (\mathbf{Q}^T\mathbf{A}\mathbf{Q})_{ii} \tag{4.16}$$

Discrete QR Method

Continuous formulas of LCE estimation suffer from the numerical difficulty of dealing with matrices whose coefficients either rapidly converge to zero or diverge. For this reason, different approaches have been formulated. The popular *discrete* QR method is based on incrementally updating the LCEs estimates with the diagonal elements of matrix $\mathbf{R}$ obtained from the QR decomposition of the state transition matrix between two consecutive time steps.

Given the state transition matrix $\mathbf{Y}(t, t_{j-1})$ from time t_{j-1} to an arbitrary time t as the solution of the problem $\dot{\mathbf{Y}} = \mathbf{f}_{/\mathbf{x}}(\mathbf{x}(t), t)\mathbf{Y}$ with $\mathbf{Y}(t_{j-1}, t_{j-1}) = \mathbf{I}$, set $\mathbf{Y}_j = \mathbf{Y}(t_j, t_{j-1})$. Consider then the QR decomposition of $\mathbf{Y}_j\mathbf{Q}_{j-1}$, which implies $\mathbf{Q}_j\mathbf{R}_j = \mathbf{Y}_j\mathbf{Q}_{j-1}$. Now, after defining $\mathbf{R}_{\Pi_j} = \Pi_{k=0}^{j}\mathbf{R}_{j-k}$, one can show that:

$$\mathbf{Y}_j\mathbf{Q}_{j-1}\mathbf{R}_{\Pi_{j-1}} = \mathbf{Q}_j\mathbf{R}_j\mathbf{R}_{\Pi_{j-1}} = \mathbf{Q}_j\mathbf{R}_{\Pi_j} \tag{4.17}$$

This way, $\mathbf{Y}_j\mathbf{Q}_{j-1}\mathbf{R}_{\Pi_{j-1}}$ can be used to construct $\mathbf{R}_{\Pi_j}$ by only considering incremental QR decompositions over $\mathbf{Y}_j\mathbf{Q}_{j-1}$, i.e. with limited contraction/expansion. The LCEs are then estimated from $\mathbf{R}_{\Pi_j}$ as,

$$\lambda_i = \lim_{j\to\infty} \frac{1}{t_j} \log r_{ii}(t_j) \tag{4.18}$$

where $j \in \mathbb{N}$ and $r_{ii}(t_j)$ are the diagonal elements of matrix $\mathbf{R}(t_j) = \mathbf{R}_{\Pi_j}$. Since the product of two upper triangular matrices $\mathbf{C} = \mathbf{AB}$ is also an upper triangular matrix, the diagonal elements are $c_{ii} =$

$a_{ii}b_{ii}$. Thus the logarithm of c_{ii} can be incrementally computed as $\log(a_{ii}b_{ii}) = \log(a_{ii}) + \log(b_{ii})$. This helps preventing overflow/underflow in numerical computations. Furthermore,

$$r_{ii}(t_j) = \Pi_{k=0}^{j} r_{(j-k)_{ii}} \tag{4.19}$$

thus,

$$\log\left(r_{ii}(t_j)\right) = \sum_{k=0}^{j} \log(r_{k_{ii}}) \tag{4.20}$$

which leads to:

$$\lambda_i = \lim_{j\to\infty} \frac{1}{t_j} \sum_{k=0}^{j} \log(r_{k_{ii}}) \tag{4.21}$$

4.2.3 Computation of State Transition Matrix

The state transition matrix is required in discrete QR decomposition method; hence, numerical integration is necessary to obtain it. For a small enough time step, Eq. 4.3 is linearized,

$$\boldsymbol{\delta}\dot{\mathbf{x}} = \mathbf{A}(\mathbf{x}(t), t)\boldsymbol{\delta}\mathbf{x} \tag{4.22}$$

where $\mathbf{A} = \mathbf{f}_{/\mathbf{x}}$, partial derivative of nonlinear function $\mathbf{f}$ with respect to state space variables $\mathbf{x}$. Generally, since $\mathbf{f}$ can be any nonlinear function of the trajectory $\mathbf{x}_j$ and time t, integration of state transition matrix require the knowledge of the trajectory, i.e. the differential equation needs to be integrated. Numerical integration of differential equations is a straightforward task and skipped here. On the other hand, computation of state transition matrix is given to clearly state the procedure. In this study, two practical methods are considered for computing state transition matrix. *One-lag trapezoid rule integration* is used to compute state transition matrix for any type of problem from linear to nonlinear non-autonomous. The other one is the *Hsu's Method*, which is used only for linear problems.

One-Lag Trapezoid Rule Integration

As explained in [106], under the assumption that a constant integration time step h is used, define the state $\mathbf{x}$ and its derivative $\dot{\mathbf{x}}$ at time t_j

as the average of and the difference between the values of the state ± half of the time step forward and backward;

$$\begin{aligned} \mathbf{x}_j &= \frac{\mathbf{x}_{j+1/2} - \mathbf{x}_{j-1/2}}{2}, \\ \dot{\mathbf{x}}_j &= \frac{\mathbf{x}_{j+1/2} - \mathbf{x}_{j-1/2}}{h} \end{aligned} \tag{4.23}$$

which corresponds to using a one-leg trapezoid rule-like approximation of the state and its derivative. Discretizing Eq. 4.22 at time t_j, using the expressions of $\mathbf{x}_j$ and $\dot{\mathbf{x}}$ from Eq. 4.25, and solved for $\mathbf{x}_{j+1/2}$, yields:

$$\mathbf{x}_{j+1/2} = \left(\mathbf{I} + \frac{h}{2}\mathbf{A}_j\right)^{-1} \left(\mathbf{I} - \frac{h}{2}\mathbf{A}_j\right) \mathbf{x}_{j-1/2} \tag{4.24}$$

implies:

$$\mathbf{Y}(t, t_j) = \left(\mathbf{I} + \frac{h}{2}\mathbf{A}_j\right)^{-1} \left(\mathbf{I} - \frac{h}{2}\mathbf{A}_j\right) \tag{4.25}$$

This equation is required to be integrated together with the Eq. 4.3 if $\mathbf{f}$ is nonlinear. For LTI systems, the state transition matrix is independent of the trajectory $\mathbf{x}(t)$, hence there is no need to integrate Eq. 4.3. It should be noted that this method is 2^{nd} order accurate, unconditionally stable (A-stable) with no algorithmic dissipation.

Integration Using Hsu's Method

When Hsu's method [94] is used to compute the state transition matrix, the formulation can be written in a more compact form. The method is applied by considering a piecewise constant approximation of matrix $\mathbf{A}(\mathbf{x}, t)$, namely $\mathbf{A}(\mathbf{x}, t) \approx \mathbf{A}(\hat{\mathbf{x}}, \hat{t}) = \hat{\mathbf{A}}$ with $\hat{t} \in [t_j, t_{j+1}]$ and $\hat{\mathbf{x}} = \mathbf{x}(\hat{t})$. The choice of $\hat{t}$ may influence the results. Then, the state transition matrix is readily obtained as,

$$\mathbf{Y}(t, t_j) \approx \mathrm{e}^{\hat{\mathbf{A}}(t - t_j)} \tag{4.26}$$

where the matrix exponential may be approximated (e.g. truncated when computed as a matrix power series) to improve the computational efficiency of the method[4].

[4] In fact, one can show using Neumann series [107] that the trapezoidal rule given in Eq. 4.25 is a second order approximation to $e^{\mathbf{A}(t-t_j)}$.

4.3 Sensitivity of Lyapunov Exponent Estimates

The analytical sensitivity problem is based on the Discrete QR method, which exploits the QR decomposition of the state transition matrix of a differential problem using the tangent manifold of the so-called *fiducial trajectory*. Such sensitivity can be useful to gain insight into the dependence of stability indicators on system parameters, or can be integrated into gradient-based (or gradient-aware) optimization procedures, or into uncertainty evaluation problems. The motivation of focusing on analytical sensitivity is the capability to capture abrupt changes in the stability properties of the system. This is typically the case when the topology of the solution changes. For example when dealing with linear systems, for parameter values that make some of the eigenvalues locally coincident, or when a pair of complex conjugate eigenvalues turn into two separate real ones; or in nonlinear systems appearance of new or disappearance of existing equilibrium points at some characteristic value of a parameter.

The sensitivity of LCE estimates is obtained using the discrete QR method can be practically performed in a cascaded manner:

- the sensitivity of the LCEs is expressed as a function of the sensitivity of the diagonal elements of matrix $\mathbf{R}$;
- the sensitivity of matrix $\mathbf{R}$ is computed as a function of the sensitivity of submatrices $\mathbf{R}_j$ resulting from the piecewise integration of the problem from time step t_{j-1} to t_j, $\mathbf{Y}_j$: $\dot{\mathbf{Y}} = \mathbf{A}\mathbf{Y}$, $\mathbf{Y}_0 = \mathbf{Y}_{j-1}$;
- the sensitivity of each submatrix is computed from the sensitivity of the piecewise solutions of the problem, $\mathbf{Y}_{j/p}$;
- the computation of the sensitivity matrix $\mathbf{Y}_{j/p}$ is written in form of a self-adjoint problem, to minimize the number of time integrations regardless of the number of parameters for which sensitivity is sought.

Consider a set of bounded parameters $\mathbf{p} \in \mathcal{P}$, and assume that the problem $\dot{\mathbf{x}} = \mathbf{f}(\mathbf{x}, t, \mathbf{p})$ depends on parameters $\mathbf{p}$. The sensitivity of the LCEs with respect to a generic parameter $p \subset \mathbf{p}$, using the form of Eq. 4.18, is:

$$\lambda_{i/p} = \lim_{t\to\infty} \frac{1}{t} \frac{r_{ii/p}(t)}{r_{ii}(t)} \tag{4.27}$$

The capability to compute the sensitivity of matrix $\mathbf{R}$, namely $\mathbf{R}_{/p}$, is obviouslSy needed. Recalling the definition of $\mathbf{R}(t_j) = \mathbf{R}_{\Pi_j}$ as formulated within the discrete QR algorithm, its sensitivity is:

$$\mathbf{R}_{/p}(t_j) = \sum_{k=0}^{j} \left(\Pi_{n=0}^{k-1}\mathbf{R}_{j-n}\right) \mathbf{R}_{k/p} \left(\Pi_{n=k+1}^{j}\right) \mathbf{R}_{j-n} \tag{4.28}$$

Since $\mathbf{R}(t_j) = \mathbf{R}_j\mathbf{R}(t_{j-1})$, the update of $\mathbf{R}_{/p}$ can be incrementally computed according to,

$$\mathbf{R}_{/p}(t_j) = \mathbf{R}_{j/p}\mathbf{R}(t_{j-1}) + \mathbf{R}_j\mathbf{R}_{/p}(t_{j-1}) \tag{4.29}$$

thus the accumulation of the perturbation is straightforward. Alternatively, using the form of Eq. 4.21, the sensitivity of LCEs can also be expressed as:

$$\lambda_{i/p} = \lim_{j\to\infty} \frac{1}{t_j} \sum_{k=1}^{j} \frac{r_{k_{ii}/p}}{r_{k_{ii}}} \tag{4.30}$$

In this case, only the sensitivity of $\mathbf{R}_j$ is needed, which is obtained in the next section by computing the sensitivity of the QR decomposition.

4.3.1 Sensitivity of QR Decomposition

The sensitivity of the QR decomposition can be obtained along the lines of the state transition matrix with differentiation of QR decomposition that is used to formulate the continuous QR method for LCE estimation (see for example [58,108]). Consider the QR decomposition of an arbitrary matrix[5] $\mathbf{M} \in \mathbb{R}^{n\times n}$,

$$\mathbf{M} = \mathbf{QR} \tag{4.31}$$

with orthogonal $\mathbf{Q}$, i.e. $\mathbf{Q}^T\mathbf{Q} = \mathbf{I}$, and $\mathbf{R}$ upper triangular, with positive diagonal elements. Next, take the derivative of $\mathbf{M}$ with respect to a scalar parameter p,

$$\mathbf{M}_{/p} = \mathbf{Q}_{/p}\mathbf{R} + \mathbf{QR}_{/p} \tag{4.32}$$

and the derivative of the orthogonality condition $\mathbf{Q}^T\mathbf{Q} = \mathbf{I}$,

$$\left(\mathbf{Q}^T\right)_{/p}\mathbf{Q} + \mathbf{Q}^T\mathbf{Q}_{/p} = \mathbf{0} \tag{4.33}$$

[5]Indeed, in LCE estimates the matrix $\mathbf{M} = \mathbf{Y}_j\mathbf{Q}_{j-1}$, i.e. equals to the state transition matrix $\mathbf{Y}_j$ multiplied by an orthonormal matrix of previous step $\mathbf{Q}_{j-1}$

i.e.

$$\left(\mathbf{Q}^T\mathbf{Q}_{/p}\right)^T + \mathbf{Q}^T\mathbf{Q}_{/p} = \mathbf{0} \tag{4.34}$$

The latter condition states that $\mathbf{Q}^T\mathbf{Q}_{/p}$ must be skew-symmetric; thus, only $n(n-1)/2$ coefficients are independent (for example, those in the strictly lower triangular portion, i.e. the lower triangular part, excluding the diagonal). Finally, premultiply $\mathbf{M}_{/p}$ by $\mathbf{Q}^T$:

$$\mathbf{R}_{/p} = \mathbf{Q}^T\mathbf{M}_{/p} - \mathbf{Q}^T\mathbf{Q}_{/p}\mathbf{R} \tag{4.35}$$

Since matrix $\mathbf{R}_{/p}$ is upper triangular, the whole problem can be re-cast in the form:

$$\begin{aligned}
&\text{compute} && \mathbf{W} = \mathbf{Q}^T\mathbf{Q}_{/p} && \text{(4.36a)}\\
&\text{such that} && \text{stril}\left(\mathbf{Q}^T\mathbf{M}_{/p} - \mathbf{W}\mathbf{R}\right) = \text{stril}\left(\mathbf{0}\right) && \text{(4.36b)}\\
&\text{subjected to} && \mathbf{W}^T + \mathbf{W} = \mathbf{0} && \text{(4.36c)}\\
&\text{compute} && \mathbf{R}_{/p} && \text{(4.36d)}\\
&\text{such that} && \text{triu}\left(\mathbf{R}_{/p}\right) = \text{triu}\left(\mathbf{Q}^T\mathbf{M}_{/p} - \mathbf{W}\mathbf{R}\right) && \text{(4.36e)}\\
&\text{and} && \text{stril}\left(\mathbf{R}_{/p}\right) = \text{stril}\left(\mathbf{0}\right) && \text{(4.36f)}
\end{aligned}$$

where the operator triu$(\cdot)$ extracts the upper triangular part of the argument and the operator stril$(\cdot)$ extracts the strictly lower triangular[6] part of the argument. The statement 4.36f is redundant since $\mathbf{W}$, computed according to the Eqs. 4.36a–c, already yields $\mathbf{R}_{/p}$ with the strictly lower triangular part set to zero.

It is worth noticing that, since $\mathbf{R}$ is upper triangular, the matrix $\mathbf{W}$ is computed as,

$$\mathbf{W}_L = \text{stril}\left(\mathbf{Q}^T\mathbf{M}_{/p}\mathbf{R}^{-1}\right) \qquad \mathbf{W} = \mathbf{W}_L - \mathbf{W}_L^T \tag{4.37}$$

where $\mathbf{R}^{-1}$ does not require any factorization, but only back-substitution. In fact, after setting $\mathbf{B} = \mathbf{Q}^T\mathbf{M}_{/p}$, the generic coefficient of stril$(\mathbf{W})$ is:

$$w_{ij} = \frac{1}{r_{jj}}\left(b_{ij} - \sum_{k=1}^{j-1} w_{ik}r_{kj}\right) \qquad j = 1, n-1 \qquad i = j+1, n \tag{4.38}$$

[6]Strictly lower refers to the elements below the main diagonal

Then:

$$\mathbf{Q}_{/p} = \mathbf{Q}\mathbf{W} \tag{4.39}$$

The discrete QR method requires the decomposition of $\mathbf{Y}_j\mathbf{Q}_{j-1}$; thus, the sensitivity of $\mathbf{M} = \mathbf{Y}_j\mathbf{Q}_{j-1} = \mathbf{Q}_j\mathbf{R}_j$ is actually required, i.e.;

$$\mathbf{M}_{/p} = \mathbf{Q}_{j/p}\mathbf{R}_j + \mathbf{Q}_j\mathbf{R}_{j/p} = \mathbf{Y}_{j/p}\mathbf{Q}_{j-1} + \mathbf{Y}_j\mathbf{Q}_{(j-1)/p} \tag{4.40}$$

where $\mathbf{Q}_{j-1}$ and $\mathbf{Q}_{(j-1)/p}$ are available from the previous iteration. First of all, Eq. 4.40 is pre-multiplied by $\mathbf{Q}_j^T$ to obtain:

$$\mathbf{Q}_j^T\mathbf{Q}_{j/p}\mathbf{R}_j + \mathbf{R}_{j/p} = \mathbf{Q}_j^T\mathbf{Y}_{j/p}\mathbf{Q}_{j-1} + \mathbf{Q}_j^T\mathbf{Y}_j\mathbf{Q}_{(j-1)/p} \tag{4.41}$$

Then the strictly lower triangular part of the equation is evaluated to compute $\mathbf{W}_L$,

$$\begin{aligned}\mathbf{W}_L &= \text{stril}\left(\left(\mathbf{Q}_j^T\mathbf{Y}_{j/p}\mathbf{Q}_{j-1} + \mathbf{Q}_j^T\mathbf{Y}_j\mathbf{Q}_{(j-1)/p}\right)\mathbf{R}_j^{-1}\right) \\ &= \text{stril}\left(\left(\mathbf{Q}_j^T\mathbf{Y}_{j/p}\mathbf{Q}_{j-1} + \mathbf{R}_j\mathbf{W}_{j-1}\right)\mathbf{R}_j^{-1}\right)\end{aligned} \tag{4.42}$$

the strictly lower triangular part of $\mathbf{W}_j = \mathbf{Q}_j^T\mathbf{Q}_{j/p} = \mathbf{W}_L - \mathbf{W}_L^T$. See Eq. 4.38 for details about the computation of $\mathbf{W}_L$. Finally, the upper triangular part of Eq. 4.41 is evaluated to obtain $\mathbf{R}_{j/p}$,

$$\begin{aligned}\mathbf{R}_{j/p} &= \mathbf{Q}_j^T\left(\mathbf{Y}_{j/p}\mathbf{Q}_{j-1} + \mathbf{Y}_j\mathbf{Q}_{(j-1)/p}\right) - \mathbf{W}_j\mathbf{R}_j \\ &= \mathbf{Q}_j^T\mathbf{Y}_{j/p}\mathbf{Q}_{j-1} + \mathbf{R}_j\mathbf{W}_{j-1} - \mathbf{W}_j\mathbf{R}_j\end{aligned} \tag{4.43}$$

Clearly, the sensitivity of the state transition matrix, $\mathbf{Y}_{j/p}$, evaluated between two consecutive times, $t = t_{j-1}$ to t_j, is required.

4.3.2 Sensitivity of State Transition Matrix

The sensitivity of state transition matrix $\mathbf{Y}$ at time t_j, namely $\mathbf{Y}_{/p}(t_j)$, is needed to compute the sensitivity of the LCEs. In principle, this is obtained by integrating the sensitivity of the problem $\dot{\mathbf{Y}} = \mathbf{A}\mathbf{Y}$. Then,

$$\begin{aligned}\dot{\mathbf{Y}}_{/p} &= \mathbf{A}\mathbf{Y}_{/p} + \left(\mathbf{A}_{/\mathbf{x}}\mathbf{x}_{/p} + \mathbf{A}_{/p}\right)\mathbf{Y} \\ &= \mathbf{A}\mathbf{Y}_{/p} + \frac{\mathrm{d}\mathbf{A}}{\mathrm{d}p}\mathbf{Y}\end{aligned} \tag{4.44}$$

i.e. a problem with the same matrix $\mathbf{A}$ of the original one, forced by a term $(\mathrm{d}\mathbf{A}/\mathrm{d}p)\mathbf{Y}$ that depends on the reference solution. The term $\mathbf{A}_{/\mathbf{x}}$ is the second-order derivative of function $\mathbf{f}$ with respect to the

state $\mathbf{x}$. It vanishes for linear problems. The sensitivity of the state to parameter p is obtained by perturbing the problem $\dot{\mathbf{x}} = \mathbf{f}(\mathbf{x}, t)$,

$$\dot{\mathbf{x}}_{/p} = \mathbf{f}_{/x}\mathbf{x}_{/p} + \mathbf{f}_{/p} \tag{4.45}$$

and integrating it in time accordingly. A similar problem needs to be solved for each parameter.

As an alternative, consider the problem $\dot{\mathbf{Y}} = \mathbf{A}\mathbf{Y}$ premultiply it by a set of unknowns (Lagrange multipliers) $\mathbf{P}^T$ and integrate it over the interval $[t_{j-1}, t_j]$,

$$\mathbf{J} = \int_{t_{j-1}}^{t_j} \mathbf{P}^T \left(\mathbf{A}\mathbf{Y} - \dot{\mathbf{Y}} \right) \mathrm{d}t = \mathbf{0} \tag{4.46}$$

Consider now its perturbation with respect to parameter p:

$$\frac{\mathrm{d}}{\mathrm{d}p}(\mathbf{J}) = \tag{4.47}$$
$$\int_{t_{j-1}}^{t_j} \left(\mathbf{P}^T_{/p} \cancel{\left(\mathbf{A}\mathbf{Y} - \dot{\mathbf{Y}} \right)} + \mathbf{P}^T \left(\frac{\mathrm{d}\mathbf{A}}{\mathrm{d}p}\mathbf{Y} + \mathbf{A}\mathbf{Y}_{/p} - \dot{\mathbf{Y}}_{/p} \right) \right) \mathrm{d}t = \mathbf{0}$$

$\dot{\mathbf{Y}}_{/p}$ is eliminated using integration by part, yielding:

$$\begin{aligned} \frac{\mathrm{d}}{\mathrm{d}p}(\mathbf{J}) &= \int_{t_{j-1}}^{t_j} \left(\mathbf{P}^T \left(\frac{\mathrm{d}\mathbf{A}}{\mathrm{d}p}\mathbf{Y} + \mathbf{A}\mathbf{Y}_{/p} \right) + \dot{\mathbf{P}}^T \mathbf{Y}_{/p} \right) \mathrm{d}t - \mathbf{P}^T \mathbf{Y}_{/p} \Big|_{t_{j-1}}^{t_j} \\ &= \int_{t_{j-1}}^{t_j} \left(\mathbf{P}^T \frac{\mathrm{d}\mathbf{A}}{\mathrm{d}p}\mathbf{Y} + \left(\mathbf{P}^T\mathbf{A} + \dot{\mathbf{P}}^T \right) \mathbf{Y}_{/p} \right) \mathrm{d}t - \mathbf{P}^T \mathbf{Y}_{/p} \Big|_{t_{j-1}}^{t_j} = \mathbf{0} \end{aligned} \tag{4.48}$$

The adjoint problem,

$$\dot{\mathbf{P}} = -\mathbf{A}^T\mathbf{P} \tag{4.49}$$

is solved first from time t_j backwards to an arbitrary time $t \in [t_{j-1}, t_j]$, with initial conditions arbitrarily set to $\mathbf{P}(t_j) = \mathbf{I}$; then,

$$\mathbf{P}(t) = \mathbf{\Phi}(t, t_j)\mathbf{P}(t_j) = \mathbf{\Phi}(t, t_j) \tag{4.50}$$

where $\mathbf{\Phi}(t, t_j)$ is the state transition matrix of the adjoint problem. Now, Eq. 4.48 becomes,

$$\int_{t_{j-1}}^{t_j} \mathbf{P}^T \frac{\mathrm{d}\mathbf{A}}{\mathrm{d}p}\mathbf{Y} \, \mathrm{d}t - \mathbf{P}^T(t_j)\mathbf{Y}_{/p}(t_j) + \mathbf{P}^T(t_{j-1})\mathbf{Y}_{/p}(t_{j-1}) = \mathbf{0} \tag{4.51}$$

i.e.:

$$\mathbf{Y}_{/p}(t_j) = \mathbf{\Phi}^T(t_{j-1}, t_j)\mathbf{Y}_{/p}(t_{j-1}) + \int_{t_{j-1}}^{t_j} \mathbf{\Phi}^T(t, t_j)\frac{\mathrm{d}\mathbf{A}}{\mathrm{d}p}(\mathbf{x}(t), t)\mathbf{Y}(t)\ \mathrm{d}t \tag{4.52}$$

In practice, one only needs to find $\mathbf{P}(t)$ (i.e. $\mathbf{\Phi}(t, t_j)$) and then compute as many finite integrals like the one of Eq. 4.52 as the parameters whose sensitivity is sought.

Special Case: Integration Using Hsu's Method

Hsu's method given in Eq. 4.26 provides a more compact form of computing the sensitivity of the state transition for linear systems. Then, the state transition matrix of a piecewise constant approximation of matrix $\mathbf{A}(\mathbf{x}, t)$, namely $\mathbf{A}(\mathbf{x}, t) \approx \mathbf{A}(\hat{\mathbf{x}}, \hat{t}) = \hat{\mathbf{A}}$ with $\hat{t} \in [t_j, t_{j+1}]$ and $\hat{\mathbf{x}} = \mathbf{x}(\hat{t})$ is readily obtained as,

$$\mathbf{Y}(t_{j+1}, t_j) \approx \mathrm{e}^{\hat{\mathbf{A}}(t_{j+1} - t_j)} \tag{4.53}$$

where the choice of $\hat{t}$ may influence the results and the matrix exponential may be approximated (e.g. truncated when computed as a matrix power series) to improve the computational efficiency. The sensitivity of the state transition matrix is:

$$\mathbf{Y}_{/p}(t_{j+1}, t_j) \approx \hat{\mathbf{A}}_{/p}(t_{j+1} - t_j)\mathrm{e}^{\hat{\mathbf{A}}(t_{j+1} - t_j)} = \hat{\mathbf{A}}_{/p}(t_{j+1} - t_j)\mathbf{Y}(t_{j+1}, t_j) \tag{4.54}$$

4.4 Illustration of the method

This section presents a linear damped oscillator example to explore the multiplicity and oscillations of LCE estimates in mechanical systems. Complex rotorcraft applications can be found in Chapter 5.

Linear Damped Oscillator

Consider the mass-spring-damper problem:

$$m\ddot{q} + c\dot{q} + kq = 0 \ \text{ or } \ \ddot{q} + 2\xi\omega\dot{q} + \omega^2 q = 0 \tag{4.55}$$

The state space representation for $\omega > 0$ can be written as:

$$\dot{\mathbf{x}} = \left\{ \begin{array}{c} \dot{q} \\ \ddot{q} \end{array} \right\} = \left[\begin{array}{cc} 0 & 1 \\ -\omega^2 & -2\xi\omega \end{array} \right] \left\{ \begin{array}{c} q \\ \dot{q} \end{array} \right\} = \mathbf{A}\mathbf{x} \tag{4.56}$$

The state transition matrix from 0 to t is defined as:

$$\mathbf{Y}(t,0) = \mathrm{e}^{\mathbf{A}t} \tag{4.57}$$

And its QR decomposition is,

$$\mathbf{Y}(t,0) = \mathbf{QR} = \begin{bmatrix} \cos\alpha & -\sin\alpha \\ \sin\alpha & \cos\alpha \end{bmatrix} \begin{bmatrix} r_{11} & r_{12} \\ 0 & r_{22} \end{bmatrix} \tag{4.58}$$

which yields,

$$r_{11} = \sqrt{Y_{11}^2 + Y_{21}^2} \ , \ r_{22} = \frac{Y_{11}Y_{22} - Y_{21}Y_{12}}{r_{11}} \tag{4.59}$$

and, of course,

$$r_{12} = \frac{Y_{11}Y_{12} + Y_{21}Y_{22}}{r_{11}} \ , \ \alpha = \tan^{-1}\left(\frac{Y_{21}}{Y_{11}}\right) \tag{4.60}$$

which are inessential for LCE estimation.

Subcritical Damping

For $0 < \xi < 1$, the state transition matrix can be formally written as,

$$\mathbf{Y}(t,0) = \mathbf{V}\mathrm{e}^{\mathbf{\Lambda}t}\mathbf{V}^{-1} \tag{4.61}$$

using the spectral decomposition of matrix $\mathbf{A}$, namely $\mathbf{A} = \mathbf{V}\mathbf{\Lambda}\mathbf{V}^{-1}$, with,

$$Y_{11} = \left(\cos\left(\sqrt{1-\xi^2}\omega t\right) + \frac{\xi}{\sqrt{1-\xi^2}}\sin\left(\sqrt{1-\xi^2}\omega t\right)\right)\mathrm{e}^{-\xi\omega t} \tag{4.62a}$$

$$Y_{12} = \frac{1}{\sqrt{1-\xi^2}\omega}\sin\left(\sqrt{1-\xi^2}\omega t\right)\mathrm{e}^{-\xi\omega t} \tag{4.62b}$$

$$Y_{21} = -\frac{\omega}{\sqrt{1-\xi^2}}\sin\left(\sqrt{1-\xi^2}\omega t\right)\mathrm{e}^{-\xi\omega t} \tag{4.62c}$$

$$Y_{22} = \left(\cos\left(\sqrt{1-\xi^2}\omega t\right) - \frac{\xi}{\sqrt{1-\xi^2}}\sin\left(\sqrt{1-\xi^2}\omega t\right)\right)\mathrm{e}^{-\xi\omega t} \tag{4.62d}$$

The singular values of $\mathbf{\Phi}(t,0)$ are,

$$\sigma_{1,2} = \hat{\sigma}_{1,2}\mathrm{e}^{-\xi\omega t} \tag{4.63}$$

where the magnitudes are,

$$\hat{\sigma}_1 = \tag{4.64a}$$

$$\sqrt{\frac{\left(1+2\omega^2\xi^2+\omega^4\right)S^2+2\omega^2\left(1-\xi^2\right)C^2 \pm S\sqrt{1+2\omega^2\xi^2+\omega^4}\sqrt{\left(1+\omega^2\right)^2S^2+4\omega^2\left(1-\xi^2\right)C^2}}{2\omega^2\left(1-\xi^2\right)}}$$

$$\hat{\sigma}_2 = \frac{1}{\hat{\sigma}_1} \tag{4.64b}$$

with $C = \cos(\sqrt{1-\xi^2}\omega t)$ and $S = \sin(\sqrt{1-\xi^2}\omega t)$. The singular values differ from each other and are time-dependent; the corresponding LCEs,

$$\lambda_1 = \lim_{t\to\infty}\frac{\log\left(\sigma_{1,2}\right)}{t} = \lim_{t\to\infty}\frac{\log\left(\hat{\sigma}_{1,2}\right)}{t} - \xi\omega = -\xi\omega \tag{4.65}$$

since $\hat{\sigma}_{1,2}$ are limited (indeed, they are periodic, with period $T = 2\pi/(\sqrt{1-\xi^2}\omega)$).

Considering now the QR decomposition, one can observe that r_{22} is actually $r_{22} = \mathrm{e}^{-2\xi\omega t}/r_{11}$; r_{11} can be written as $r_{11} = \hat{r}(t)\mathrm{e}^{-\xi\omega t}$, where $\hat{r}(t) > 0$ is a non-trivial but otherwise regular periodic function,

$$\hat{r}(t) = \tag{4.66}$$

$$\sqrt{\frac{1}{2}\frac{1+\omega^2}{1-\xi^2} + \frac{\xi}{\sqrt{1-\xi^2}}\sin\left(2\sqrt{1-\xi^2}\omega t\right) + \frac{1}{2}\frac{1-2\xi^2-\omega^2}{1-\xi^2}\cos\left(2\sqrt{1-\xi^2}\omega t\right)} > 0$$

thus, $r_{22} = \mathrm{e}^{-\xi\omega t}/\hat{r}(t)$. The LCEs associated with this problem are,

$$\begin{aligned}\lambda_1 = \lim_{t\to\infty}\frac{\log\left(r_{11}\right)}{t} &= \lim_{t\to\infty}\frac{\log\left(\hat{r}(t)\right) - \xi\omega t}{t} \\ &= \lim_{t\to\infty}\frac{\log\left(\hat{r}(t)\right)}{t} - \xi\omega = -\xi\omega \qquad (4.67a)\\ \lambda_2 = \lim_{t\to\infty}\frac{\log\left(r_{22}\right)}{t} &= \lim_{t\to\infty}\frac{\log\left(1/\hat{r}(t)\right) - \xi\omega t}{t} \\ &= -\lim_{t\to\infty}\frac{\log\left(\hat{r}(t)\right)}{t} - \xi\omega = -\xi\omega \qquad (4.67b)\end{aligned}$$

since $\hat{r}(t)$, being regular, is limited; thus its logarithm is also limited, and the limits of $\hat{r}(t)/t$ in Eqs. 4.67 tend to zero. It is worth noticing that the mean value of the two LCE estimates,

$$\frac{\lambda_1+\lambda_2}{2} = \lim_{t\to\infty}\frac{\log\left(r_{11}\right)+\log\left(r_{22}\right)}{2t} = -\xi\omega \tag{4.68}$$

is exactly the real part of complex conjugate eigenvalues of matrix $\mathbf{A}$ $\forall t$, since the spurious oscillations related to $\hat{r}(t)$ and $1/\hat{r}(t)$ cancel out. The sensitivity of the LCEs to the two parameters, ξ and ω, of the equation are:

$$\lambda_{/\xi} = -\omega = \lambda/\xi \tag{4.69a}$$
$$\lambda_{/\omega} = -\xi = \lambda/\omega \tag{4.69b}$$

which are clearly non-oscillatory.

Critical Damping

Consider now the case $\xi = 1$, i.e. critical damping, which yields two real, coincident eigenvalues for matrix $\mathbf{A}$, hence the trajectory of the transient solution does not involve oscillations. The state transition matrix, considering a Jordan canonical form [109] of the system matrix, $\mathbf{A} = \mathbf{U}\mathbf{J}\mathbf{U}^{-1}$, is now:

$$\mathbf{Y}(t,0) = \mathbf{U}\mathrm{e}^{\mathbf{J}t}\mathbf{U}^{-1} = \begin{bmatrix} 1+\omega t & t \\ -\omega^2 t & 1-\omega t \end{bmatrix} \mathrm{e}^{-\omega t} \tag{4.70}$$

The QR decomposition yields again $r_{11} = \hat{r}(t)\mathrm{e}^{-\omega t}$ and $r_{22} = \mathrm{e}^{-\omega t}/\hat{r}(t)$, now with,

$$\hat{r}(t) = \sqrt{1 + 2\omega t + \omega^2(1+\omega^2)t^2} \tag{4.71}$$

The LCEs are:

$$\begin{aligned} \lambda_1 = \lim_{t\to\infty} \frac{\log(r_{11})}{t} &= \lim_{t\to\infty} \frac{\log(\hat{r}(t)) - \omega t}{t} \\ &= \lim_{t\to\infty} \frac{\log(\hat{r}(t))}{t} - \omega = -\omega \end{aligned} \tag{4.72a}$$
$$\begin{aligned} \lambda_2 = \lim_{t\to\infty} \frac{\log(r_{22})}{t} &= \lim_{t\to\infty} \frac{\log(1/\hat{r}(t)) - \omega t}{t} \\ &= -\lim_{t\to\infty} \frac{\log(\hat{r}(t))}{t} - \omega = -\omega \end{aligned} \tag{4.72b}$$

Again, the mean value of the two LCEs is directly $-\omega$.

Supercritical Damping

Consider now supercritical damping, $\xi > 1$; the elements of the state transition matrix are:

$$Y_{11} = \left(\cosh\left(\sqrt{\xi^2-1}\omega t\right) + \frac{\xi}{\sqrt{\xi^2-1}} \sinh\left(\sqrt{\xi^2-1}\omega t\right) \right) \mathrm{e}^{-\xi\omega t} \tag{4.73a}$$

$$Y_{12} = \frac{1}{\sqrt{\xi^2-1}\omega} \sinh\left(\sqrt{\xi^2-1}\omega t\right) \mathrm{e}^{-\xi\omega t} \tag{4.73b}$$

$$Y_{21} = \frac{-\omega}{\sqrt{\xi^2-1}} \sinh\left(\sqrt{\xi^2-1}\omega t\right) \mathrm{e}^{-\xi\omega t} \tag{4.73c}$$

$$Y_{22} = \left(\cosh\left(\sqrt{\xi^2-1}\omega t\right) - \frac{\xi}{\sqrt{\xi^2-1}} \sinh\left(\sqrt{\xi^2-1}\omega t\right) \right) \mathrm{e}^{-\xi\omega t} \tag{4.73d}$$

which, after setting $\lambda_{1,2} = (-\xi \pm \sqrt{\xi^2-1})\omega$, can be rewritten as:

$$\mathbf{Y}(t,0) = \begin{bmatrix} \dfrac{\lambda_2 \mathrm{e}^{\lambda_1 t} - \lambda_1 \mathrm{e}^{\lambda_2 t}}{\lambda_2 - \lambda_1} & \dfrac{-\mathrm{e}^{\lambda_1 t} + \mathrm{e}^{\lambda_2 t}}{\lambda_2 - \lambda_1} \\ \dfrac{\lambda_1\lambda_2 \mathrm{e}^{\lambda_1 t} - \lambda_1\lambda_2 \mathrm{e}^{\lambda_2 t}}{\lambda_2 - \lambda_1} & \dfrac{-\lambda_1 \mathrm{e}^{\lambda_1 t} + \lambda_2 \mathrm{e}^{\lambda_2 t}}{\lambda_2 - \lambda_1} \end{bmatrix} \tag{4.74}$$

Since $\lambda_1 > \lambda_2$, one obtains $r_{11} = \hat{r}(t)\mathrm{e}^{\lambda_1 t}$ and $r_{22} = \mathrm{e}^{\lambda_2 t}/\hat{r}(t)$, with

$$\hat{r}(t) = \sqrt{\frac{\lambda_2^2\left(1+\lambda_1^2\right) - 2\lambda_1\lambda_2\left(1+\lambda_1\lambda_2\right)\mathrm{e}^{(\lambda_2-\lambda_1)t} + \lambda_1^2\left(1+\lambda_2^2\right)\mathrm{e}^{2(\lambda_2-\lambda_1)t}}{\left(\lambda_2-\lambda_1\right)^2}}, \tag{4.75}$$

which tends to a finite value for $t \to \infty$. As such,

$$\lim_{t\to\infty} \frac{\log\left(r_{11}\right)}{t} = \lambda_1 + \lim_{t\to\infty} \frac{\log\left(\hat{r}(t)\right)}{t} \tag{4.76}$$

$$\lim_{t\to\infty} \frac{\log\left(r_{22}\right)}{t} = \lambda_2 - \lim_{t\to\infty} \frac{\log\left(\hat{r}(t)\right)}{t} \tag{4.77}$$

and $\log(\hat{r}(t))/t \to 0$ for $t \to \infty$.

Comparison with Numerical Solution

The linear damped oscillator is analyzed for stability and sensitivity of LCEs with respect to the damping coefficient, $p := c$. In the numerical analysis, the values of mass ($m = 1$ kg) and stiffness ($k = 0.25$ Nm^{-1}) are chosen such that $c = 1$ Nsm^{-1} is the critical damping value ($\xi = 1$). The problem has the analytical solution of the damping exponents:

$$\lambda_{1,2} = \begin{cases} -\dfrac{c}{2m} & \text{if } c^2 - 4mk \leq 0 \\ \dfrac{-c \pm \sqrt{c^2 - 4mk}}{2m} & \text{if } c^2 - 4mk > 0 \end{cases} \tag{4.78}$$

Figs. 4.1 and 4.2 present the convergence of a critically and supercritically damped oscillator, respectively. Both cases show contracting behavior (i.e. negative LCEs). A subcritically damped system shows oscillatory convergence, as illustrated in Fig. 4.3 and in Fig. 4.4 with the final portion is zoomed. It can be observed that while critically damped and over-damped systems converge without oscillations, the LCE estimate of a subcritically damped system, which has two complex conjugate eigenvalues, oscillates as pointed out in Ref. [110]. The Figs. 4.3 and 4.4, as proposed above, also show that the actual damping parameter, i.e. the real part of the eigenvalues of the problem, is the mean value of the two LCEs at any time step, regardless of the amplitude of the oscillation. Although the same time passes between two adjacent peaks of the LCE estimates, the curves are not periodic, owing to the division by t as given in Eq. 4.7. Periodicity (with period half of $2\pi/(\omega\sqrt{1-\xi^2})$) can be restored by multiplying the LCE estimates by t after removing the mean value. Such behavior of the LCE estimates may be useful when detecting values associated with complex conjugate eigenvalues in problems with a large number of states.

The LCE estimates for the mass-spring-damper problem are shown in Fig. 4.5 with respect to the damping coefficient c as it is changed from 0.5 Nsm^{-1} (subcritical) to 1.5 Nsm^{-1} (supercritical). As expected, for $c \leq 1$, i.e. before the critical damping condition, when the system has two complex conjugate eigenvalues, the two LCEs are coincident, and become more and more negative as the damping increases. After that point, the two LCE estimates split, as the system's eigenvalues become real and distinct, but their mean value still follows the same slope of the subcritical damping case. The numerical results are in very good agreement with the analytical solution.

The sensitivity of LCEs with respect to the damping coefficient, ($\lambda_{/p}$, $p := c$) are compared again with the analytical solution for the same set of parameter values. The analytical derivative of LCEs is straightforward using Eq.4.78,

$$\lambda_{1,2/p} = \begin{cases} -\dfrac{1}{2m} & \text{if } c^2 - 4mk < 0 \\ \text{undefined} & \text{if } c^2 - 4mk = 0 \\ -\dfrac{1}{2m} \pm \dfrac{c}{2m\sqrt{c^2 - 4mk}} & \text{if } c^2 - 4mk > 0 \end{cases} \tag{4.79}$$

Notice that the left and right limits of $\lambda_{i/p}$ differ for $c = 2\sqrt{mk}$, i.e. at critical damping; specifically, the right limit is $\pm\infty$, whereas the left limit is $-1/(2m)$. The estimates of LCE sensitivity are shown in Fig. 4.6 with respect to the damping coefficient c as it is changed from 0.5 Nsm^{-1} (subcritical) to 1.5 Nsm^{-1} (supercritical). The sensitivity results of the numerical method are matching well with that of analytical solution except the point where bifurcation occurs at $c = 1$. It should be noted that at this point the derivative does not exist as explained, hence sensitivity is not defined as stated in Eq. 4.79. Therefore when the proposed method is used, such non-differentiable points should be detected.

Discussion of Results

It is worth noticing that regardless of the value of ξ,

$$\begin{aligned} \lim_{t\to\infty} \frac{\log\left(\det(\mathbf{R})\right)}{t} &= \lim_{t\to\infty} \frac{\log\left(\Pi_{i=1}^{2} r_{ii}\right)}{t} = \lim_{t\to\infty} \frac{\sum_{i=1}^{2} \log\left(r_{ii}\right)}{t} \\ &= \lim_{t\to\infty} \frac{\lambda_1 t + \log\left(\hat{r}(t)\right) + \lambda_2 t - \log\left(\hat{r}(t)\right)}{t} \\ &= \lambda_1 + \lambda_2 \end{aligned} \tag{4.80}$$

i.e. the sum of the LCEs is exact from the beginning and $\forall t$. When $|\xi| \leq 1$, the two LCEs are identical, although their estimates oscillate while converging to the exact value.

Detecting LCE estimates whose oscillatory behavior indicates the existence of LCEs with multiplicity η greater than 1 may not be straightforward. In this example and in subsequent ones of Chapter 5, we infer the convergence of two oscillating LCE estimates to a value with multiplicity $\eta = 2$ from the behavior of their mean value. We speculate,

without further investigation, that the use of a decomposition capable of dealing with characteristic values with multiplicity $\eta > 1$ is needed to make such detection more robust. A development in this sense is considered as a future work.

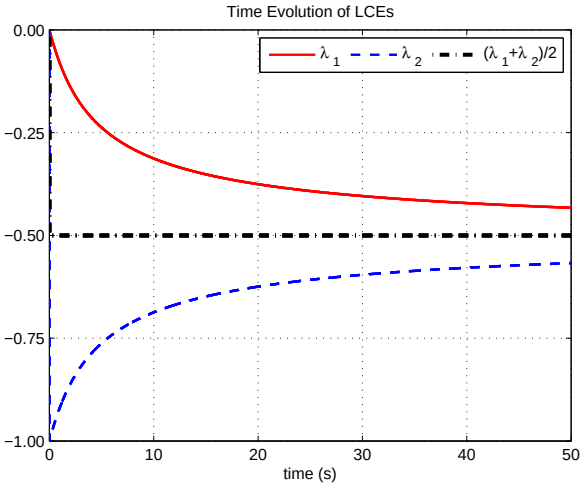

Figure 4.1: *Damped oscillator: time evolution of LCE estimates for critically damped ($\xi = 1$)*

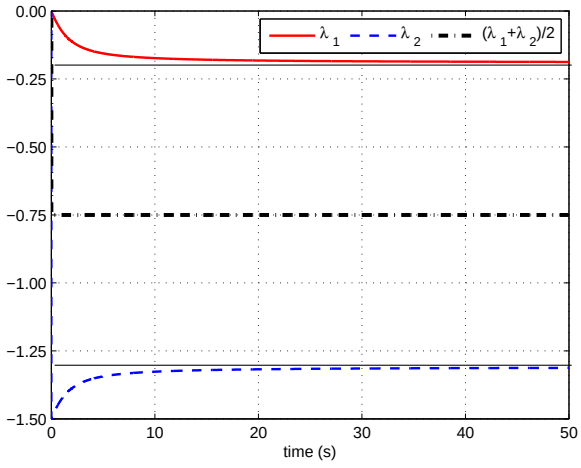

Figure 4.2: *Damped oscillator: time evolution of LCE estimates for supercritically damped system ($\xi = 1.5$).*

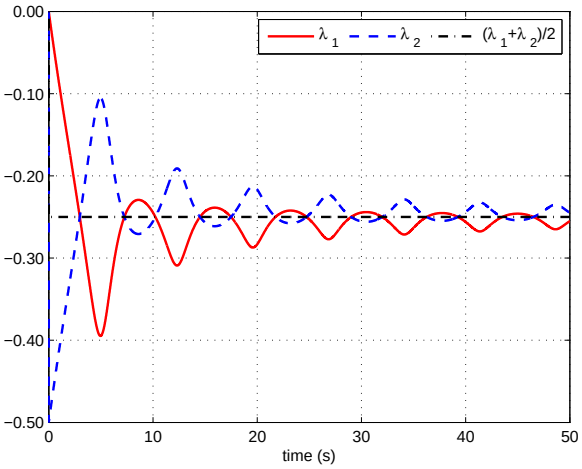

Figure 4.3: *Damped oscillator: time evolution of LCE estimates for subcritically damped system ($\xi = 0.5$)*

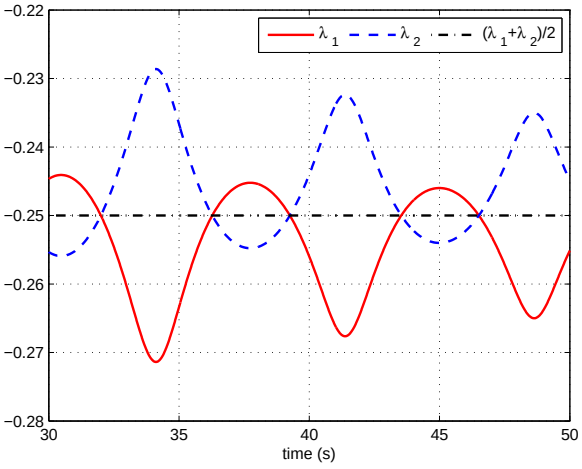

Figure 4.4: *Damped oscillator: time evolution of LCE estimates for subcritically damped system ($\xi = 0.5$), zoomed view after convergence*

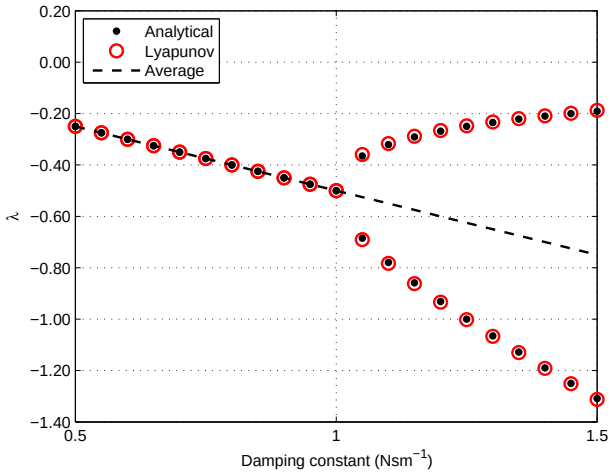

Figure 4.5: *Damped oscillator: LCE estimates with respect to damping constant c.*

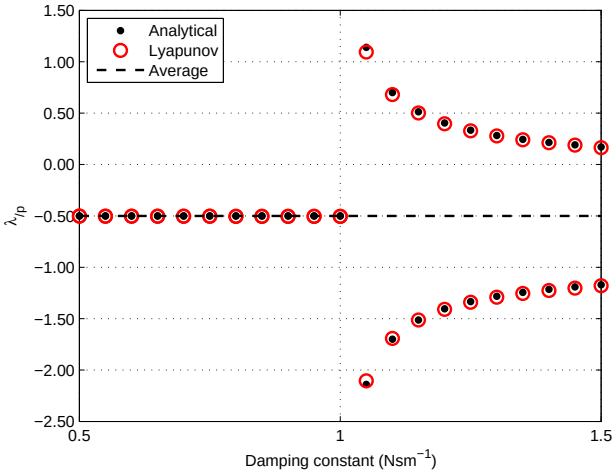

Figure 4.6: *Damped oscillator: Sensitivity estimation of LCEs with respect to damping coefficient c*

CHAPTER 5

Numerical Examples

5.1 Introduction

This chapter presents the numerical examples using the rotor aeroelastic tool introduced in Chapter 2, the stability and sensitivity using Floquet Method explained in Chapter 3 and using Lyapunov Characteristic Exponents (LCEs) described in Chapter 4. The aim of this chapter is to illustrate the tools and methods for their verification using rotorcraft related problems involving periodic and nonlinear terms in their equations of motion. The occurrence of characteristic nonlinear phenomena in the solutions are addressed and discussed.

The first problem is related to rotor blade flapping with perturbation aerodynamics and presented in Section 5.2. The non-dimensional forward flight speed, the so-called advance ratio (μ) causes azimuth-dependent aerodynamic operation; leading to periodicity in the equivalent stiffness and damping matrices. Stability and sensitivity of stability properties are performed using Floquet Method and Lyapunov Characteristic Exponents. The periodicity of the problem with multiplicity of the stability properties is addressed.

Section 5.3 is devoted to a helicopter ground resonance analysis.

The problem is analyzed for possible changes in the configuration of dampers such as malfunction and nonlinearity. The first case is selected to analyze a linear time periodic problem (LTP) and compare stability and sensitivity results obtained by Lyapunov and Floquet. In order to do this, the damping constant of one of the blade lead-lag dampers are selected as the parameter and varied from zero to its nominal value while the rest are kept at their nominals. In the second case the blade dampers are represented by a second order polynomial function with saturation in order to capture some nonlinear phenomena. The coefficient related to the linear term of the damping force is selected as the parameter and it is varied from zero to the nominal value of the linear damping of the model. The results are compared with the time history of the blade motion. In the third case first and second cases are mixed and a nonlinear non-autonomous problem is analyzed.

The final set of problems of Section 5.4 presents a large scale helicopter model which includes detailed descriptions of rotor aeroelastic modes, fuselage rigid body and elastic modes, control system and sensors. First, the aeroelastic rotor model is verified against respected tools and stability analyses are performed for an helicopter at hovering condition. In the second case, a periodic problem is set by differentiating one blade damper from others. LCEs are compared with the characteristic exponents obtained using Floquet Theory together with their sensitivity .

5.2 Helicopter Blade Flapping

Consider the Floquet analysis of the fundamental flap dynamics of a helicopter rotor blade as presented in Ref. [84]. The problem is a linear, second-order time periodic system; the periodicity arising from the equivalent aerodynamic stiffness and damping in forward flight. The results of the Floquet analysis, with the principal component of the imaginary part of the eigenvalues, are provided in Fig. 5.1. Owing to the forward flight operation of the helicopter, in which asymmetry of the aerodynamic environment interacts with the dynamics of the blade, the system is periodic, with a fundamental frequency equal to the angular speed of the rotor, Ω. In hover condition (i.e. when the ratio between the airstream velocity and the tip speed of the rotor blades, μ, is zero), the eigenvalues ($s = \lambda + \mathrm{j}\omega$) are complex conjugated. As the advance ratio μ increases, a decrease in the imaginary part (ω) is observed first, whereas the real part (λ) remains constant. When

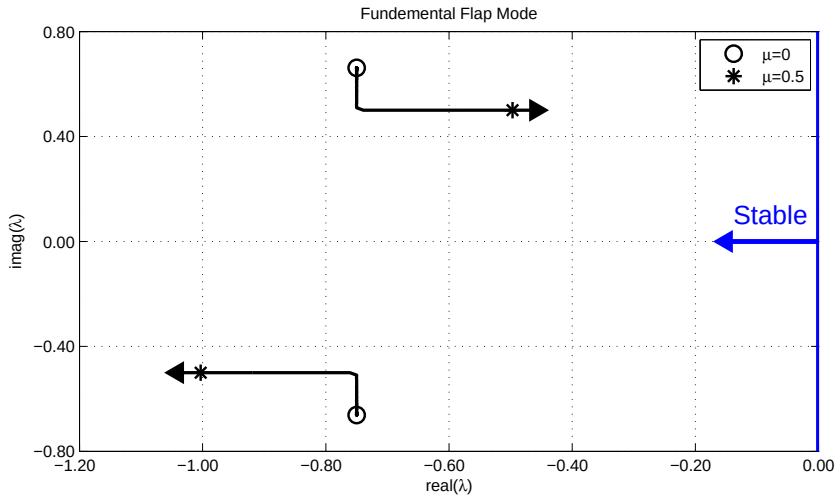

Figure 5.1: *Floquet eigenanalysis of the fundamental flapping mode of a helicopter (Figure adopted from Ref. [84]).*

the non-dimensional imaginary part approaches 0.5/rev, it remains constant; the real part of one of the eigenvalues (the one at the bottom of the figure) increases in magnitude, while the other (the one at the top of the figure) reduces. As explained in Ref. [92], in some cases this behavior can have significant repercussions on the stability of the system, reducing stability margins and in some cases even leading to instability.

Rigid blade flapping can be modeled as a second order single degree of freedom LTP problem (from Ref. [92]) under simplifying assumptions. Since the purpose of this example is to address LTP systems, rather than using a more realistic but complex helicopter blade dynamics model, only periodicity is retained, and the model is oversimplified by linearizing the dynamics, using quasi-static aerodynamics and neglecting reverse flow conditions. The dots represent differentiation with respect to the azimuth angle t (in this context it represents non-dimensional time). The equation of motion can be written as,

$$\ddot{\beta} + \frac{\gamma}{8}\left(1 + \frac{4}{3}\mu\sin(t)\right)\dot{\beta} + \left(\nu_\beta^2 + \frac{\gamma}{8}\left(\frac{4}{3}\mu\cos(t) + \mu^2\sin(2t)\right)\right)\beta = 0 \tag{5.1}$$

that represents the flapping of a rigid helicopter blade, where β is the blade flap angle, γ is the Lock number (the non-dimensional ratio

between aerodynamic and inertial flapping loads, which in the present context loosely represents the damping factor), μ is the advance ratio (the ratio between the helicopter forward velocity and the blade tip velocity in hover, which weighs the periodic part of the coefficients) and ν_β is the flapping frequency non-dimensionalized by rotor angular speed Ω. In order to demonstrate the trend of LCE estimates with respect to a parameter, the advance ratio μ is chosen. The problem is rewritten in first order form,

$$\left\{ \begin{array}{c} \dot{\beta} \\ \ddot{\beta} \end{array} \right\} = \left[\begin{array}{cc} 0 & 1 \\ -K_\beta & -C_\beta \end{array} \right] \left\{ \begin{array}{c} \beta \\ \dot{\beta} \end{array} \right\} \tag{5.2}$$

where stiffness K_β and damping C_β terms are:

$$K_\beta = \nu_\beta^2 + \frac{\gamma}{8}\left(\frac{4}{3}\mu\cos(t) + \mu^2\sin(2t)\right) \tag{5.3a}$$

$$C_\beta = \frac{\gamma}{8}\left(1 + \frac{4}{3}\mu\sin(t)\right) \tag{5.3b}$$

Then, the state space matrix is directly $\mathbf{A}(t) = \mathbf{f}_{/\mathbf{x}}$, and its sensitivity with respect to μ is:

$$\mathbf{A}_{/\mu} = \left[\begin{array}{cc} 0 & 0 \\ -\frac{\gamma}{8}\left(\frac{4}{3}\cos(t) + 2\mu\sin(2t)\right) & -\frac{\gamma}{6}\sin(t) \end{array} \right] \tag{5.4}$$

LCEs and their sensitivity are estimated according to the proposed approach for the values of lock number $\gamma = 12$ and flapping natural frequency $\nu_\beta = 1$. Clearly, a trivial fiducial trajectory is $\beta(t) = 0$, which is obtained for $\beta(0) = 0$ and $\dot{\beta}(0) = 0$. Other non-trivial trajectories can be obtained starting from arbitrary initial conditions; were $\beta(t) = 0$ asymptotically stable, the solution converges to it. Since this problem is linear and homogeneous, $\beta(t) = 0$ is the unique equilibrium point and it is necessary and sufficient to analyze the stability of the trivial solution $\beta(t) = 0$ (See introduction of Chapter 4). The expected fiducial trajectory is readily obtained within a few periods when it is asymptotically stable.

The evolution of LCE estimates associated with complex conjugate eigenvalues for $\mu = 0.15$ are shown in Fig. 5.2 and with zoomed plot in Fig. 5.3. The figures show a different behavior from that of the mass-spring-damper system. Owing to periodicity, the mean value of two

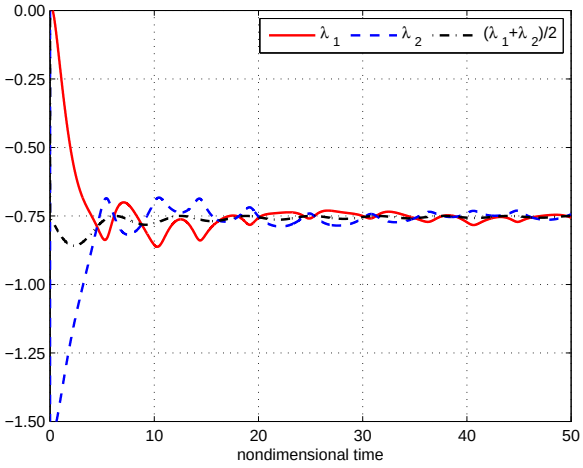

Figure 5.2: *Blade flapping: non-dimensional time evolution of LCE estimates associated with complex conjugate eigenvalues,* $\mu = 0.15$

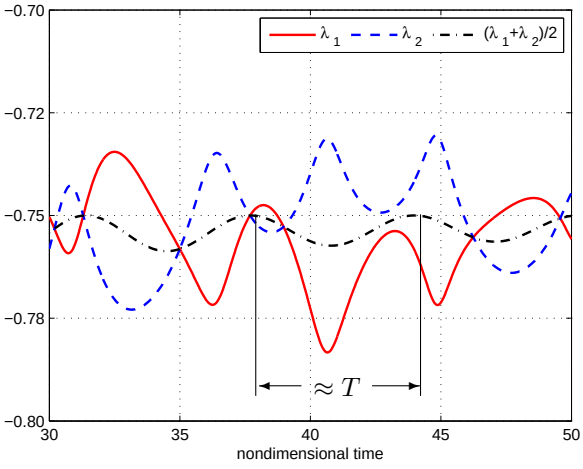

Figure 5.3: *Blade flapping: non-dimensional time evolution of LCE estimates associated with complex conjugate eigenvalues,* $\mu = 0.15$*; zoom after convergence*

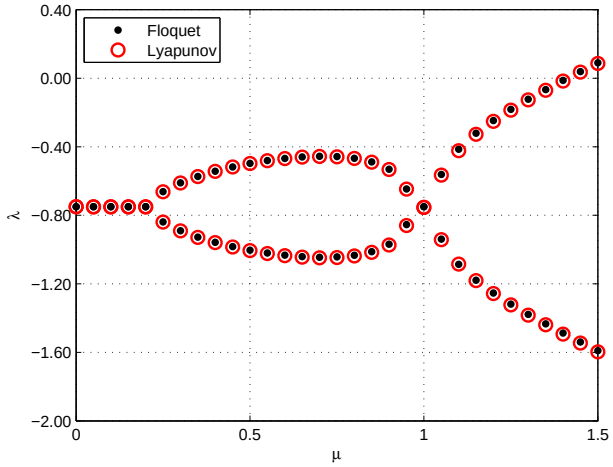

Figure 5.4: *Blade flapping: estimates of LCEs with respect to advance ratio μ*

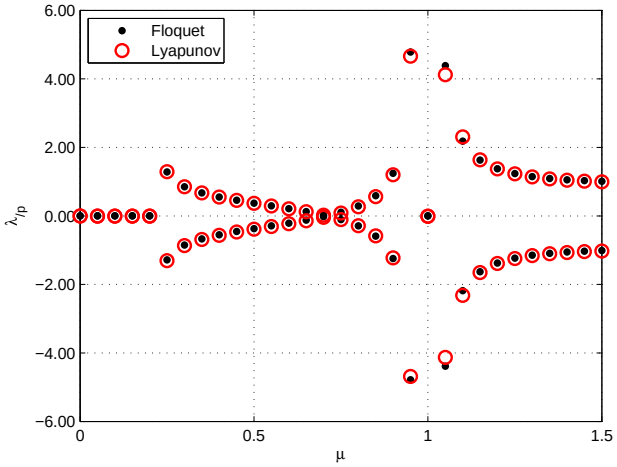

Figure 5.5: *Blade flapping: estimates of sensitivity of LCEs with respect to advance ratio μ*

LCEs associated with complex conjugate eigenvalues shows a decaying oscillatory behavior with the period of the system, $T = 2\pi$. The decay is caused by division by t, according to Eq. 4.7. In order to have an accurate estimate of the LCEs, integration needs to be performed for a large enough non-dimensional time, to let the oscillations vanish. Remember that there was no periodicity in the mean value of the two LCEs resulting from the LTI system consisting of a sub-critically damped oscillator, which has two imaginary eigenvalues, as given in Figs. 4.1 to 4.4.

The LCE and sensitivity estimates are compared in Fig. 5.5 with the corresponding values obtained using the Floquet theory for a range of advance ratio $0 \leq \mu \leq 1.5$. This range of advance ratios is way beyond the maximum flight speed of conventional helicopters (about 0.4) but may be of interest for slowed rotors. Both results of Floquet and Lyapunov methods are in good agreement. Up to $\mu = 0.22$ the system has two complex conjugate eigenvalues with equal real part that does not depend on μ; consistently, sensitivity with respect to μ is zero. Beyond that value, the periodic nature of the system leads to distinct real part for the two modes; i.e. the stability properties start becoming sensitive to μ. Then, the stability of one of the modes increases, whereas that of the other one reduces, as also can be verified with the real part of Fig 5.1.

5.3 Helicopter Ground Resonance

Helicopter Ground Resonance is a mechanical instability associated with the in-plane degrees of freedom of the rotor (see for example [111], or the seminal work by Coleman and Feingold [112]). The combination of the in-plane motion of the blades causes an overall in-plane motion of the rotor center of mass which couples with the dynamics of the airframe and undercarriage system. For this reason, the damping of the in-plane motion of the blades is essential in articulated and soft-inplane rotor, and is usually provided by lead-lag dampers.

The problem has been studied using models of various complexity levels. Hammond's model [113] has been extensively used due to its simplicity; as such, it is chosen as the helicopter ground resonance model in this study. A schematic is given in Fig. 5.6, where one blade is shown for clarity. The blades have only lead-lag degrees of freedom and lead-lag hinge is supported by spring and damper. Helicopter and undercarriage system is modeled using dampers and springs in

two directions providing a minimum complexity model analyzing the ground resonance.

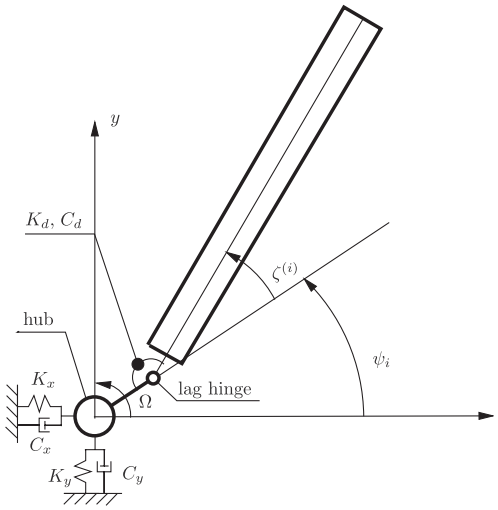

Figure 5.6: *Schematic of Hammond's Helicopter ground resonance Ref. [114]. There are two hub modes connected to the ground and rotating blades which include lead-lag degrees of freedom. (Only one blade is presented for clarity)*

The isotropic rotor case, i.e. equally spaced blades with identical properties, are analyzed and verified with Ref. [113]. The stability results for the isotropic rotor are not included here in order not to duplicate the original work. However, the equations of motion is briefly described to clearly address the sources of periodicity and nonlinearity in the analysis. The equations of motion in the rotating reference frame can be written as;

$$\mathbf{M}_r(t)\ddot{\mathbf{q}}_r + \mathbf{C}_r(t)\dot{\mathbf{q}}_r + \mathbf{K}_r(t)\mathbf{q}_r = \mathbf{0} \tag{5.5}$$

where $\mathbf{q}_r$, $\mathbf{M}_r$, $\mathbf{C}_r$ and $\mathbf{K}_r$ are degrees of freedom vector and mass, damping and stiffness matrices in rotating frame with periodic terms as given in original work [113]. In Hammond's model there are 4 blades with an allowed motion around lead-lag hinge(ζ_i, i being blade index) having an offset e, static moment S_ζ, mass moment of inertia J_ζ, lead-lag damper C_d and lead-lag spring K_d. Moreover the two hub in-plane degrees of freedom represent the dynamics of the fuselage and undercarriage system; x being longitudinal and y being lateral and characterized by $M_{x,y}$ $C_{x,y}$ and $K_{x,y}$, namely mass, damper and spring constants. The parameter values are reported in Table 5.1. Then, the

degree of freedom vector of the system is;

$$\mathbf{q}_r = [\zeta_1 \;\; \zeta_2 \;\; \zeta_3 \;\; \zeta_4 \;\; x \;\; y]^T \tag{5.6}$$

where $\psi_i = \psi + i2\pi/N$ is the azimuth angle of the corresponding blade with blade index i, whereas ψ is the reference azimuth angle. The corresponding mass, damping and stiffness matrices in rotating frame of reference are:

$$\mathbf{M}_r(\psi) = \begin{bmatrix} J_\zeta & 0 & 0 & 0 & -S_\zeta\cos\psi & -S_\zeta\sin\psi \\ 0 & J_\zeta & 0 & 0 & S_\zeta\sin\psi & -S_\zeta\cos\psi \\ 0 & 0 & J_\zeta & 0 & S_\zeta\cos\psi & S_\zeta\sin\psi \\ 0 & 0 & 0 & J_\zeta & -S_\zeta\sin\psi & S_\zeta\cos\psi \\ -S_\zeta\cos\psi & S_\zeta\sin\psi & S_\zeta\cos\psi & -S_\zeta\sin\psi & M_x & 0 \\ -S_\zeta\sin\psi & -S_\zeta\cos\psi & S_\zeta\sin\psi & S_\zeta\cos\psi & 0 & M_y \end{bmatrix} \tag{5.7a}$$

$$\mathbf{C}_r(\psi) = \begin{bmatrix} C_\zeta & 0 & 0 & 0 & 0 & 0 \\ 0 & C_\zeta & 0 & 0 & 0 & 0 \\ 0 & 0 & C_\zeta & 0 & 0 & 0 \\ 0 & 0 & 0 & C_\zeta & 0 & 0 \\ 2\Omega S_\zeta\sin\psi & 2\Omega S_\zeta\cos\psi & -2\Omega S_\zeta\sin\psi & -2\Omega S_\zeta\cos\psi & C_x & 0 \\ -2\Omega S_\zeta\cos\psi & 2\Omega S_\zeta\sin\psi & 2\Omega S_\zeta\cos\psi & -2\Omega S_\zeta\sin\psi & 0 & C_y \end{bmatrix} \tag{5.7b}$$

$$\mathbf{K}_r(\psi) = \begin{bmatrix} K_\zeta & 0 & 0 & 0 & 0 & 0 \\ 0 & K_\zeta & 0 & 0 & 0 & 0 \\ 0 & 0 & K_\zeta & 0 & 0 & 0 \\ 0 & 0 & 0 & K_\zeta & 0 & 0 \\ \Omega^2 S_\zeta\cos\psi & -\Omega^2 S_\zeta\sin\psi & -\Omega^2 S_\zeta\cos\psi & \Omega^2 S_\zeta\sin\psi & K_x & 0 \\ \Omega^2 S_\zeta\sin\psi & \Omega^2 S_\zeta\cos\psi & -\Omega^2 S_\zeta\sin\psi & -\Omega^2 S_\zeta\cos\psi & 0 & K_y \end{bmatrix} \tag{5.7c}$$

The degree of freedom vector and matrices can be transformed into the non-rotating frame using the multi-blade coordinate transformation explained in Section 2.7. The transformation matrices, which are normalized with the angular speed of the rotor, Ω, are $\mathbf{T}_1$, its first time derivative $\mathbf{T}_2$ and second time derivative $\mathbf{T}_3$. For a rotor having

Table 5.1: *Ground resonance: numerical values of Hammond model parameters*

Number of blades, N	4
Blade static moment, S_ζ	189.1 kgm
Blade mass moment of inertia, J_ζ	1084.7 kg m^2
Lag hinge offset, e	0.3048 m
Lag spring, K_d	0 Nmrad^{-1}
Lag damper, C_d	4067.5 Nmsrad^{-1}
Hub mass, M_x, M_y	8026.6 kg , 3283.6 kg
Hub spring, K_x, K_y	1240481.8 Nm^{-1}, 1240481.8 Nm^{-1}
Hub damper, C_x, C_y	51078.7 Nsm^{-1}, 25539.3 Nsm^{-1}

4 blades, these transformation matrices are:

$$\mathbf{T}_1 = \begin{bmatrix} 1 & \cos(\psi_1) & \sin(\psi_1) & -1 & 0 & 0 \\ 1 & \cos(\psi_2) & \sin(\psi_2) & 1 & 0 & 0 \\ 1 & \cos(\psi_3) & \sin(\psi_3) & -1 & 0 & 0 \\ 1 & \cos(\psi_4) & \sin(\psi_4) & 1 & 0 & 0 \\ 0 & 0 & 0 & 0 & 1 & 0 \\ 0 & 0 & 0 & 0 & 0 & 1 \end{bmatrix} \tag{5.8a}$$

$$\mathbf{T}_2 = \frac{\mathrm{d}\mathbf{T}_1}{\mathrm{d}\psi} \tag{5.8b}$$

$$\mathbf{T}_3 = \frac{\mathrm{d}\mathbf{T}_2}{\mathrm{d}\psi} \tag{5.8c}$$

Then, the degrees of freedom vector in the non-rotating frame is given as,

$$\mathbf{q}_{nr} = \mathbf{T}_1^{-1}\mathbf{q}_r = [\zeta_0 \;\; \zeta_{1c} \;\; \zeta_{1s} \;\; \zeta_{N/2} \;\; x \;\; y]^T; \tag{5.9}$$

where $\mathbf{q}_{nr}$ includes collective, ζ_0, cyclic, ζ_{1c} and ζ_{1s}, and reactionless, $\zeta_{N/2}$ blade lead-lag modes, and the two hub displacement modes x and y. Note that for a general system with periodic and nonlinear terms, the collective and reactionless degrees of freedom are expected to contribute to the dynamics of the rotor when coupled with the motion of the hub. Hence, as opposed to the isotropic rotor case, which was an LTI system; all degrees of freedom must be retained for periodic and nonlinear stability analysis. The equation of motion in the non-rotating frame can be written as,

$$\mathbf{M}_{nr}\ddot{\mathbf{q}}_{nr} + \mathbf{C}_{nr}\dot{\mathbf{q}}_{nr} + \mathbf{K}_{nr}\mathbf{q}_{nr} = \mathbf{0} \tag{5.10}$$

with the corresponding mass $\mathbf{M}_{nr}$, damping $\mathbf{C}_{nr}$ and stiffness $\mathbf{K}_{nr}$ ma-

trices in the non-rotating frame:

$$\mathbf{M}_{nr} = \mathbf{T}_1^{-1}\mathbf{M}_r\mathbf{T}_1 \tag{5.11a}$$

$$\mathbf{C}_{nr} = \mathbf{T}_1^{-1}(2\Omega\mathbf{M}_r\mathbf{T}_2 + \mathbf{C}_r\mathbf{T}_1) \tag{5.11b}$$

$$\mathbf{K}_{nr} = \mathbf{T}_1^{-1}(\Omega^2\mathbf{M}_r\mathbf{T}_3 + \Omega\mathbf{C}_r\mathbf{T}_2 + \mathbf{K}_r\mathbf{T}_1) \tag{5.11c}$$

Using the matrices formulated in Section 2.7 and the matrices of mixed-coordinates given in Eq. 5.7, the corresponding matrices in non-rotating frame are obtained for the isotropic rotor as a basis of periodic and nonlinear models, which are modified in the analyses depending on the characteristics of periodicity and nonlinearity. The matrices are:

$$\begin{aligned}\mathbf{M}_{nr} &= \mathbf{T}^{-1}\mathbf{M}_r\mathbf{T} \\ &= \begin{bmatrix} J_\zeta & 0 & 0 & 0 & 0 & 0 \\ 0 & J_\zeta & 0 & 0 & 0 & S_\zeta \\ 0 & 0 & J_\zeta & 0 & -S_\zeta & 0 \\ 0 & 0 & 0 & J_\zeta & 0 & 0 \\ 0 & 0 & -2S_\zeta & 0 & M_x & 0 \\ 0 & 2S_\zeta & 0 & 0 & 0 & M_y \end{bmatrix}\end{aligned} \tag{5.12a}$$

$$\begin{aligned}\mathbf{C}_{nr} &= \mathbf{T}^{-1}\left(2\Omega\mathbf{M}_r\mathbf{T}_{/\psi} + \mathbf{C}_r\mathbf{T}\right) \\ &= \begin{bmatrix} C_\zeta & 0 & 0 & 0 & 0 & 0 \\ 0 & C_\zeta & 2\Omega J_\zeta & 0 & 0 & 0 \\ 0 & -2\Omega J_\zeta & C_\zeta & 0 & 0 & 0 \\ 0 & 0 & 0 & C_\zeta & 0 & 0 \\ 0 & 0 & 0 & 0 & C_x & 0 \\ 0 & 0 & 0 & 0 & 0 & C_y \end{bmatrix}\end{aligned} \tag{5.12b}$$

$$\begin{aligned}\mathbf{K}_{nr} &= \mathbf{T}^{-1}\left(\Omega^2\mathbf{M}_r\mathbf{T}_{/\psi\psi} + \Omega\mathbf{C}_r\mathbf{T}_{/\psi} + \mathbf{K}_r\mathbf{T}\right) \\ &= \begin{bmatrix} K_\zeta & 0 & 0 & 0 & 0 & 0 \\ 0 & K_\zeta - \Omega^2 J_\zeta & \Omega C_\zeta & 0 & 0 & 0 \\ 0 & -\Omega C_\zeta & K_\zeta - \Omega^2 J_\zeta & 0 & 0 & 0 \\ 0 & 0 & 0 & K_\zeta & 0 & 0 \\ 0 & 0 & 0 & 0 & K_x & 0 \\ 0 & 0 & 0 & 0 & 0 & K_y \end{bmatrix}\end{aligned} \tag{5.12c}$$

5.3.1 Helicopter GR with Dissimilar Lead-Lag Dampers

In the non-rotating frame, i.e. in multi-blade coordinates as given in Eq. 5.12, the elements of the matrices of a ground resonance problem do not depend on the azimuth angle; hence, its stability can be analyzed using eigenvalue decomposition as a linear time invariant system. For this reason Hammond's model is not periodic for an isotropic rotor (i.e. with identical, equally spaced blades) unless the isotropy of the system is spoiled, e.g. by removing or modifying one of the characteristics of the blades such as the lead-lag damper or spring restraint. Whenever the isotropy of the rotor is broken, time dependence surfaces and eigenvalue decomposition may fail in reflecting the actual stability characteristics.

A typical case of engineering interest with periodic equations of motion is that of one blade damper inoperative or has dissimilar damping constant as compared to the dampers of the other blades. Such a problem is not a normal operating condition; yet, it needs to be analyzed to assess stability in case of a malfunction in dampers. In this analyses the estimates of the stability and sensitivity of stability properties are illustrated by removing the damper from one blade, and by considering the rotor angular speed Ω as the parameter. Since the model has a total of 12 states, only the most critical damping indicators, i.e. the largest two LCEs, are provided in results for clarity.

The sensitivity of the state space matrix with respect to Ω is straightforward using the transformation matrices formulated in Section 2.7 and the matrices of mixed-coordinates given in Eq. 5.7. The sensitivities of mass, damping and stiffness matrices can be obtained in a similar way to the sensitivities given in the flapping problem and then sensitivity of the state space model can be formed. In order to skip lengthy matrices, they are not included here.

For a rotor angular speed range of $\Omega = 0$ RPM to $\Omega = 400$ RPM, Fig. 5.7 presents the estimation of the largest two LCEs and Fig. 5.8 shows the sensitivity estimation of the corresponding LCEs with respect to rotor angular speed for the same range. The estimated LCEs and their sensitivity well match with the results obtained using the Floquet theory. Fig. 5.9 presents the time evolution of LCE estimates for the angular speed $\Omega = 400$ RPM and Fig. 5.10 gives the zoomed view of the same case after convergence is achieved. The first two LCEs show an oscillating behavior; their average slowly converges to the value given in Fig. 5.8.

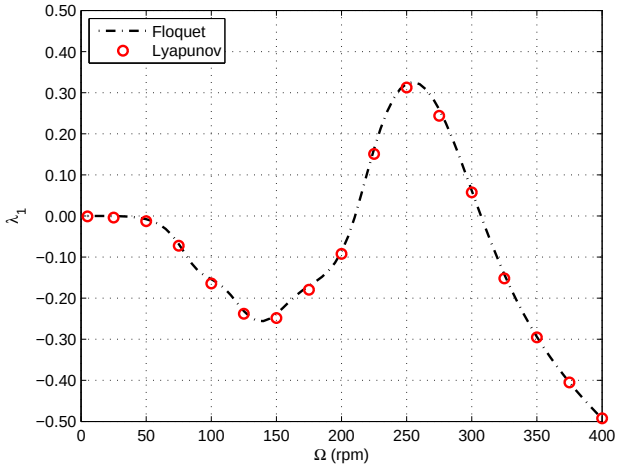

Figure 5.7: *Helicopter ground resonance with one blade damper inoperative: estimate of the largest LCE with respect to rotor angular speed* Ω

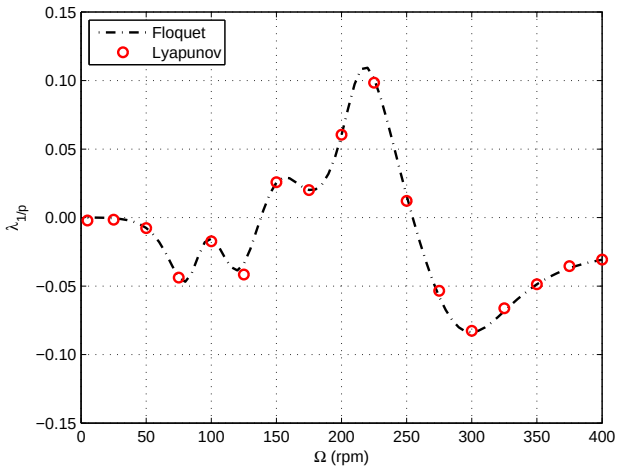

Figure 5.8: *Helicopter ground resonance with one blade damper inoperative: sensitivity estimate of the largest LCE given in Fig. 5.7 with respect to rotor angular speed* Ω

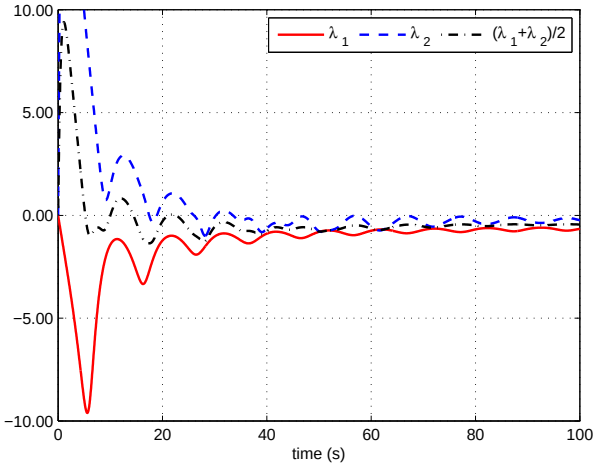

Figure 5.9: *Helicopter ground resonance with one blade damper inoperative: time evolution of the estimates of the largest two LCEs ($\Omega = 400$ rpm)*

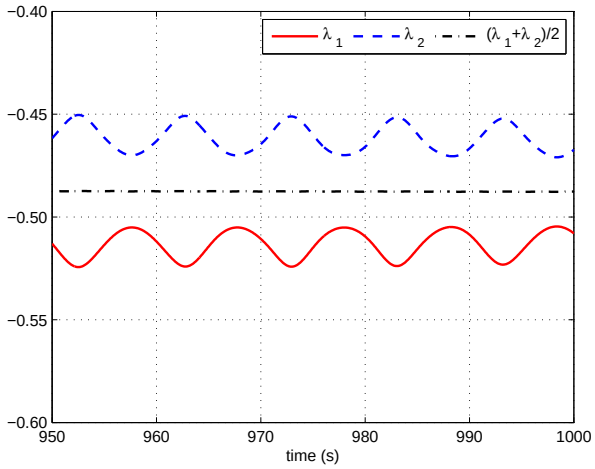

Figure 5.10: *Helicopter ground resonance with one blade damper inoperative: time evolution of estimates of the largest two LCEs ($\Omega = 400$ rpm), zoomed view after convergence*

5.3.2 Helicopter Ground Resonance with Nonlinear Lead-Lag Dampers

A distinctive advantage of LCEs is their capability to analyze and quantify the stability of the trajectories of nonlinear, non-autonomous dynamical systems. The dynamics of rotorcraft is generally described by nonlinear, time-dependent equations [65]. Among nonlinear phenomena, limit cycle oscillations (LCO) are defined as isolated closed trajectories of nonlinear dynamical systems; when an LCO develops, the system oscillates in a self-sustained manner without the need of an external input as described in Ref. [100]. Although being bounded seems to be in the favor of the system integrity in the sense that oscillations do not grow in amplitude; the occurrence of LCOs can affect structural life, flight safety and ride comfort of a rotorcraft. As in the case of nonlinear phenomena, the occurrence of LCOs can only be detected considering the nonlinearity of the problem [101].

For this purpose, the same ground resonance model of the previous example is studied with lead-lag dampers; characterized by a nonlinear constitutive law, to verify the application of the method to nonlinear problems. The simple nonlinear constitutive law of the damper considered in Ref. [114] (a moment quadratic in the angular velocity, modeling turbulent viscous flow, with saturation), which is plotted in Fig. 5.11, is modified by adding a linear term to the quadratic characteristic, yielding the moment

$$f_d = \begin{cases} \chi\dot{\zeta}|\dot{\zeta}| + C_L\dot{\zeta} & \dot{\zeta} < \dot{\zeta}_L \\ \bar{\chi}\dot{\zeta}_L|\dot{\zeta}_L| & \dot{\zeta} \geq \dot{\zeta}_L \end{cases} \tag{5.13}$$

about the lead-lag hinge, where $\chi = \bar{\chi} - C_L/\dot{\zeta}_L$ to ensure that the value of damping at the discontinuity point $\dot{\zeta}_L$ remains the same when the slope at zero angular velocity, C_L, is changed. The slope is chosen as the parameter for investigating the sensitivity of the LCE estimates. It is expressed as a fraction of the nominal linear damper C_b given in Table 5.1. The same parameter values of the damper given in Ref. [114] are used for the other parameters, as reported in Table 5.2.

Table 5.2: *Helicopter ground resonance with nonlinear blade damper: saturated hydraulic damper parameters, data from Ref. [114].*

$\bar{\chi}$	1.2203×10^6	Nms ^{2} rad $^{-2}$
$\dot{\zeta}_L$	1.0	degs $^{-1}$

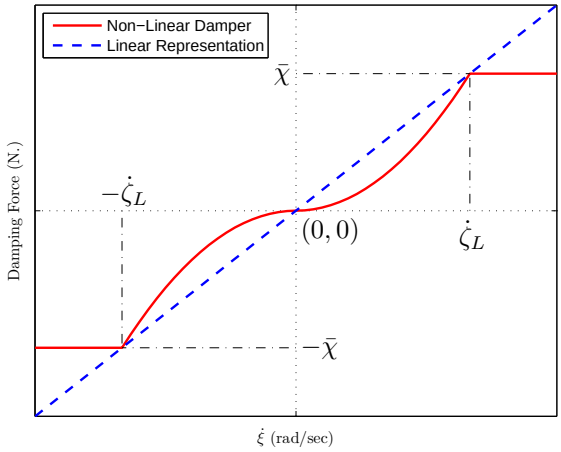

Figure 5.11: *Representation of a nonlinear damper with saturation and its linear representation, Ref. [114]*

In the model of Ref. [114] the slope C_L is zero, and Limit Cycle Oscillations (LCO) are reported. Without the linear term, the model is not realistic, since flow in a hydraulic damper tends to be laminar at small flow rates. Thus, the linear term better describes the physics of the device in the low speed regime and the addition of the linear parameter C_L can improve the accuracy of the model. Nevertheless, this problem has been selected to obtain a LCO in an otherwise reasonably realistic model and to test estimation of LCEs and their sensitivity with a nonlinear problem that may include LCO, exponential stability, and unstable equilibria.

As explained in Section 5.3, the original form of Hammond's model is linear. Whereas in this ground resonance with nonlinear damper problem, we are interested in changing one linear parameter to a nonlinear one while the linearity of the rest of the model is preserved. In such a case, if nonlinearity is in one or few components and the rest of the model is linear, the linearized model of Chapter 2 can be used to represent the linear dynamics and the nonlinear components can be included as a force caused by the nonlinear effects. In this particular case, the nonlinearity is in damping force caused by the lead-lag motion of the blades. The relation can be written as,

$$\mathbf{M}\ddot{\mathbf{x}} + \mathbf{C}\dot{\mathbf{x}} + \mathbf{K}\mathbf{x} + \mathbf{f_{NL}}(\dot{\boldsymbol{\zeta}}^2) = \mathbf{0} \tag{5.14}$$

where $\dot{\boldsymbol{\zeta}}$ is the vector of lead lag angle including contributions of all blades. Since all the matrices are in non-rotating reference frame, the nonlinear damping force $\mathbf{f_{NL}}$ should also be converted into multi-blade coordinates using the method explained in Section 2.7. Then the equations in state space form is:

$$\begin{bmatrix} \dot{\mathbf{x}} \\ \ddot{\mathbf{x}} \end{bmatrix} = \begin{bmatrix} \mathbf{O} & \mathbf{I} \\ -\mathbf{M}^{-1}\mathbf{K} & -\mathbf{M}^{-1}\mathbf{C} \end{bmatrix} \begin{bmatrix} \mathbf{x} \\ \dot{\mathbf{x}} \end{bmatrix} + \begin{bmatrix} \mathbf{0} \\ -\mathbf{M}^{-1}\mathbf{f_{NL}} \end{bmatrix} \tag{5.15}$$

Similar discussion also holds for the Jacobian matrix evaluation, which is required in estimating LCEs. Clearly, the derivative of the nonlinear forcing function with respect to its states $\mathbf{f_{NL/x}}$, i.e. the Jacobian, is a function of the rate of the lead-lag angle. For this reason, in nonlinear systems, the stability properties depends on initial conditions, as they also determine the trajectory and hence the Jacobian. Note that, Jacobian matrix is constant for LTI systems and periodic for LTP systems; in any case it is not a function of the state in linear systems.

The blade lag motion ζ (only one of four blades is shown for clarity) is discussed first. In plots, there are two curves each related to simulations starting from different initial conditions. Fig. 5.12 shows the blade lag motion for the cases in which the blade experiences LCO in the absence of linear damping therm ($C_L = 0$). The two curves with the same amplitude and period are obtained for different initial conditions, although a time shift can be observed. Such a behavior confirms the limit cycle interpretation of the attractor. Fig. 5.13 presents an exponentially stable system when the linear damping term is equal to the nominal value ($C_L = C_d$). The resulting curves converge to $\zeta = 0$, confirming the interpretation of the attractor as a stable point.

It is worth noticing that $\zeta = 0$ is also an equilibrium solution for the case $C_L = 0$. However, since solutions obtained with initial conditions in the vicinity of $\zeta = 0$ converge to the previously mentioned limit cycle, the solution $\zeta = 0$ is topologically an unstable equilibrium point, a so-called *repellor*. The instability of such solution is confirmed by the present analysis, which estimates a positive LCE.

The same phenomena can also be observed by looking at the phase plots of the blade motion. Fig. 5.14 presents the map of the blade lag motion and its time derivative for the cases in which the blade experiences LCO ($C_L = 0$) and whereas Fig. 5.15 gives the phase plane for an exponentially stable system ($C_L = C_d$). In both plots, the simulations start from different initial conditions, marked with "$*$". Again in Fig. 5.14, both the inner and outer trajectories converge to an

ellipse with the horizontal axis of $\zeta = 0.015$ deg and the vertical one of $\dot{\zeta} = 0.2$ deg/s. In Fig. 5.15, starting from the same initial conditions, the solutions converge to equilibrium, i.e. $\zeta = 0$ deg and $\dot{\zeta} = 0$ deg in case of sufficiently large damping slope at zero lag rate, $C_L = C_d$. It should be noted here that only the motion of one blade is shown here, and the intersections observed in the plot (for example the one on Fig. 5.14 starting from an outer trajectory) does not mean that two solutions exist at the intersection point. In fact, the problem has 12 states and the plot only shows one pair, projected on a 2D plane.

If the system has a periodic attractor, a so-called LCO, zero-valued LCE estimates (or very close to zero from a numerical analysis point of view) are expected [99]. In order to observe this and also further investigate sensitivity, LCEs and their sensitivity are estimated for a range of damper slopes at zero lag rate, C_L ($C_L = 0$ was used in Ref. [114]). Results are shown in Fig. 5.16 for largest two LCEs and in Fig. 5.16 for the corresponding sensitivity of LCEs; as it can be observed, starting from $C_L = 0$ the largest LCE is zero and remains approximately zero until $C_L \approx 0.35 C_d$. Hence, a LCO occurs in this range after the system encounters a perturbation. For larger values of C_L, the two largest LCEs (nearly) merge (i.e. they become quite close from a numerical point of view) and the system becomes exponentially stable with all LCEs being negative. This is verified by looking at the lag motion of the blade, as given in Fig. 5.12, which corresponds to $C_L = 0$, the blade motion converges to a stable LCO with magnitude 0.015 deg, as also reported in Ref. [114]. Increasing the zero lag rate slope provides asymptotic stability: for example, when $C_L = C_d$, all LCEs are negative; as shown in Fig. 5.13, system is exponentially stable.

The time evolution of LCE estimates corresponding to the cases of Fig. 5.12 and Fig. 5.13 are shown in Fig. 5.18 and Fig. 5.19 respectively. In the case resulting in an LCO, ($C_L = 0$ values of Fig. 5.16), the first two LCE estimates are distinct and the first LCE, λ_1, quickly converges to zero, corresponding to the stable LCO with magnitude 0.015 deg. A zero-valued LCE indicates a LCO; hence, the LCE estimates and the time simulations are in agreement. Increasing the slope at zero lag rate provides stability; for a sufficiently large value of C_L, as shown in Fig. 5.16, the first two LCE estimates converge to the same value, suggesting that they are coincident, with multiplicity 2, as if they were associated with complex conjugate eigenvalues in a LTI system. This solution is stable, as observed from the time simulations and indicated by the negative largest LCEs.

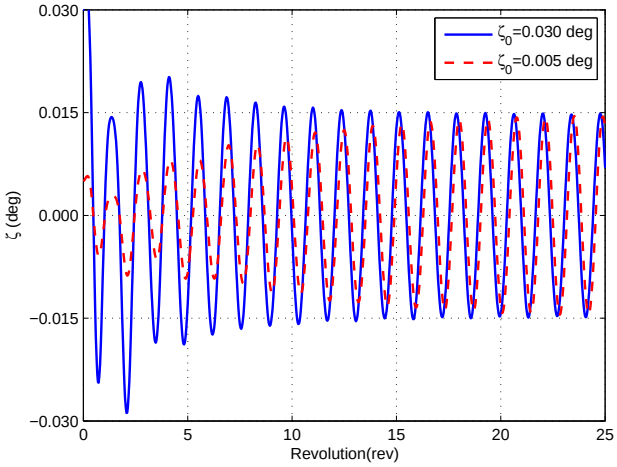

Figure 5.12: *Helicopter ground resonance with nonlinear blade damper: blade lag motion starting from different initial conditions for no damping at zero lag rate ($C_L = 0$) , resulting in limit cycle oscillations*

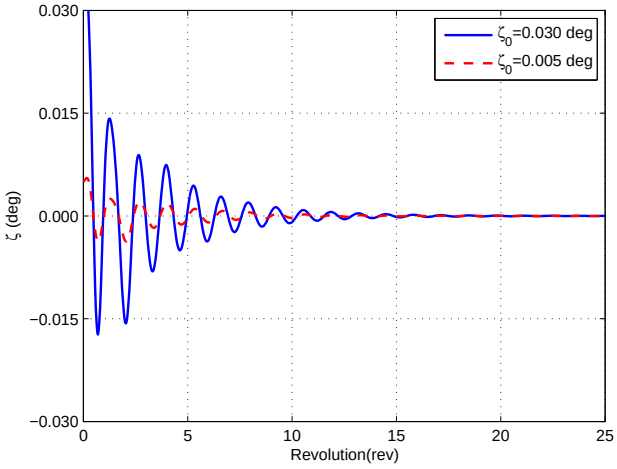

Figure 5.13: *Helicopter ground resonance with nonlinear blade damper: blade lag motion starting from different initial conditions for nominal damping at zero lag rate ($C_L = C_d$) , resulting in exponential stability.*

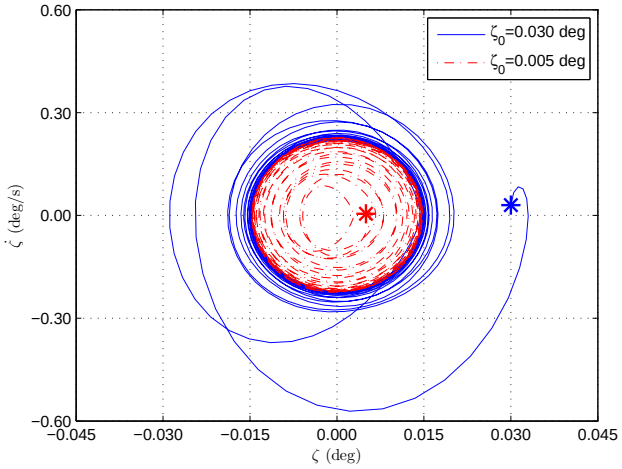

Figure 5.14: *Helicopter ground resonance with nonlinear blade damper: phase plane of blade lag motion starting from different initial conditions for no damping at zero lag rate ($C_L = 0$) which corresponds to blade lag motion given in Fig. 5.12, resulting in LCO*

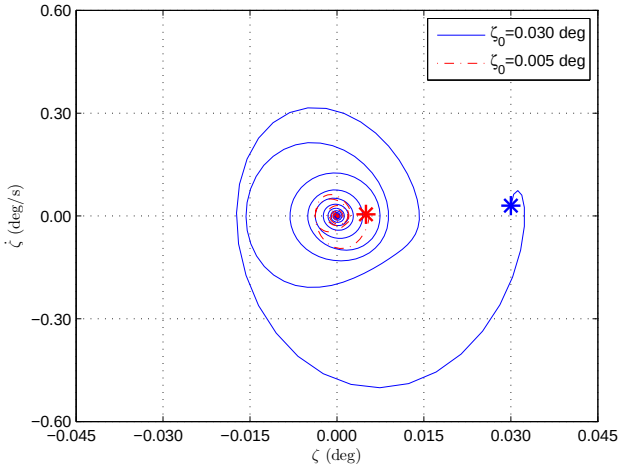

Figure 5.15: *Helicopter ground resonance with nonlinear blade damper: phase plane of blade lag motion starting from different initial conditions for nominal damping at zero lag rate ($C_L = C_d$) which corresponds to blade lag motion given in Fig. 5.13, resulting in exponential stability*

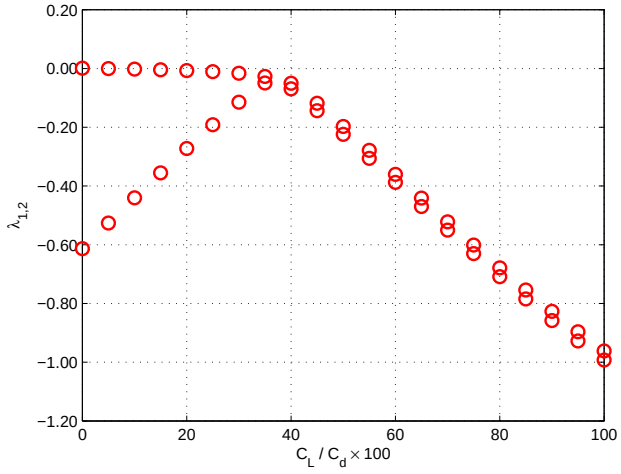

Figure 5.16: *Helicopter ground resonance with nonlinear blade damper: the largest two LCE estimates with respect to damper slope at zero lag rate C_L*

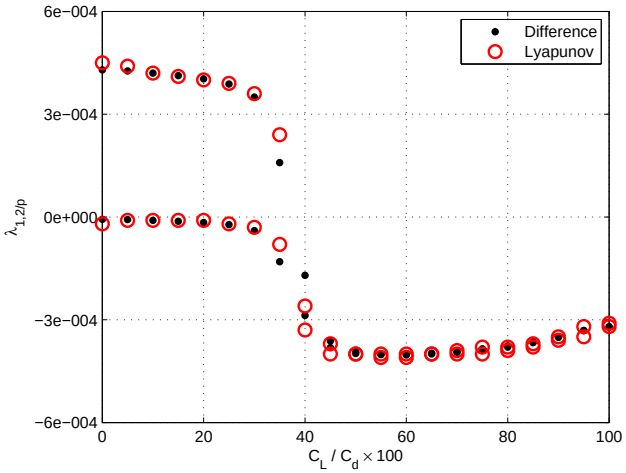

Figure 5.17: *Helicopter ground resonance with nonlinear blade damper: sensitivity estimates of the largest two LCEs given in Fig. 5.16 with respect to damper slope at zero lag rate C_L*

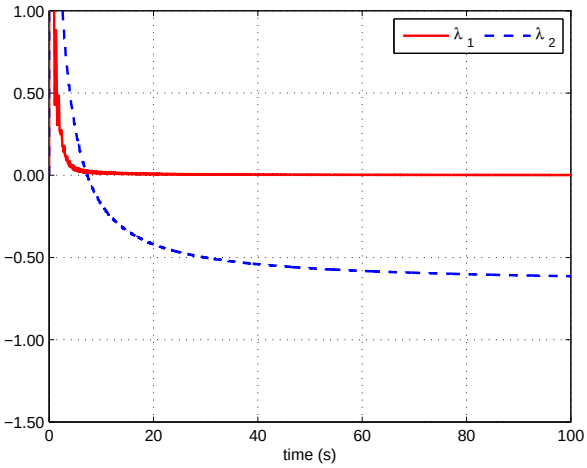

Figure 5.18: *Helicopter ground resonance with nonlinear blade damper: time evolution of the largest two LCE estimates for no damping at zero lag rate ($C_L = 0$), system with LCO*

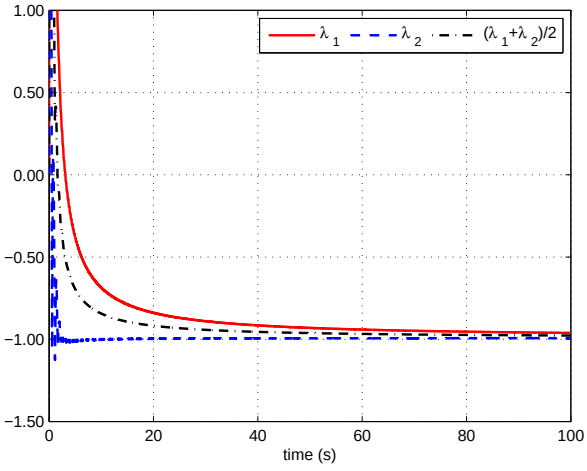

Figure 5.19: *Helicopter ground resonance with nonlinear blade damper: time evolution of LCE estimates for nominal damping at zero lag rate ($C_L = C_d$), exponentially stable system*

5.3.3 Helicopter Ground Resonance with Dissimilar and Nonlinear Lead-Lag Dampers

In order to apply the proposed approach to a nonlinear non-autonomous problem, the one damper inoperative model is modified using the nonlinear damper of Eq. 5.13. Linear damping constant (C_L) is selected as the parameter and stability and sensitivity analyses are performed for the range of the parameter given in the previous subsection. The first two LCEs are shown in Fig. 5.20 as functions of the percentage of linear damping C_L. For C_L/C_d region up to 75% the first LCE is greater than zero. Since, for a nonlinear system, a positive LCE indicates chaos as described in Ref. [99], chaotic behavior is expected in this region. Then the largest two, hence all, LCEs become smaller than zero, we can expect a stable system.

Fig. 5.21 presents the analytical sensitivity results corresponding to the largest two LCEs and compared with the finite difference results which are simply obtained by taking first derivative of the curves in Fig. 5.20. While the positive LCE remains almost constant the sensitivity for C_L/C_d region up to 75%, the other mode has positive gradient and two modes are merging. Analytical and finite difference results can be considered close and follow the similar pattern.

In order to check the results, we further analyze the two extreme points of Fig. 5.20. Fig. 5.22 shows the lag motion of one blade (only one blade is presented for simplicity) for null slope at zero lag rate ($C_L = 0$) and compares it with Fig. 5.14, i.e. the results of an isotropic rotor with identical nonlinear dampers. The solution seems unstable in the sense that it does not converge to an equilibrium point or a periodic orbit but at the same time remains within a bounded region of state space. In fact, this is the distinctive property of chaos, a never repeating bounded trajectory as explained in Refs. [99] and [100]. Hence, the positive largest LCE and the chaotic motion of the blade are in agreement. The time evolution of LCEs for this case is given in Fig. 5.23, which show two separates LCEs.

On the contrary, Fig. 5.24 presents the lag motion of the one blade for the damper having nominal slope at zero lag rate ($C_L = C_d$). Again there is no dominant period and the motion seems arbitrary but this time the amplitude converges to zero, resulting in a stable system. The corresponding time evaluation of LCEs in time are presented in Fig. 5.25 showing two LCEs converging to the same value leading to multiplicity of the largest two LCEs.

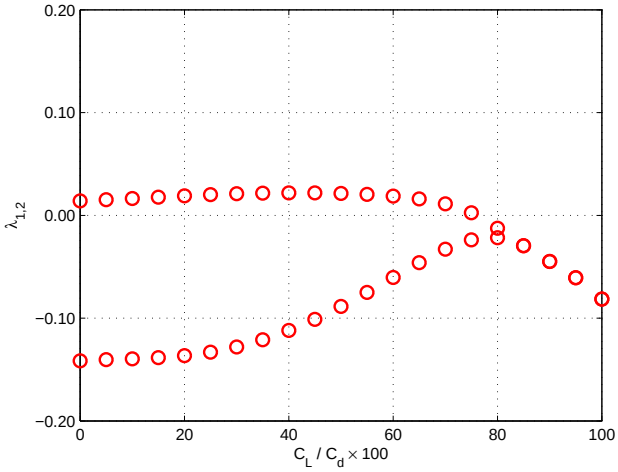

Figure 5.20: *Helicopter ground resonance with dissimilar nonlinear blade damper: the largest two LCE estimates vs. damper slope at zero lag rate C_L.*

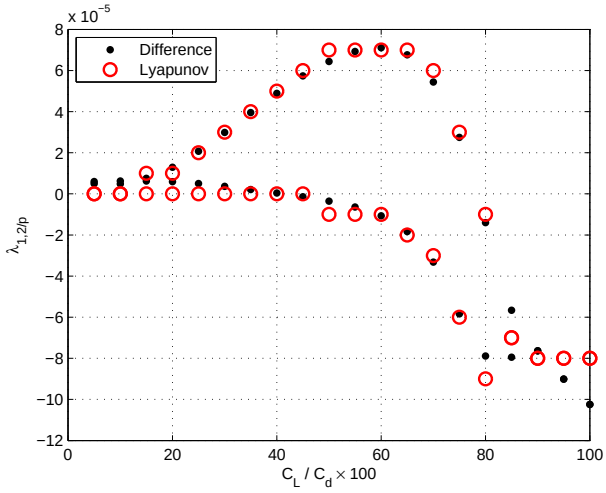

Figure 5.21: *Helicopter ground resonance with dissimilar nonlinear blade damper: sensitivity estimates of largest two LCEs given in Fig. 5.20 vs. damper slope at zero lag rate C_L.*

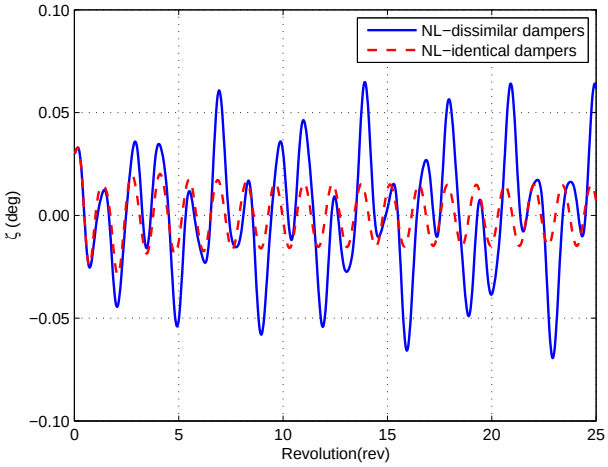

Figure 5.22: *Helicopter ground resonance with dissimilar nonlinear blade damper: blade lag motion for no damping at zero lag rate ($C_L = 0$) starting from different initial conditions, compared with the isotropic damper case*

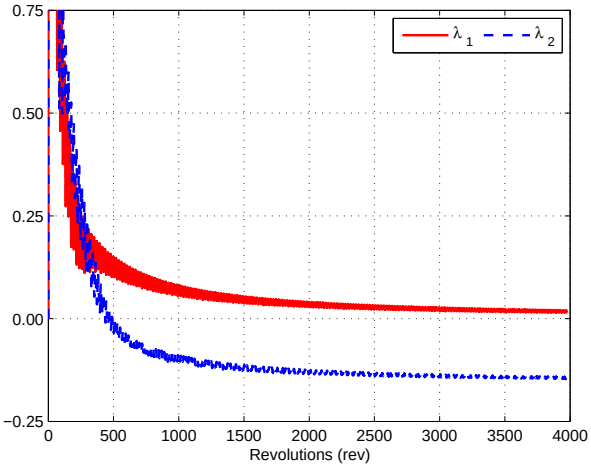

Figure 5.23: *Helicopter ground resonance with dissimilar nonlinear blade damper: time evolution of largest two LCEs for no damping at zero lag rate ($C_L = 0$)*

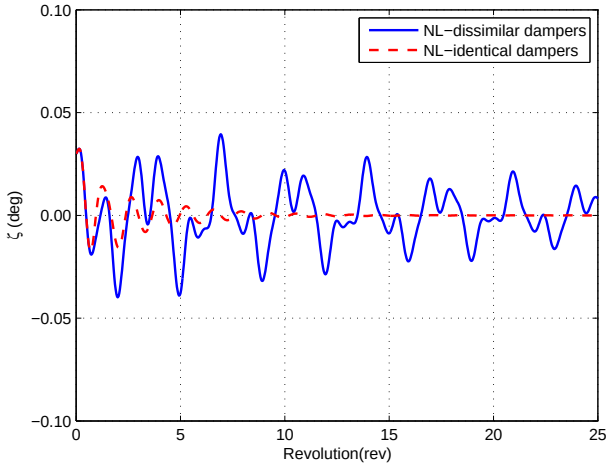

Figure 5.24: *Helicopter ground resonance with dissimilar nonlinear blade damper: blade lag motion for nominal damping at zero lag rate ($C_L = C_d$) starting from different initial conditions, compared with the isotropic damper case*

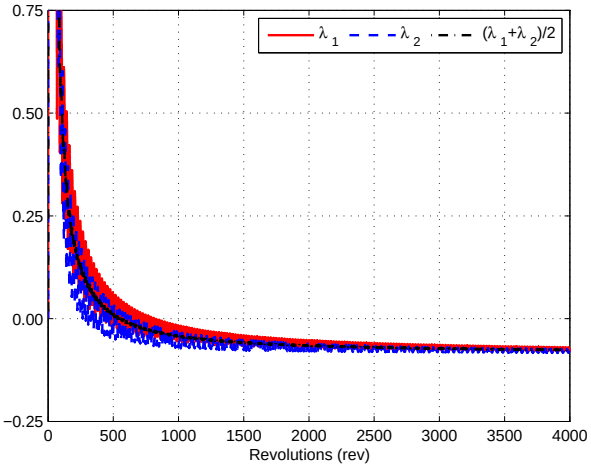

Figure 5.25: *Helicopter ground resonance with dissimilar nonlinear blade damper: time evolution of first two LCEs for nominal damping at zero lag rate ($C_L = C_d$)*

5.4 Analysis of a Detailed Helicopter Model

The nature of the rotorcraft aeroservoelasticity possesses interaction of structural dynamics, aerodynamics and control systems of rotorcraft; with each field having considerable numbers of degrees of freedom, even in their simplest and the most compact forms. As described in Chapter 4; the methods of estimating LCEs, including discrete QR, requires matrix manipulations at each step, with multiplication and orthogonalization. In the sensitivity estimation, things become more complicated; the number of manipulations increase as the derivative of the state transition matrix, hence the derivative of the decomposition, add more matrix manipulations. More severely, the procedure should be continued theoretically for an infinite limit and practically till the convergence of LCEs. As a consequence, the nature of the LCE estimation may cause high computational cost and problems in convergence as the number of state variables increases.

In such a case where there exist many degrees of freedom; extracting the most critical LCEs, i.e. the few largest, can be a solution, which may help improving computation efficiency as stated in Ref. [115,116]. However, there can be many lightly damped LCEs in a detailed rotorcraft model. Such lightly damped modes can be critical and are required to be estimated for an unknown number of LCEs. Therefore, within the scope of this work, the method should be verified for a detailed system for its whole spectra.

An aeroservoelastic model of hovering rotorcraft is selected. As opposed to the ground resonance, which is a purely mechanical problem as stated in Ref. [22], the aerodynamic contribution of the rotor and aerodynamic derivatives of the fuselage are involved. Moreover, the body is not supported, hence there exist unconstrained rigid body modes. The directional control should be maintained by means of a tail rotor and sensors for yaw rate. In this section of the chapter; first, the model is verified in Section 5.4.1 against existing results for the LTI model using classical eigenvalue decomposition. Then, in Section 5.4.2, periodicity is introduced using dissimilarity in lead-lag dampers. Stability and sensitivity of stability properties are estimated using Floquet method and Lyapunov Characteristice Exponents (LCEs).

5.4.1 Aeroservoelastic Stability of LTI model

This section presents the aeroservoelastic stability analysis of a detailed helicopter model for the comparison of linearized aeroelastic ro-

tor model formulated in Chapter 2 with respected a reference model. Since the capability of MASST prior to this work is limited to the stability analysis of LTI systems, hover condition is presented here (a forward flight condition with averaged matrices over the rotor disc could be a possible application as well). The MASST model developed for the analysis given in Ref. [89] is considered as a basis; the comparison is made for rotor matrices originating from different sources. The fuselage model involves 6 rigid body modes with flight mechanics derivatives and 10 elastic modes, whereas the aeroelastic rotor modes involve 3 bending which makes a total of 12 rotor modes in multi-blade coordinates. The directional controller and corresponding sensors are also included. This model also serves as a basis for the stability and sensitivity of the periodic problem of Section 5.4.2.

The aeroelastic eigenvalues ($s = \lambda + \omega \mathrm{j}$) of the model described in Chapter 2 (LARotor) and reference model of Ref. [89] are compared in non-rotating frame. The results are presented in Fig. 5.26 in which the horizontal axis represents the real part of the eigenvalues ($\lambda = Re(s)$), whereas the vertical axis gives the imaginary part of the eigenvalues ($\omega = Im(s)$); in other words damping and frequency respectively. Good agreement can be observed both in terms of the damping and frequency values.

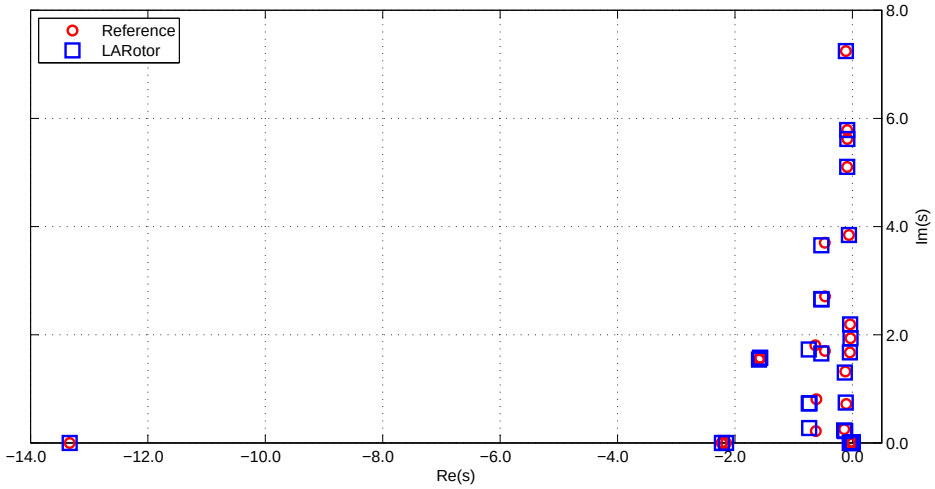

Figure 5.26: *Aeroservoelastic Stability of detailed helicopter model in hover: comparison of the eigenvalues with Reference solution from Ref. [89]. The differences in the models originate from the rotor matrices*

5.4.2 Aeroservoelastic Stability with Dissimilar Lead Lag Dampers

This section presents the analysis of stability and sensitivity of stability properties for a detailed helicopter model with periodic characteristics and aeroserveolastic interactions, as an extension to the stability of LTI system given in Section 5.4.1. An aeroelastic model closely related to PUMA helicopter that was developed and used in Ref. [89] is selected for the analysis. The periodic rotor matrices, obtained by the aeroelastic model of Chapter 2, are added to the MASST model.

In order to introduce periodicity, the lead-lag damper of one blade is considered as a parameter varying from zero ($C_L = 0$) to the two times of the nominal value ($C_L = 2C_d$), while the other dampers are kept at their nominal values ($C_L = C_d$). Hence the resulting model is linear time periodic. Stability and sensitivity analyses of the LTP model are performed using Floquet theory as described in Chapter 3 and Lyapunov Theory as explained in Chapter 4 and characteristic exponents are compared.

In Fig. 5.27 the characteristic exponents are estimated for the parameter range using both Floquet and Lyapunov. The LCEs show good correlation with Floquet within the range of the analysis. It can also be observed that the higher modes are not sensitive to the parameter change. On the other hand the lightly damped modes, which has higher contribution from in-plane motion of the rotor, have higher sensitivity to the dissimilarity in the rotor. This can be better seen in Fig. 5.28 where only lightly damped modes are captured.

Among those, the mode which is the most sensitive to the parameter change, is the lightly damped lag mode. The corresponding characteristic exponents are separately plotted in Fig. 5.29. It can be observed that even when one damper is completely inoperative the system does not lose stability in lead-lag direction. This is mainly due to the presence of the aerodynamic damping coming from the coupled lag-flap motion. Moreover, on the contrary to a ground resonance, helicopter is free from ground and hence the dynamics of landing gear on rolling motion does not cause additional coupling with the in-plane motion of the rotor center of gravity. The corresponding sensitivity of the LCE of Fig. 5.29 is given in Fig. 5.30. Comparison of sensitivity estimate of the LCE with the Floquet sensitivity and with finite difference values of Fig. 5.29 is also provided. Results show the estimates using LCEs is close to those obtained by Floquet and finite difference.

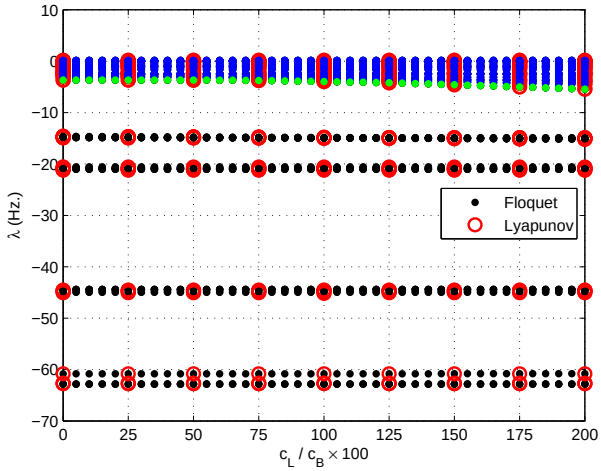

Figure 5.27: *Detailed LTP H/C model: Characteristic Exponents estimated by Floquet Analysis and Lyapunov Theory (LCEs), whole range where lightly damped modes are marked with blue.*

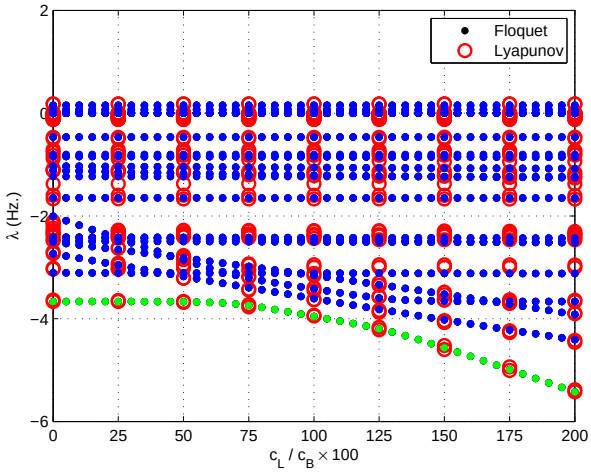

Figure 5.28: *Detailed LTP H/C model: Characteristic Exponents estimated by Floquet Analysis and Lyapunov Theory (LCEs), lightly damped modes zoomed from Fig. 5.27 where lightly damped blade lag mode marked with yellow.*

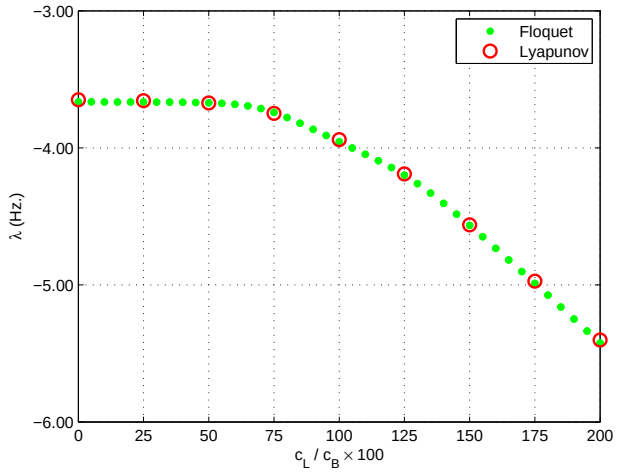

Figure 5.29: *Detailed LTP H/C model: Characteristic Exponents estimated by Floquet Analysis and Lyapunov Theory (LCEs) corresponding to the lightly damped blade lag mode, zoomed from Fig. 5.28*

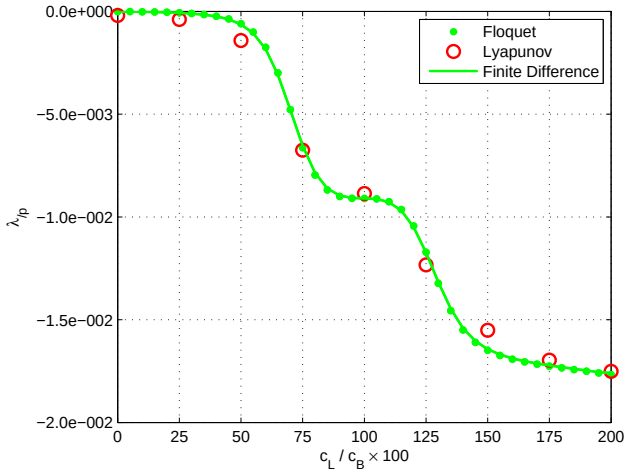

Figure 5.30: *Detailed LTP H/C model: Sensitivity estimates of characteristic Exponents estimated by Floquet Analysis and Lyapunov Theory (LCEs) corresponding to the lightly damped blade lag mode of Fig. 5.29.*

CHAPTER 6

Conclusions and Future Work

This work presents our research with the scope of achieving a complete rotorcraft aeroservoelastic analysis capability. An aeroelastic rotor model is developed and coupled with MASST aeroservoelastic analysis platform. The quantitative stability analysis and sensitivity of stability properties are formulated using Floquet method for linear time periodic (LTP) and Lyapunov Characteristic Exponents (LCEs) for nonlinear non-autonomous rotorcraft systems. The tools and methods are illustrated and discussed on rotorcraft related problems and the capacity of capturing periodic and nonlinear phenomena is proved.

The aeroelastic rotor model is verified against respected tools. It is showed that aeroservoelastic stability of rotorcraft can be performed with a capacity close to the commercial codes. Still, rotor is a very complex mechanism and the aeroelastic rotor tool is always open to improvement. The development will continue especially with higher fidelity aerodynamics.

The numerical methods of stability and sensitivity of linear time invariant and linear time periodic systems using eigenvalue calculation and Floquet analysis are robust. Unless the state space matrix is singular they can be used with confidence. Moreover stability and

sensitivity of stability estimates of linear systems can be obtained quite fast. On the other hand, estimation of LCEs and their sensitivity require an infinity limit in the estimation and hence much more slower than eigen-solution and Floquet Analysis. The methods for estimation of Lyapunov Exponents are also less robust and efficient when the size of the system increases with multiplicity of LCEs. Although this is the price of generalizing stability analysis and increasing the capacity of quantitative estimation of stability properties, more robust techniques can be developed in order to automatically capture the multiplicity of the exponents and match the multiple ones. This will help reducing the computational cost; since when correctly recognized, multiplicity of Lyapunov Exponent estimates presents a much faster convergence to the correct value. This is also true for increasing computational efficiency of the sensitivity of Lyapunov Exponents.

It is believed that a robust and cost efficient estimation of Lyapunov Characteristic Exponents, with the increasing power of computer, can make it the standard stability estimation. Especially for several aerospace related applications including rotorcraft aeroservoelasticity; time dependence, often in conjunction with non-strict periodicity and quasi-periodicity, as well as nonlinearity, cannot be neglected. LCEs correspond to the real part of the eigenvalues for linear time invariant systems, and to Floquet multipliers for linear time periodic systems; hence, they represent a natural generalization of stability indicators that are familiar in current engineering practice.

The nature of the rotorcraft aeroservoelasticity possesses interaction of different fields with each field having considerable number of degrees of freedom, even in their simplest and most compact forms. The methods of estimating LCEs, including discrete QR, requires matrix manipulations at each step, which include multiplication and orthogonalization. In the sensitivity estimation, the number of manipulations increase as the derivative of the state transition matrix is needed. More severely, the procedure should be continued theoretically for an infinite limit and practically for convergence of LCEs; which causes increase in the computational cost and problems in convergence. Although, there can be many lightly damped LCEs in a detailed rotorcraft model, extracting the few largest instead of its whole spectra can help in reducing computational cost.

Another extension of this work is to make use of the sensitivity of the stability estimates. Analytical sensitivity of Floquet multipliers and LCEs that are formulated in this work can proficiently support

the sensitivity analysis of systems with increasing levels of complexity. These sensitivities can be used to determine the robustness of stability, to detect bifurcations and to provide the gradients of stability parameters required in optimization and continuation algorithms.

Bibliography

[1] Stanley S. McGowen. *Helicopters, an illustrated history of their impact*. ABC Clio, Santa Barbara, CA, 2005.

[2] John Watkinson. *Art of the Helicopter*. Elsevier, 2004.

[3] Wayne Johnson. *Rotorcraft Aeromechanics*. Cambridge University Press, 2013.

[4] Antonio Filippone. *Flight Performance of Fixed and Rotary Wing Aircraft*. Elsevier, 2006.

[5] F.D. Harris and M.P. Scully. Rotorcraft cost too much. *Journal of the American Helicopter Society*, 43(1):3–13, 1998. doi:10.4050/JAHS.43.3.

[6] Anonymous. Rotorcraft flying handbook. FAA H-8083-21, Federal Aviation Administration, 2000.

[7] Thomas E. Noll. Aeroservoelasticity. TM 102620, NASA, March 1990.

[8] Jan R. Wright and Jonathan E. Cooper. *Introduction to Aircraft Aeroelasticity and Loads*. John Wiley & Sons, Chichester, 2007.

[9] John D. Anderson Jr. *Fundamental of Aerodynamics*. McGraw-Hill, Inc., New York, 3rd edition, 2001.

[10] J. Gordon Leishman. *Principles of Helicopter Aerodynamics*. Cambridge University Press, Cambridge, UK, 2000.

[11] K.S. Brentner and F. Farassat. Modeling aerodynamically generated sound of helicopter rotors. *Progress in Aerospace Sciences*, 39(2):83–120, April 2003. 10.1016/j.paerosci.2005.01.001.

[12] W. Johnson. Airloads, wakes and aeroelasticity. CR 177551, NASA, 1990.

[13] T. H. G. Megson. *Aircraft Structures for Engineering Students*. Halsted Press, New York, USA, 2nd edition, 1990.

[14] J. Seddon. *Basic Helicopter Aerodynamics*. BSP Professional Books, London, 1990.

[15] Gloria K. Yamauchi and Larry A. Young. A status of NASA rotorcraft research. TP 2009-215369, NASA, September 2009.

[16] Dewey H. Hodges. Review of composite rotor blade modeling. *AIAA Journal*, 28(3):561–565, March 1990.

[17] Olivier A. Bauchau and C. H. Hong. Large displacement analysis of naturally curved and twisted composite beams. *AIAA Journal*, 25(11):1469–1475, November 1987.

[18] Dewey H. Hodges. Nonlinear equations for dynamics of pretwisted beams undergoing small strains and large rotations. TP 2470, NASA, May 1985.

[19] R. Ferrer, T. Krysinski, P.A. Auborg, and S. Belizzi. New methods for rotor tracking and balance tuning and defect detection applied to eurocopter products. In *American Helicopter Society 57th Annual Forum*, Washington, DC, May 9–11 2001.

[20] Donald L. Kunz. A survey and comparison of engineering beam theories for helicopter rotor blades. *Journal of Aircraft*, 31(3):473–479, 1994.

[21] Pierangelo Masarati and Marco Morandini. On the modeling of rotating beams for rotorcraft blade analysis. In *28th European Rotorcraft Forum*, pages 62.1–11, Bristol, UK, 17–20 September 2002.

[22] A. R. S. Bramwell, George Done, and David Balmford. *Bramwell's Helicopter Dynamics*. Butterworth-Heinemann, 2001.

[23] G. S. Doman. Research requirements for the reduction of helicopter vibration. CR 145116, NASA, 1976.

[24] Raymond G. Kvaternik and T. Sreekanta Murthy. Airframe structural dynamic considerations in rotor design optimization. TP 212490, NASA, 2006.

[25] R.M. Heffernan and M. Gaubert. Vibration analysis SA349/2 helicopter. TM 102794, NASA, 1991.

[26] A.C. VECA. Vibration effects on helicopter reliability and maintainability. TM 73-11, NASA, 1973.

[27] Kristin L. Harrer, Debra Yniguez, Maria Majar Maria, David Ellenbecker, Nancy Estrada, and Mark Geiger. Whole body vibration exposure for MH-60s pilots. In *43th SAFE*, Utah, USA, 2005.

[28] Rendy P. Cheng, Mark B. Tischler, and Roberto Celi. A high-order, linear time-invariant model for application to higher harmonic control and flight control system interaction. TR 04-005, NASA, 2006.

[29] Alfred Gessow and Garry C. Myers Jr. *Aerodynamics of the Helicopter*. Frederick Ungar Publishing, New York, 1976.

[30] L. R. Stiles, J. Mayo, A. L. Freisner, K. H. Landis, and B. D. Kothmann. "Impossible to Resist" the development of rotorcraft fly-by-wire technology. In *American Helicopter Society 60th Annual Forum*, Baltimore, MD, June 8-10 2004.

[31] Raymond W. Prouty and H. C. Curtiss. Helicopter control systems: A history. *J. of Guidance, Control, and Dynamics*, 26(1):12–18, 2003. doi: 10.2514/2.5039.

[32] Ch. Kessler. Active rotor control for helicopters: motivation and survey on higher harmonic control. *CEAS Aeronaut. J.*, available online, 2011. doi:10.1007/s13272-011-0005-9.

[33] Aykut Tamer, Vincenzo Muscarello, Pierangelo Masarati, Giuseppe Quaranta, and Yavuz Yaman. Helicopter vibratory loads and vibrations reduction using higher-harmonic control. In *39th European Rotorcraft Forum*, Moscow, RU, 3–6 September 2014.

[34] M.N.H . Hamouda and G.A. Pierce. Helicopter vibration suppression using simple pendulum absorbers on the rotor blade. CR NSG-1592, NASA, 1982.

[35] Peretz P. Friedmann and T. A. Millot. Vibration reduction in rotorcraft using active control: a comparison of various approaches. *J. of Guidance, Control, and Dynamics*, 18(4):664–673, July-August 1995.

[36] J. Becker, B. Caldwell, and V. Vaccaro. The interaction of flight control system and aircraft structure. In *RTO AVT SpecialistsMeeting on Structural Aspects of Flexible Aircraft Control*, Ottawa, Canada, October 18–20 1999.

[37] Wolfgang Luber. Aeroservoelastic flight control design for a military combat aircraft weapon system. In *28th Congress of the International Council of the Aeronautical Sciences*, Brisbane, Australia, September 23–28 2012.

[38] O. Dieterich, J. Götz, B. DangVu, H. Haverdings, P. Masarati, M. D. Pavel, M. Jump, and M. Gennaretti. Adverse rotorcraft-pilot coupling: Recent research activities in Europe. In *34th European Rotorcraft Forum*, Liverpool, UK, September 16–19 2008.

[39] J. Serafini, M. Gennaretti, P. Masarati, G. Quaranta, and O. Dieterich. Aeroelastic and biodynamic modeling for stability analysis of rotorcraft-pilot coupling phenomena. In *34th European Rotorcraft Forum*, Liverpool, UK, September 16–19 2008.

[40] Pierangelo Masarati and Giuseppe Quaranta. Bioaeroservoelastic analysis of involuntary rotorcraft-pilot interaction. *J. of Computational and Nonlinear Dynamics*, 9(3):031009, July 2014. doi:10.1115/1.4025354.

[41] Pierangelo Masarati, Giuseppe Quaranta, Massimo Gennaretti, and Jacopo Serafini. An investigation of aeroelastic rotorcraft-pilot interaction. In *37th European Rotorcraft Forum*, Gallarate, Italy, September 13–15 2011. Paper no. 112.

[42] John R. Mayo. The involuntary participation of a human pilot in a helicopter collective control loop. In *15th European Rotorcraft Forum*, pages 81.1–12, Amsterdam, The Netherlands, 12–15 September 1989.

[43] T. Parham, Jr., David Popelka, David G. Miller, and Arnold T. Froebel. V-22 pilot-in-the-loop aeroelastic stability analysis. In *American Helicopter Society 47th Annual Forum*, Phoenix, Arizona (USA), May 6–8 1991.

[44] Pierangelo Masarati, Giuseppe Quaranta, and Michael Jump. Experimental and numerical helicopter pilot characterization for aeroelastic rotorcraft-pilot couplings analysis. *Proc. IMechE, Part G: J. Aerospace Engineering*, 227(1):124–140, January 2013. doi:10.1177/0954410011427662.

[45] Vincenzo Muscarello, Pierangelo Masarati, and Giuseppe Quaranta. Robust aeroservoelastic analysis for the investigation of rotorcraft pilot couplings. In *3rd CEAS Air & Space Conference*, Venice, Italy, October 24–28 2011.

[46] Giuseppe Quaranta, Aykut Tamer, Vincenzo Muscarello, Pierangelo Masarati, Massimo Gennaretti, Jacopo Serafini, and Marco Molica Colella. Rotorcraft aeroelastic stability using robust analysis. *CEAS Aeronaut. J.*, 5(1):29–39, March 2014. doi:10.1007/s13272-013-0082-z.

[47] Wayne Johnson. Development of a comprehensive analysis for rotorcraft — I. rotor model and wake analysis. *Vertica*, 5:99–129, 1981.

[48] Wayne Johnson. Development of a comprehensive analysis for rotorcraft — II. aircraft model, solution procedure and applications. *Vertica*, 5:185–216, 1981.

[49] Wayne Johnson. Technology drivers in the development of CAMRAD II. In *American Helicopter Society Aeromechanics Specialists Conference*, San Francisco, California, January 19–21 1994.

[50] Olivier A. Bauchau and N. K. Kang. A multibody formulation for helicopter structural dynamic analysis. *Journal of the American Helicopter Society*, 38(2):3–14, April 1993.

[51] MBDyn: Multibody dynamics. http://www.mbdyn.org/ (last accessed June 2014).

[52] Pierangelo Masarati, Vincenzo Muscarello, and Giuseppe Quaranta. Linearized aeroservoelastic analysis of rotary-wing aircraft. In *36th European Rotorcraft Forum*, pages 099.1–10, Paris, France, September 7–9 2010.

[53] Pierangelo Masarati, Vincenzo Muscarello, Giuseppe Quaranta, Alessandro Locatelli, Daniele Mangone, Luca Riviello, and Luca Viganò. An integrated environment for helicopter aeroservoelastic analysis: the ground resonance case. In *37th European Rotorcraft Forum*, pages 177.1–12, Gallarate, Italy, September 13–15 2011.

[54] Morris W. Hirsch, Stephen Smale, and Robert L. Devaney. *Differential Equations, Dynamical Systems, and an Introduction to Chaos*. Elsevier, San Diego, California, 2004.

[55] David G. Hull. *Fundamentals of Airplane Flight Mechanics*. Springer-Verlag, Berlin, 2007.

[56] Robert H. Bishop Richard C. Dorf. *Modern Control Systems*. Pearson - Prentice Hall, New Jersey, 2005.

[57] Sergio Bittanti and Patrizio Colaneri. *Periodic Systems*. Springer, 2009.

[58] Giancarlo Benettin, Luigi Galgani, Antonio Giorgilli, and Jean-Marie Strelcyn. Lyapunov characteristic exponents for smooth dynamical systems and for Hamiltonian systems; a method for computing all of them. part 1: Theory. *Meccanica*, 15(1):9–20, March 1980. doi:10.1007/BF02128236.

[59] S. S. Rao. *Engineering Optimization*. John Wiley & Sons, 1996.

[60] H.M. Osinga B. Krauskopf and K. Galan-Vioque. *Numerical Continuation Methods for Dynamical Systems*. Bristol.

[61] Aykut Tamer. Analysis and design of helicopter rotor blades for reduced vibrational level. Master's thesis, Middle East Technical University, Ankara, Turkey, 2011.

[62] Aykut Tamer and Yavuz Yaman. Optimization of an helicopter rotor for minimum vibratory loads. In *Ankara International Aerospace Conference*, Ankara, TR, September 14–16 2011.

[63] Aykut Tamer and Pierangelo Masarati. Linearized structural dynamics model for the sensitivity analysis of helicopter rotor blades. In *Ankara International Aerospace Conference*, Ankara, TR, September 11–13 2013.

[64] G. Orosz and G. Stépán. Hopf bifurcation calculations in delayed systems with translational symmetry. *Journal of Nonlinear Science*, 14(6):505–528, 2004. doi:10.1007/s00332-004-0625-4.

[65] Richard L. Bielawa. *Rotary Wing Structural Dynamics and Aeroelasticity*. AIAA, Washington, DC, 2005.

[66] Sigurd Skogestad and Ian Postlethwaite. *Multivariable Feedback Control*. John Wiley & Sons, Chichester, 2005.

[67] Roy R. Craig, Jr. and Mervyn C. C. Bampton. Coupling of substructures for dynamic analysis. *AIAA Journal*, 6(7):1313–1319, July 1968.

[68] John C. Houbolt and George W. Brooks. Differential equations of motion for combined flapwise bending, chordwise bending, and torsion of twisted nonuniform rotor blades. TN 3905, NACA, 1957. Updated in 1975.

[69] John C. Houbolt and George W. Brooks. Differential equations of motion for combined flapwise bending, chordwise bending, and torsion of twisted nonuniform rotor blades. TR 1346, NASA, 1975. Supersedes NACA TN 3905, 1957.

[70] D. H. Hodges and E. H. Dowell. Nonlinear equation for the elastic bending and torsion of twisted nonuniform rotor blades. TN D-7818, NASA, 1974.

[71] P. P. Friedmann and F. Straub. Application of the finite element method to rotary-wing aeroelasticity. *Journal of the American Helicopter Society*, 25(1):36–44, January 1980.

[72] D. H. Hodges and M. J. Rutkowski. Free vibration analysis of rotating beams by a variable-order finite element method. *AIAA Journal*, 19(11):1459–1466, November 1981. doi:10.2514/2.933.

[73] Anubav Datta. *Fundamental Understanding and Prediction of Vibratory Loads of a Helicopter*. PhD thesis, University of Maryland, 2006.

[74] Gian Luca Ghiringhelli, Pierangelo Masarati, and Paolo Mantegazza. A multi-body implementation of finite volume beams. *AIAA Journal*, 38(1):131–138, January 2000. doi:10.2514/2.933.

[75] Thomas J. R. Hughes. *The Finite Element Method: Linear Static and Dynamic Finite Element Analysis*. Prentice Hall International Inc., New Jersey, 1987.

[76] Vittorio Giavotto, Marco Borri, Paolo Mantegazza, Gian Luca Ghiringhelli, V. Caramaschi, G. C. Maffioli, and F. Mussi. Anisotropic beam theory and applications. *Computers & Structures*, 16(1–4):403–413, 1983. doi:10.1016/0045-7949(83)90179-7.

[77] Klaus Jürgen Bathe. *Finite Element Procedures*. Prentice-Hall, Upper Saddle River, New Jersey, 1996.

[78] S.S. Rao. *Finite Element Method in Engineering*. Elsevier, 2004.

[79] A. T. Conlisk. Modern helicopter aerodynamics. *Annual Review of Fluid Mechanics*, 29:515–167, 1997.

[80] J. Gordon Leishman. *Principles of Helicopter Aerodynamics*. Cambridge University Press, Cambridge, UK, 2nd edition, 2006.

[81] Giuseppe Quaranta. *A Study of Fluid-Structure Interactions for Rotorcraft Aeromechanics: Modeling and Analysis Methods*. PhD thesis, Dipartimento di Ingegneria Aerospaziale, Politecnico di Milano, Milano, Italy, 2004.

[82] Giuseppe Quaranta, Pierangelo Masarati, and Paolo Mantegazza. A conservative mesh-free approach for fluid structure interface problems. In *Coupled Problems 2005*, Santorini, Greece, May 24–27 2005.

[83] John Dugundji and John. H. Wendell. Some analysis methods for rotating systems with periodic coefficients. *AIAA Journal*, 21(6):890–897, August 1982.

[84] Wayne Johnson. *Helicopter Theory*. Princeton University Press, Princeton, New Jersey, 1980.

[85] G. Bir. Multiblade coordinate transformation and its application to wind turbine analysis. In *ASME Wind Energy Symposium*, Reno, Nevada, January 7–10 2008. NREL/CP-500-42553.

[86] Cesare Cardani and Paolo Mantegazza. Continuation and direct solution of the flutter equation. *Computers & Structures*, 8:185–192, 1976.

[87] W. Keats Wilkie, Paul H. Mirick, and Chester W. Langston. Rotating shake test and modal analysis of a model helicopter rotor blade. TM 4760, NASA, June 1997. (ARL Technical Report 1389).

[88] William G. Bousman, Colin Young, François Toulmay, Neil E. Gilbert, Roger C. Strawn, Judith V. Miller, Thomas H. Maier, Michel Costes, and Philippe Beaumier. A comparison of lifting-line and CFD methods with flight test data from a research Puma helicopter. TM 110421, NASA, October 1996.

[89] Vincenzo Muscarello, Pierangelo Masarati, and Giuseppe Quaranta. Multibody analysis of rotorcraft-pilot coupling. In P. Eberhard and P. Ziegler, editors, *2nd Joint International Conference on Multibody System Dynamics*, Stuttgart, Germany, May 29–June 1 2012.

[90] Norman M. Wereley. *Analysis and Control of Periodically Time Varying Systems*. PhD thesis, Massachusetts Institute of Technology, 1990.

[91] David A. Peters and Kurt H. Hohenemser. Application of the Floquet transition matrix to problems of lifting rotor stability. *Journal of the American Helicopter Society*, 16(2):25–33, 1971. doi:10.4050/JAHS.16.25.

[92] David A. Peters, Sydnie M. Lieb, and Loren A. Ahaus. Interpretation of Floquet eigenvalues and eigenvectors for periodic systems. *Journal of the American Helicopter Society*, 56(3):1–11, July 2011. doi:10.4050/JAHS.56.032001.

[93] C. L. Bottasso and S. Cacciola. Periodic stability analysis of wind turbines. In *European Wind Energy Conference & Exhibition 2012*, pages 1021–1028, Copenhagen, Denmark, April 16–19 2012.

[94] C. S. Hsu. On approximating a general linear periodic system. *Journal of Mathematical Analysis and Applications*, 45(1):234–251, 1974.

[95] P. Friedmann and J. Silverthorn. Aeroelastic stability of periodic systems with application to rotor blade flutter. In *AIAA/ASME/SAE 15th Structures, Structural Dynamics and Materials Conference*, Las Vegas, Nevada, April 17–19 1974.

[96] G. H. Gaonkar, D. S. Simha Prasad, and D. Sastry. On computing Floquet transition matrices of rotorcraft. *Journal of the American Helicopter Society*, 26(3):56–61, 1981. doi:10.4050/JAHS.26.56".

[97] Cleve Moler and Charles Van Loan. Nineteen dubious ways to compute the exponential of a matrix, twenty-five years later. *SIAM Review*, 45(1):3–49, 2003.

[98] L. Ya. Adrianova. *Introduction to Linear Systems of Differential Equations*, volume 146 of *Translations of Mathematical Monographs*. American Mathematical Society, Providence, Rhode Island, 1995.

[99] Alfredo Medio and Marji Lines. *Nonlinear Dynamics A Primer*. Cambridge Univ Press, 2001.

[100] Steven H. Strogatz. *Nonlinear Dynamics and Chaos publisher =*. 1994.

[101] Dewey Hodges and G. Alvin Pierce. *Introduction to Structural Dynamics and Aeroelasticity*. Cambridge University Press, Cambridge, England, 2002.

[102] Earl H. Dowell. *A Modern Course in Aeroelasticity*. Springer, 5th edition, 2015.

[103] Bernard Etkin and Lloyd Duff Reid. *Dynamics of Flight*. John Wiley & Sons, New York, 3 edition.

[104] Karlheinz Geist, Ulrich Parlitz, and Werner Lauterborn. Comparison of different methods for computing Lyapunov exponents. *Progress of Theoretical Physics*, 83(5), May 1990. doi:10.1143/PTP.83.875.

[105] Firdaus E. Udwadia and Hubertus F. von Bremen. Computation of Lyapunov characteristic exponents for continuous dynamical systems. *Zeitschrift für angewandte Mathematik und Physik ZAMP*, 53(1):123–146, 2002. doi:10.1007/s00033-002-8146-7.

[106] Pierangelo Masarati. Estimation of Lyapunov exponents from multibody dynamics in differential-algebraic form. *Proc. IMechE Part K: J. Multi-body Dynamics*, 227(4):23–33, 2012. doi:10.1177/1464419312455754.

[107] Kaare Brandt Petersen and Michael Syskind Pedersen. *The Matrix Cookbook*. 2008.

[108] L. Dieci and E. Van Vleck. Lyapunov spectral intervals: Theory and computation. *SIAM Journal on Numerical Analysis*, 40(2):516–542, 2002. doi:10.1137/S0036142901392304.

[109] Lawrance Perko. *Differential Equations and Dynamical Systems*. Springer-Verlag, Berlin-Heidelberg-New York, 2000.

[110] L. Dieci, R. D. Russell, and E. S. Van Vleck. On the computation of Lyapunov exponents for continuous dynamical systems. *SIAM Journal on Numerical Analysis*, 34(1):402–423, 1997. doi:10.1137/S0036142993247311.

[111] Gareth D. Padfield. *Helicopter Flight Dynamics: The Theory and Application of Flying Qualities and Simulation Modelling*. AIAA Education Series, 1996.

[112] Robert P. Coleman and Arnold M. Feingold. Theory of self-excited mechanical oscillations of helicopter rotors with hinged blades. Report 1351, NACA, 1958.

[113] C. E. Hammond. An application of Floquet theory to prediction of mechanical instability. *Journal of the American Helicopter Society*, 19(4):14–23, 1974. doi:10.4050/JAHS.19.14.

[114] Giuseppe Quaranta, Vincenzo Muscarello, and Pierangelo Masarati. Lead-lag damper robustness analysis for helicopter ground resonance. *J. of Guidance, Control, and Dynamics*, 36(4):1150–1161, July 2013. doi:10.2514/1.57188.

[115] Michael T. Rosenstein, James J. Collins, and Carlo J. De Luca. A practical method for calculating largest Lyapunov exponents from small data sets. *Physica D: Nonlinear Phenomena*, 65(1–2):117–134, May 1993. doi:10.1016/0167-2789(93)90009-P.

[116] Shihui Fu and Qi Wang. Estimating the largest Lyapunov exponent in a multibody system with dry friction by using chaos synchronization. *Acta Mechanica Sinica*, 22:277–283, 2006. doi:10.1007/s10409-006-0004-y.